Aptamer-Based Sensors: Developing Electrochemical and Surface Plasmon Resonance Sensors Using Aptamers as Target Recognition Elements

by

David A. D. Blair, B.Sc.

A thesis submitted to the Faculty of Graduate Studies and Research

in partial fulfillment of the requirement for the degree of

Master of Science

to

The Faculty of Graduate Studies and Research

Department of Chemistry

Carleton University

Ottawa, Ontario

Canada

Abstract

The development of an aptamer-based electrochemical sensor focused on the synthesis and characterization of a redox-active [Co(4-(3-carboxypropyl)-4'-methyl-2,2'-bipyridine)(2,2'-bipyridine)$_2$]$^{3+}$ complex. The cobalt bis(bipyridyl) and modified bipyridine reagents were successfully synthesized and subsequent reactions to produce the desired complex were performed. Characterization of the reaction products confirmed the successful synthesis of the cobalt complex, with the best purity being achieved using water as a solvent. Preliminary electrochemical characterization and conjugation attempts indicated that the label complex may be applicable in the desired sensor design.

A different aptamer-based sensor was created by exciting surface plasmon resonance (SPR) at the surface of a gold-plated optical using tilted fiber Bragg gratings that were written into the core of the fiber. A measureable change in the SPR was observed during the immobilization of a thiolated aptamer to the gold surface, and during the subsequent binding of the aptamer to its target. Microscopic characterization techniques were used to correlate the shift in SPR to the visual conformation of the surface immobilization of the aptamer and target binding.

Acknowledgments

I have to mention that I would not have been able to do any of this without my family. Their love, support and patience is really more than anyone could ask for, and I consider myself very lucky that they are always there for me when I need encouragement and food and a washing machine.

I would like to thank my supervisor Dr. Maria DeRosa an infinite amount of times for giving me this amazing opportunity. She was an incredible source of information, and all of her advice and support were an invaluable help for me, and it is greatly appreciated. She also hosts some of the greatest lab gatherings that, I am sure, have ever occurred in history. I would also like to thank Dr. Jeff Manthorpe, Dr. Seán Barry, Dr. Rob Letcher, Tony O'Neil and Keith Bourque in the Chemistry Department for sharing their knowledge with me when books just would not do the job. Thanks to Dr. Jacques Albert and Yanina Shevchenko for giving me the opportunity to work on the fiber project, and Tuan Guo for all of his help. Thanks also to Anne-Fook Yang, Denise Chabot, Graham Galway, Nur Uddin Ahamad and Dr. Anatoli Ianoul for the use of their microscopes and their vast wealth of knowledge. Special thanks to Dr. Bob Burk, who has been there for me with help and advice for my entire University career.

The lab has been a second home to me throughout this project, and as such the lab members have made it incredibly easy to come in by being like a second, rather large, family. Tariq Francis was a huge asset to have throughout the entire cobalt project, and Ryan Walsh, Elyse Bernard, Yasir Sultan and Maureen McKeague were incredible friends inside and outside of the lab. I am also indebted to all of the undergrads who have come and gone, or stayed, whose enthusiasm and knowledge I am sure will bring them much success.

I am grateful to have so many amazing friends who help me get back to the outside life occasionally. Joe and Nic (my KS brothers), Mike W, Pete, Colin, Lindsay, Fin, Connor, Rob and Mike Y have been the most amazing friends since as far back as I can remember, and the road trips and midnight breakfasts are unforgettable. I can remember meeting Mike B, Peter, Becky, the Marion building, and my volleyball teams, but they are better friends than anyone can hope for. Thanks to Robert Randolph, moe., the Weakerthans, the Rheostatics, Michael Franti and Luke Doucet for making writing this report even more enjoyable than it already was.

As with everything I do, this report is dedicated to the memory of all my friends and family whose lives, short or long, are a constant inspiration for me every step of the way.

Table of Contents

List of Figures

List of Tables

List of Abbreviations

AFM – atomic force microscopy

bipy – 2,2'-bipyridine

bipy' – 4-(3-carboxypropyl)-4'-methyl-2,2'-bipyridine

CLSM – confocal laser scanning microscopy

COSY – H-H correlation spectroscopy

Cy3, Cyanine 3 – 1-(e-carboxypentynyl)-14-ethyl-3,3,34,34-tetramethylindocarbocyanine-5,54-disulfonate

DCM – dichloromethane

DEA – diethylamine

DIPEA – diisopropylethylamine

DMF – dimethylformamide

DNA – deoxyribonucleic acid

DTNB – 5,5'-dithiobis-(2-nitrobenzoic acid)

EDC – 1-ethyl-3-(3-dimethylaminopropyl) carbodiimide hydrochloride

EDTA – ethylenediaminetetra-acetic acid disodium salt

FBG – fiber Bragg grating

FRET – fluorescence resonance energy transfer

HPLC – high performance liquid chromatography

LDA – lithium diisopropylamide

LPFG – long-period fiber grating

MS – mass spectrometry

MW – molecular weight

NHS – N-hydroxysuccinimide

NMR – nuclear magnetic resonance

PAGE – polyacrylamide gel electrophoresis

PyBOP – (benzotriazol-1-yloxy)tripyrrolidinophosphonium hexafluorophosphate

Redox potential – reduction/oxidation potential

RI – refractive index

RNA – ribonucleic acid

rpm – revolutions per minute

SAM – self-assembled monolayer

SPM – scanning probe microscope

SPR – surface plasmon resonance

SPW – surface plasma wave

TBAB – tetrabutylammonium bromide

TBE buffer – TRIS/boric acid/EDTA buffer

TCEP – tris(2-carboxyethyl) phosphine hydrochloride

TEA – triethylamine

TFBG – tilted fiber Bragg grating

THF – tetrahydrofuran

TLC – thin-layer chromatography

TNB – 2-nitro-5-thiobenzoate

List of Publications

Y. Y. Shevchenko, D. A. D. Blair, M. C. Derosa, and J. Albert. "DNA Target Detection Using Gold-Coated Tilted Fiber Bragg Gratings in Aqueous Media." In *Conference on Lasers and Electro-Optics/Quantum Electronics and Laser Science Conference and Photonic Applications Systems Technologies*, OSA Technical Digest (CD) (Optical Society of America, 2008), paper CMJ4.

Y.Y. Shevchenko, D.A.D. Blair, M.C. DeRosa, and J. Albert. "A simple fiber optic surface plasmon resonance sensor for label-free detection of small biomolecules." *CIPI-Photons technical review*, **2008**, in press.

Chapter 1

Development of an aptamer-based electrochemical sensor

1.1 Introduction

1.1.1 Aptamers

Aptamers are nucleic acid (DNA or RNA) sequences that can be selected *in vitro* to bind to targets with high affinity and selectivity. Aptamers have been selected to bind to a number of different types of targets, such as small molecules, peptides, proteins, and cells.[1] Aptamers can also be selected to bind to non-biological targets, such as pollutants, although this application has not been explored to the extent of biological uses.[2]

Aptamers are selected from large libraries of random sequences to bind to targets using a process known as systematic evolution of ligands by exponential enrichment (SELEX).[3] The process, shown in Figure 1.1, allows the isolation of strongly binding nucleic acid sequences through a repetitive target-binding, elution and amplification process. A library of 10^{14}-10^{15} different random nucleic acid sequences is first incubated with the target. The nucleotide sequences in the library are typically composed of a random sequence zone with two constant sequences on either end (primer binding sites used for the amplification of the DNA), with the number of nucleotides in the random zone dictating how many total random sequences are in the library. The sequences bound to the target can be separated from the unbound sequences using filtration (if the target is a protein) or affinity column chromatography (if the target is a small molecule).[4] The binding sequences are then amplified, and the new, enriched library is incubated with the target, and separated from unbound sequences, amplified, etc., until the desired amount of repetitions of the process has been reached. Usually, 8-15 repetitions of this process are enough to yield suitable aptamers.[5]

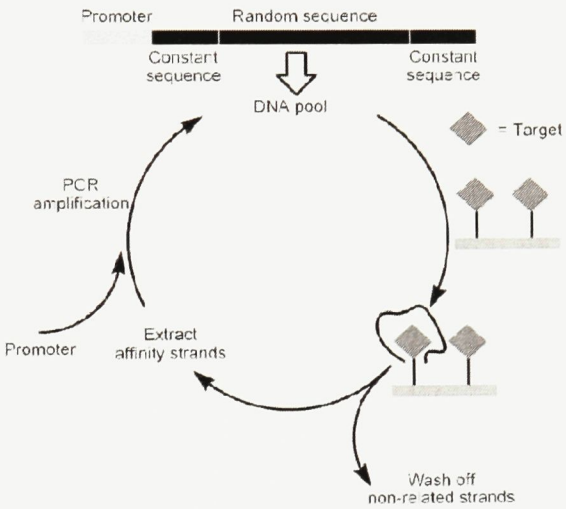

Figure 1.1. The selection of an aptamer by the SELEX cycle procedure. PCR: polymerase chain reaction.[5]

The strength of affinity of aptamers is measured by determining the dissociation constant (K_d) of the aptamer-target bound complex, and can be thought of as the concentration (in mol/L) at which half of the aptamers are bound to the target. Therefore, the lower the dissociation

constant, the higher the affinity the aptamer has for its target. Aptamers selected against small molecules typically have micromolar to sub-micromolar dissociation constants, while aptamers selected against proteins can have dissociation constants in the nanomolar range.[4] The ability of aptamers to discriminate between similar targets has also been shown in many cases. In one study, it was found that the aptamer for caffeine had a dissociation constant 10000 times lower for theophylline, whose structure differs from caffeine by only one methyl group.[6] In another study, the chiral discrimination of the aptamer for L-adenosine over D-adenosine was approximately 1700-fold.[7]

The name aptamer is derived from the Latin word *aptus*, meaning 'to fit.' In solution, aptamers are mostly unstructured, but in the presence of targets they fold into three-dimensional architectures, in which the target takes an integral role.[8] Nuclear magnetic resonance studies of target-bound aptamers have revealed that aptamers form unique overall shapes and form binding pockets to accommodate targets, and that functional groups on an aptamer are brought in close proximity to each other and form a cluster of molecular forces that specify target interaction.[9] An example of such a structural change is the cocaine-binding aptamer,[10] shown in Figure 1.2. In the absence of cocaine, a section of the aptamer is unstructured. However, when cocaine is present, a three-way junction forms, closing a second and third stem that were open in the absence of the target. This conformational change was also used to turn the aptamer into a fluorescence-based sensor, as the absence of cocaine separated the fluorophore (F) and quencher (D) so that the fluorescence could be monitored. When the cocaine was added, the formation of the three-way junction brought the fluorophore and quencher close together, so the fluorescence was reduced in a concentration-dependent fashion.[10]

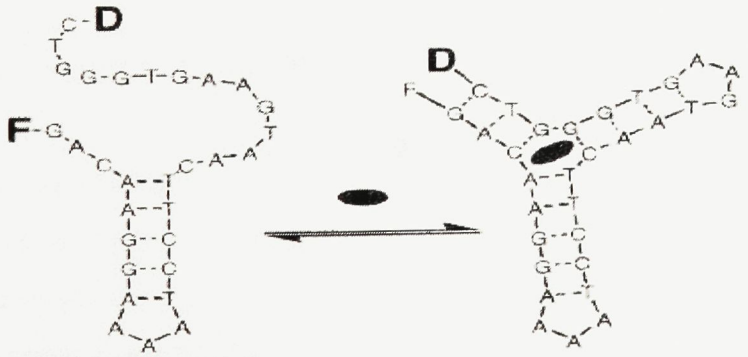

Figure 1.2. A fluorescent biosensor based on the cocaine-binding aptamer.[10] Addition of the target (black ellipsoid) quenches the emission of the fluorophore (F).

1.1.2 Aptamers and biosensing

Due to the affinity and specificity of aptamer binding, a major use for aptamers in analytical chemistry has been as stationary phases in separation techniques, such as capillary electrophoresis.[4] However, the attributes of aptamers described above are suitable for their use as the biomolecular recognition elements of biosensors, as well. Moreover, the use of aptamers in biosensors can provide advantages over immunosensors using antibodies, some of which are listed in Table 1.1.

Table 1.1. Advantages of using aptamers over antibodies in biosensing. Adapted from O'Sullivan.[1]

Antibodies	Aptamers
A significant immune response towards the target is required	Toxins and molecules that do not generate strong immune responses can still be selected against
Limited shelf life, sensitive to temperature and may undergo denaturation	Stable to long-term storage and transport at ambient temperature, can be regenerated when denatured
Finding antibodies that recognize targets in non-physiological conditions is not feasible	Selection in non-physiological conditions can be used to select aptamers for use *in vitro*
Batch-to-batch variation	No batch-to-batch variation due to chemical synthesis
Requires the use of animals	Identified *in vitro* and synthesized chemically
Labelling can result in a loss of binding affinity	Labels can be attached to areas not involved in binding and not affect binding affinity

Of those listed in Table 1.1, one advantage that makes aptamers a very attractive alternative to antibodies is their ability to be denatured and renatured several times, and as a result allow multiple readings with one sensor. Heat, salt concentration, solution pH and chelating molecules can all be used in order to denature the aptamer and release the target, so that the aptamer-based sensor may be used again. With the exception of pH, these factors may be used at any extreme without causing damage to the aptamer.[9]

Although the field of aptasensing is still in its infancy, aptamers have been used in several ways, including their use in molecular beacon sensors, surface plasmon resonance sensors, fluorescence sensors and in quartz crystal microbalances.[4]

1.1.3 Molecular beacon biosensors

Molecular beacons are a form of biomolecular recognition probe, which have gained popularity in fields such as chemistry, biology and medical sciences.[11] Molecular beacons undergo a conformational change in order to allow detection of a specific target. The molecular beacon probe consists of a short nucleotide sequence and can be broken down into three parts.[12] The first part is a loop consisting of 15-30 nucleotides, which is the area that binds with the target. The second part is a stem consisting of 5-8 nucleotide base pairs. During the binding of the molecular beacon to a target, the stem section is designed to dissociate. The third part of the molecular beacon is a fluorophore attached at the 5'-end of the oligonucleotide, and a non-fluorescent quencher attached at the 3'-end.[13] The advantage of molecular beacons is their simplicity to construct, as well as the specificity that results from their binding interactions that will be described below.

The functioning principle of the molecular beacon is shown in Figure 1.3.[11] The binding of the molecular beacon to its target is based on Watson-Crick base pairing, so in the case of DNA guanine and cytosine form base pairs, and adenine and thymine form base pairs. This base pairing is what allows the formation of the stem of the initial conformation of the molecular beacon. Two nucleotide strands which have sequences such that their nucleotides form base pairs when they are placed together in solution are called complementary. In the absence of the target sequence, the molecular beacon forms the stem-and-loop structure, due to the base pairing of the stem sequences. However, when the complementary target sequence is present, it forms base pairs with the loop portion of the molecular beacon. Since more base pairs are formed

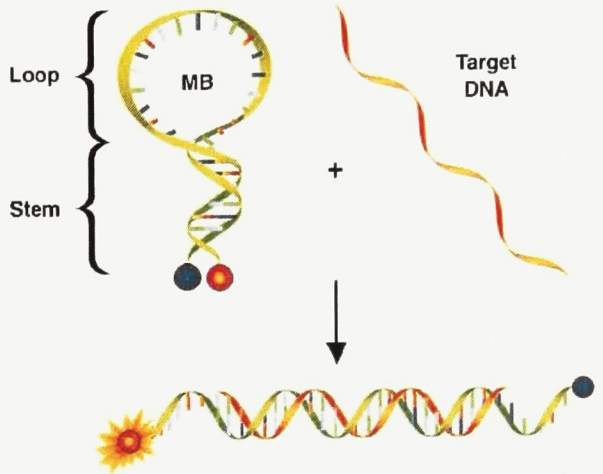

Figure 1.3. The principle of molecular beacon biosensor detection.[11]

by the binding of the beacon to its target, the base pairs of the stem section of the beacon come apart and the beacon and target form a linear double helix.

Detection using a molecular beacon is made possible by attaching a fluorophore to the 5'-end of the molecular beacon, and a non-fluorescent quencher at the 3'-end. In the absence of the target sequence, the stem-and-loop formation of the beacon brings the fluorophore and quencher close together. In this situation, the fluorescence emitted by the fluorophore is almost completely absorbed by the quencher and emitted as heat, so no signal can be seen. However, the addition of the target sequence forms the linear double helix, which separates the fluorophore and the quencher. Since the quencher is not close enough to absorb most of the fluorophore's emissions, the fluorescence can be easily observed using a fluorometer. The specificity of a molecular beacon results from the requirement of complementary base pairing in order to produce the signal. Base pair mismatches in the beacon and target sequences will not favour the formation of the double helix, and therefore a signal will not be observed.

Although molecular beacon biosensors are designed specifically for the sensing of target nucleotide sequences, which makes them unusable with aptamer-target binding, the idea of conformational change to create a signal is a major factor in the architecture of the proposed sensor. In this sense, the proposed aptamer-based biosensor could be considered a form of molecular beacon biosensor.

1.1.4 Electrochemical biosensors

The use of electrochemical methods in biosensing has gained much interest, and has potential advantages over biological and chemical assays due to their simplicity, use of small sample volumes, and reliability,[14] as well as their high sensitivity, low cost and portability.[15]

The basic principle of an electrochemical sensor is that an electroactive species is reduced or oxidized at an electrode surface. The redox reaction causes a change in the electrical parameters of the electrode, which was given a predefined pattern of constant or varied potential. This change, the result of the type or concentration of the analyte, can be measured as a result.[16] The change in the electrical parameter of the electrode can be measured using any number of electrochemical methods, although cyclic voltammetry and linear sweep voltammetry comprise 40% of the reported analyses.[16]

1.1.4.1 Redox labels in electrochemical biosensors

Redox labels have been mostly used in the electrochemical detection of DNA hybridization, as redox-active intercalating labels can be developed to specifically interact with double-stranded DNA over single-stranded DNA. The interaction of the redox label with the double-stranded DNA at the electrode surface would enhance the peak potential current of the labels, and enable the detection of the hybridization.[17]

Many transition metal complexes have proven to be useful redox-active labels in electrochemical biosensing, including ruthenium, copper, cobalt, and cadmium complexes (reviewed by Sassolas *et al.*[15] and Li *et al.*[18]). Among those compounds, tris(bipyridyl) ruthenium[19] and cobalt[20] complexes were used to probe biomolecular interactions electrochemically.

1.1.4.2 Aptamer-based electrochemical biosensors

Increasing creativity in the development of electrochemical biosensor design has facilitated the adaptation of aptamers into different forms of electrochemical biosensors. In one form, aptamers can be labelled with catalysts or nanoparticles in order to generate electrochemically detectable products.[5] In another form, the conformational changes that aptamers undergo upon binding can be used in order to initiate or disrupt electron-transfer communication between a redox-active molecule and the electrode.[5]

In the electron-transfer form of the electrochemical biosensor, detection may occur when binding of the aptamer to its target either enables or disables the transfer of electrons between the redox-active molecule and the electrode. Figure 1.4 displays designs using both of these ideas. In the first example (Figure 1.4a), a methylene blue (MB) labelled aptamer for thrombin was immobilized on an electrode. In the absence of the target, the unstructured nature of the aptamer allowed electrical contacting of the redox label with the electrode, so that a voltammetric signal was observed. Upon the addition of thrombin, the aptamer formed a structured conformation, distancing the label from the electrode and reducing the voltammetric response.[21] In another study, both the 5'- and 3'-ends of the aptamer for thrombin were elongated with hexamethylene spacers, in order to create a separation between the redox label (ferrocene in this experiment) and electrode before the addition of the target (Figure 1.4b). When the target was present, the newly-

formed structured conformation of the aptamer brought the label close to the surface, resulting in an amperometric response.[22]

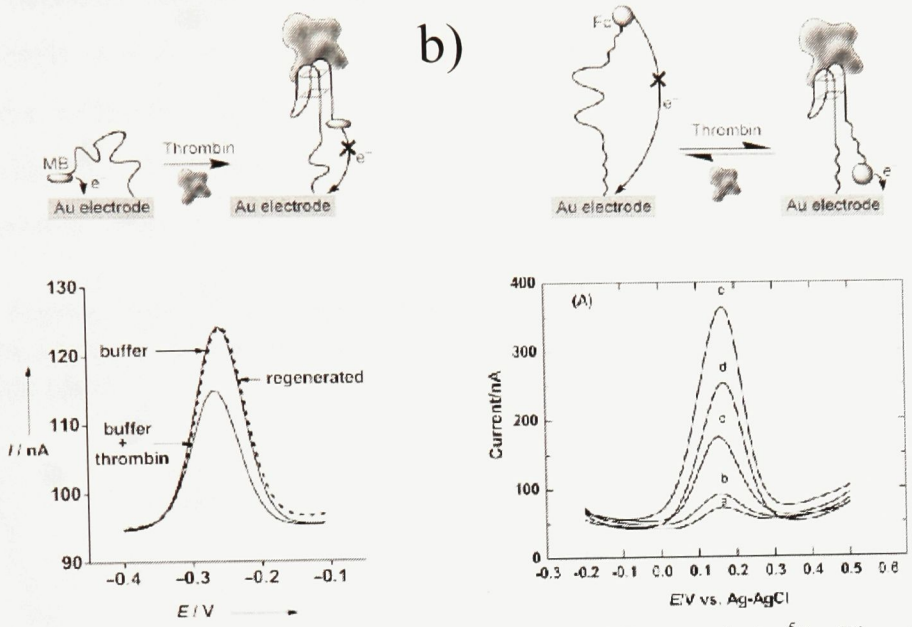

Figure 1.4. Two aptamer-based electrochemical biosensors. a) An "off" sensor design[5] by Xiao et al., with a voltammogram displaying the electrochemical response in buffer (dashed line), and after the addition of thrombin (solid line).[21] b) An "on" sensor design[5] by Radi et al., with a voltammogram displaying the electrochemical chemical response of the sensor in buffer (b) and concentrations of thrombin up to 30nM (e).[22]

Both of the biosensor designs described above rely on the conformational change of the aptamer to enable the detection of the analyte. The first example can be considered an "off" sensor, where the addition of the target causes a negative readout signal, while the second can be considered an "on" sensor. Of the two, a sensor that provides a positive readout signal is more desirable.[5] A major advantage of both of these sensors was that regeneration of the sensors was possible.[5]

1.1.5 Peptide coupling

An advantage to using aptamers in biosensing is the fact that at any point along the aptamer, a specific label may be tethered. The labels, when attached, can allow the aptamer to be used in a variety of imaging methods (by attaching dyes or magnetic resonance contrasting agents) or detection methods (by attaching metal nanoparticles or redox-active compounds).

Carbodiimides (N=C=N) can be used to catalyze covalent binding between a carboxylic acid and amines by activating the acid to form an O-acylurea.[23] The acylurea intermediate can then react with an amine to form the desired amide. The carbodiimide 1-ethyl-3-(3-

dimethylaminopropyl) carbodiimide hydrochloride (EDC) is an example of a compound that can activate a carboxylic acid. A problem that arises when a carbodiimide is used is that the intermediate becomes susceptible to hydrolysis when water is present, which considerably lowers the overall yield of the coupling.[23] To overcome this, a hydrophobic ester can be used to slow down the hydrolysis of the intermediate and stabilize it in the presence of water. N-hydroxysuccinimide (NHS) and N-hydroxysulfosuccinimide can be used to accomplish this, and improve the overall yield of the coupling reaction.

Scheme 1.1. Peptide coupling accomplished using EDC to activate the carboxylic acid and NHS to stabilize the acylurea intermediate. Amine-modified DNA reacts with the NHS intermediate to form the amide bond.[24]

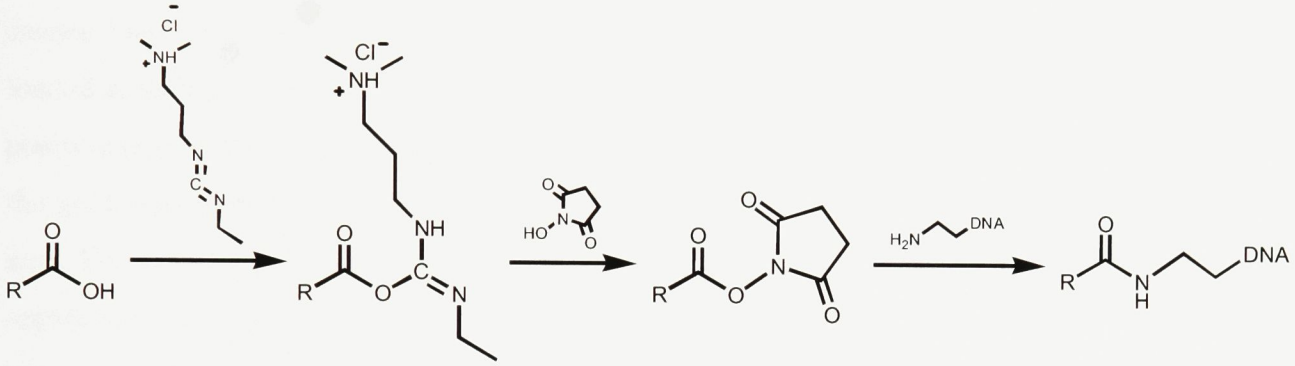

Scheme 1.2. Peptide coupling by deprotonation with diisopropylethylamine and reaction with PyBOP. Amine-modified DNA reacts with the PyBOP intermediate to form the amide bond.[25]

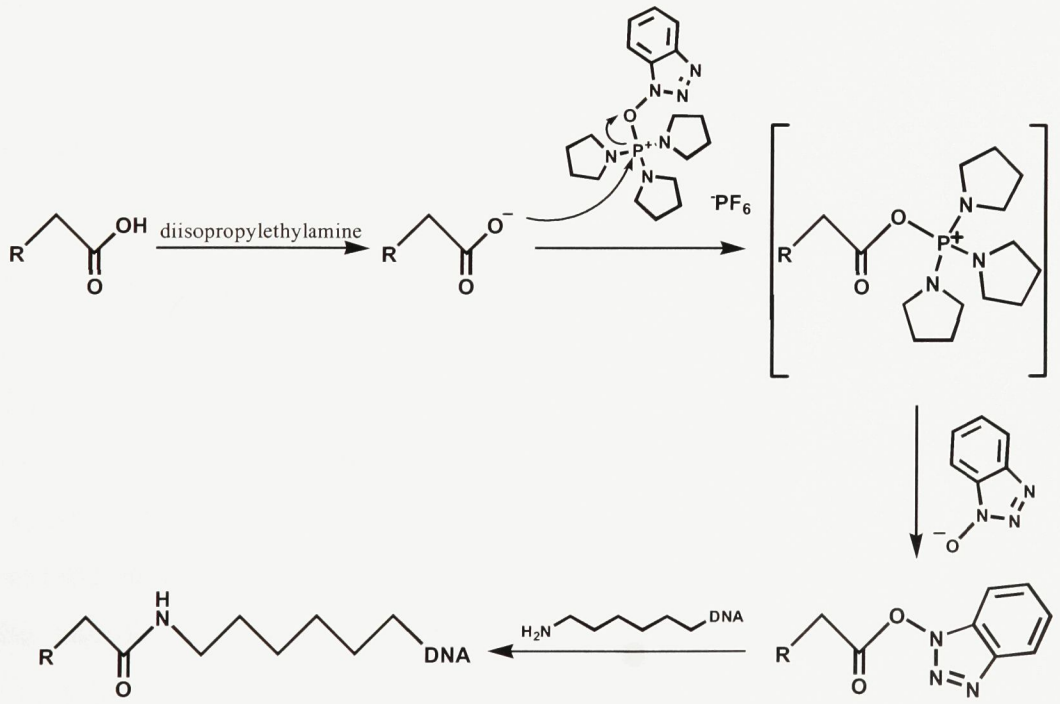

Hydroxybenzotriazoles are another family of compound that can be used to activate a carboxylic acid. After deprotonating the acid using diisopropylethylamine (DIPEA), PyBOP ((benzotriazol-1-yloxy)tripyrrolidinophosphonium hexafluorophosphate)[26] can be used to form the reactive intermediate as shown in Scheme 1.2.

1.1.6 Polyacrylamide gel electrophoresis (PAGE)

In 1960, Raymond and Wang[27] discovered that a cross-linked acrylamide and methylenebisacrylamide gel produced a flexible, stable and insoluble matrix that could be used for gel electrophoresis. Gel electrophoresis is the most widely used separation technique for biological macromolecules.[28] The technique exploits the negative charge of nucleic acids, and causes them to migrate in an electric field. The gels are mounted vertically, and samples are loaded at the top. The negative pole of the electric field is introduced at the top of the gel, and the positive pole at the bottom, making the negatively-charged nucleic acids migrate from the top of the gel towards the bottom. The gel can then be used to separate the migrating molecules by their size. The gel slows the migration of larger molecules more than smaller molecules, allowing the separation of oligonucleotide strands by length (since longer sequences are larger).[28] The migration of the nucleotides through the gel can be monitored by UV-vis spectrophotometric methods or fluorescent methods if the molecules are fluorescently labelled. For a solution of mixed biological macromolecules, gel electrophoresis has proven to be invaluable in the detection, purification, characterization of the desired molecule.[29]

1.1.7 Proposed electrochemical biosensor

The goal of this research project is to design and construct an aptamer-based electrochemical biosensor. One advantage of an aptamer-based sensor is that the aptamer can be changed in order to accommodate the detection of a wide range of analytes, even ranging into non-biological targets. The design of the sensor is depicted in Figure 1.5. The proposed sensor will consist of three parts: the electrode, the aptamer and the redox-active label. In the absence of the target, the unstructured nature of the aptamer would result in a distance between the electrode surface and the redox-active label, and therefore no electron transfer would occur between them. Upon the addition of the target, however, the aptamer's change to a more structured

configuration would bring the label close to the electrode, allowing electron transfer and creating a measurable voltammetric response.

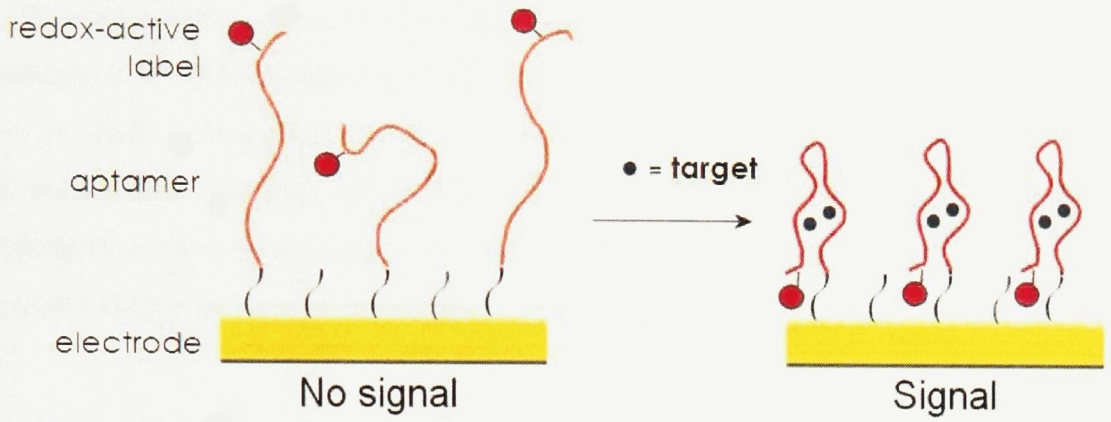

Figure 1.5. The design of the proposed sensor. The presence of the analyte brings the redox-active label close to the electrode surface, creating a measurable signal.

1.1.7.1 Electrode

Gold electrodes are common for use in aptamer-based electrochemical sensors, since thiol-modified aptamer sequences can be immobilized on the electrodes using well-studied chemistry. However, if measurements *in vivo* are to be possible, a more biocompatible material should be used as the electrode. The incorporation of carbon electrodes, then, may provide a possible system to allow *in vivo* measurements.

1.1.7.2 Aptamer

The aptamer section of the sensor consists of a single-stranded DNA aptamer. The creation of the signal is heavily dependent on the structure assumed by the aptamer when it binds to its analyte. Firstly, a change in the aptamer's structure upon binding is necessary, in order to distinguish between the voltammetric response before and after the addition of the analyte. Secondly, the conformational change that the aptamer undergoes in the presence of the target must have an effect on the electron-transfer communication between the label and the electrode.

This biosensor design is identical to the one used as described in Section 1.2.2 (see Figure 1.4b). Another study[30] used a similar design for the electrochemical detection of theophylline using the RNA aptamer. In another study, a tris-bipyridyl ruthenium complex was used as a tethered label on the DNA aptamer for cocaine.[31] The aptamer response to the addition

of the target resulted in electrogenerated chemiluminescence of the ruthenium label, which was detected using a photomultiplier.

The incorporation of both DNA and RNA aptamers could potentially be used for this sensor design, with each nucleic acid possessing its own advantages. A major advantage of RNA aptamers is their well-studied ability to fold into three-dimensional structures, which may provide more suitable binding pockets for the targets. On the other hand, the advantage of using DNA aptamers in biosensing is the added stability of DNA in solution. RNA is very susceptible to enzymatic degradation, and in serum the half life of an RNA molecule is less than one minute.[4]

Using peptide coupling, described in Section 1.1.5, an amine-modified aptamer sequence can be bound to the redox-active label at its 5'-end. The 3'-end of the aptamer can also be modified in order to tether the aptamer to the electrode. In the case of a gold electrode, a gold-thiol (Au-S) bond could be used. The gold-thiol reaction is

$$R\text{–}SH + Au^0 \longrightarrow R\text{–}S^- Au^+ + 0.5H_2$$

Sulphur moieties are notoriously reactive with noble metals. The sulphur-gold interaction is a favoured "soft-soft" interaction, whereas many functional groups present in biological molecules (amines, acids, etc.) are "hard," and as a result do not interact strongly with a gold surface. As a result, the gold-thiol interaction is highly favoured over other interactions, which allows the displacement of other weakly-interacting species by thiol-modified species.[32] Upon the introduction of thiol-modified species to a gold surface, there is an initial rapid reaction to form the gold-thiol bond, followed by a period with the species assembling on the surface to maximise the Van der Waals interactions between them.[32]

1.1.7.3 Redox-active label

The redox-active label, in order to be effective in this sensor design, must satisfy two requirements: it must be able to bind covalently to DNA, and its redox potential must be low enough that there is no attraction between the DNA aptamer and the gold electrode during the experiment. Covalent binding of the label to the aptamer will allow control of the electron transfer between the label and the electrode, as only the conformational change of the aptamer

should allow contact between them. Non-specific interactions between the positively-charged redox label and the negatively-charged DNA backbone could be used in this design, but the random position at which the label would attach to the aptamer would be detrimental to the reproducibility of the results. A low redox potential for the label is also desired for this design, in order to decrease the potential needed in the electrode. It was discovered that a positive electrode potential greater than 0.45V against a silver wire resulted in DNA lying flat on the surface.[33] In the context of the designed sensor, this would bring the redox label in contact with the electrode, allowing electron transfer and creating a false positive signal. Moreover, extreme electrode potentials, lower than -0.5V and higher than +1V versus a silver wire electrode, result in the desorption of thiol-modified DNA from the surface of the electrode, due to redox reactions that take place at the gold-thiol linkages.[34]

The proposed redox-active label in this project is shown in Figure 1.6. The label is a complex based on a cobalt tris(bipyridyl) complex, with a modified bipyridine ligand. The carboxylic acid functional group on the modified bipyridine ligand will allow covalent attachment to DNA. A cobalt tris(bipyridyl) complex was chosen because the redox potential for the one-electron transition for $[Co(bipy)_3]^{3+}/[Co(bipy)_3]^{2+}$ has been reported as being 0.305V vs. standard hydrogen electrode in 1M NaCl[35] and -0.368V against a $Ag/AgNO_3$ reference electrode in water with ammonium perchlorate as a supporting electrolyte.[36] Both of these values fall within the desired redox potential range, and make the implementation of a $[Co(bipy)_3]^{3+}$ compound in the sensor an attractive prospect.

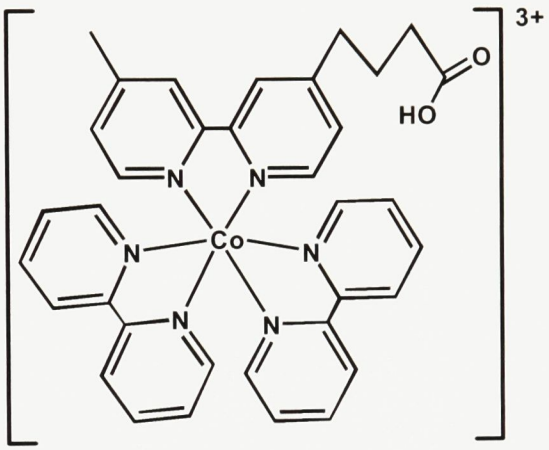

Figure 1.6. $[Co(4\text{-}(3\text{-carboxypropyl})\text{-}4'\text{-methyl-}2,2'\text{-bipyridine})(2,2'\text{-bipyridine})_2]^{3+}$: The redox-active label.

1.1.8 Project objectives

The primary objective of this project is to successfully synthesize the desired cobalt tris(bipyridyl) redox-active label complex. Then, electrochemical analysis of the complex will determine whether the redox potential of the complex would make it suitable for use in the

designed sensor. Also, attempts to conjugate the redox label to DNA will be required in order to confirm that the label complex would satisfy the two requirements of the sensor design.

1.2 Experimental Procedure

1.2.1 Equipment

For the *in vacuo* evaporation of large volumes of solvents, a Büchi REIII rotovapor was used. For the evaporation of smaller volumes, a Thermo Savant DNA120 SpeedVac Concentrator was used. Nuclear magnetic resonance (NMR) characterization was performed on a Bruker 300MHz NMR with an UltraShield magnet. All NMR solvents (acetone-d_6, dimethyl-d_6 sulfoxide, chloroform-d) were purchased from CDN Isotopes (Pointe-Claire, PQ). UV-Visible spectroscopy was performed on a Cary 300 Bio system. Mass spectrometry (MS) analysis of the redox label complex was done using a VG Platform Electrospray-Quadrupole mass spectrometer by Dr. Clement Kazakoff at the University of Ottawa (Ottawa, ON). MS analysis of the label-DNA and bipy'-DNA conjugates was done using an Oligo HTCS Electrospray-ion trap liquid chromatography/mass spectrometer by Dr. Kenneth Ray at Novatia, LLC (Monmouth Junction, NJ).

Electrochemical characterization was performed on a CH Instruments Electrochemical Workstation. The working electrode was a MW-2030 gold electrode (1.6mm in diameter). The auxiliary electrode was a MW-4130 platinum wire electrode. The reference electrode was a MW-2030 silver/silver chloride electrode. All electrodes were purchased from Bioanalytical Systems, Inc. (Mount Vernon, IN).

1.2.2 Synthesis of 4-(3-carboxypropyl)-4'-methyl-2,2'-bipyridine (bipy')

1.2.2.1 Materials

Chloroform (Spectro grade), acetone (Spectro grade), toluene (Spectro grade), hexanes (Spectro grade), tetrahydrofuran (THF), anhydrous magnesium sulphate ($MgSO_4$) and sodium carbonate were purchased from Caledon Laboratories (Georgetown, ON). Diisopropylamine (99%), *n*-butyllithium (2.5M in hexanes), 2-(2-bromoethyl)-1,3-dioxolane (96%), ethyl acetate, sodium bicarbonate, 4,4'-dimethyl-2,2'-bipyridine and potassium permanganate ($KMnO_4$, 99+%) were purchased from Sigma-Aldrich (Oakville, ON). Dichloromethane (Technical grade) was purchased from ACP Chemicals (Montreal, PQ). Silica products and triethylamine (TEA) were purchased from Fluka Analytical (through Sigma-Aldrich, Oakville, ON).

Ethylenediaminetetra-acetic acid disodium salt (EDTA) was purchased from BDH (through VWR, Mississauga, ON). Concentrated hydrochloric acid was purchased from Anachemia Science (Mississauga, ON).

The procedure for the synthesis of 4-(3-carboxypropyl)-4'-methyl-2,2'-bipyridine (bipy') was according to the method reported by Della Ciana et al.,[37] with slight modifications. All glassware was rinsed with EDTA-saturated deionized water, acetone and dichloromethane, and dried in an oven at 120°C. Upon removal from the oven, the glassware was placed in a desiccator to prevent condensation during cooling.

1.2.2.2 Preparation of the lithium diisopropylamide (LDA) solution

A glass syringe was used to add 25mL of dry THF to a three-necked round-bottom flask that had been flame-dried and sealed with rubber stoppers. With a syringe, diisopropylamine (7.5mL, 0.053 mol) was added, and the flask was placed in a dry ice/acetone bath. Then, n-butyllithium (22mL, 0.0212 mol) was added to the flask. The reaction was then left for approximately 30 minutes.

1.2.2.3 Synthesis of 4-[3-(1,3-dioxolan-2-yl)propyl]-4'-methyl-2,2'-bipyridine

In a three-necked round-bottom flask, 4,4'-dimethyl-2,2'-bipyridine (10g, 0.054 mol) was dissolved in approximately 250mL of dry THF. Heat was used to dissolve the bipyridine completely, after which the flask was placed in a dry ice/acetone bath. This solution was left for approximately 30 minutes.

A syringe was used to transfer the previously synthesized LDA solution slowly into the bipyridine solution. As more LDA was added, the solution became a dark brown colour. After the entire LDA solution had been added, the reaction solution was left for one hour in the dry ice/acetone bath.

To the solution, 2-(2-bromoethyl)-1,3-dioxolane (6.4mL, 0.053 mol) was added slowly, and the dry ice/acetone bath was replaced with only dry ice. The colour of the solution changed from dark brown to dark green. The reaction was left to stir and warm to room temperature overnight, during which time the colour of the solution changed from dark green to yellow and an orange precipitate formed.

The solution and precipitate were transferred to a separatory funnel and 100mL of deionized water was added. Then, the solution was extracted with 5x100mL dichloromethane (DCM). The organic solution was washed with 2x 100mL of saturated sodium chloride solution, and then dried over anhydrous magnesium sulphate ($MgSO_4$), and the solvent was removed *in vacuo*.

All silica used for column chromatography and thin-layer chromatography (TLC) was treated with a 10% TEA in hexanes solution. It was found that the product did not dissolve in a small enough volume of the suggested 30:70 solution of ethyl acetate to hexanes, so it was dissolved in as little DCM as possible and dried onto a minimum of silica. This was done by adding silica to the DCM solution and removing the solvent *in vacuo* until the silica appeared dry. If the silica did not look dry after all of the solvent had been removed, more DCM was added along with more silica and the solvent was removed again *in vacuo*.

A 30:70 solution of ethyl acetate to hexanes was used to elute the products from the column. The fractions collected were approximately 10mL each, with the starting material migrating the fastest (r_f=0.81) through the column, followed by the mono-alkylated product (r_f=0.57) and bisalkylated product (r_f=0.24). Fractions containing the three components were identified using TLC with a 30:70 solution of ethyl acetate to hexanes as the eluent, and fractions containing similar products were combined. The solvent was removed *in vacuo*. The yield of mono-alkylated product was 44% (with TEA pretreatment of silica) and 37% (without pretreatment).

^{1}H NMR (300MHz, $CDCl_3$) δ 8.51 (d, 2H), 8.21 (s, 2H), 7.10 (d, 2H), 4.85 (d, 1H), 3.92 (d, 2H), 3.81 (d, 2H), 2.72 (t, 2H), 2.40 (s, 3H), 1.82 (t, 2H), 1.71 (t, 2H).

1.2.2.4 Synthesis of 4-(3-formylpropyl)-4'-methyl-2,2'-bipyridine

In an Erlenmeyer flask, the mono-alkylated product was dissolved in approximately 250mL of 1M hydrochloric acid yielding a pale yellow solution. Deionized water was saturated with EDTA and either sodium bicarbonate or sodium carbonate. This solution was added until the pH of the reaction solution reached 10.

At higher pH levels, the solution turned cloudy and the colour changed from yellow to pink due to iron contamination. Iron contamination was minimized by adding more EDTA to the solution, although this did not remove the contamination altogether.

The pink solution was extracted with 5x100mL of DCM. The organic layers were collected and dried over anhydrous $MgSO_4$. The magnesium sulphate also decoloured the solution. The $MgSO_4$ was then filtered out by gravity and the organic solvent was removed *in vacuo*.

After waiting overnight the aqueous solution turned transparent yellow. The solution was extracted with another 2x100mL of DCM. The organic layers were then dried and the solvent was removed as described above. The yield of the aldehyde was 82% when sodium bicarbonate was used and 95% when sodium carbonate was used.

^{1}H NMR (300MHz, $CDCl_3$) δ 9.61 (s, 1H), 8.43 (d, 2H), 8.39 (d, 2H), 6.97 (s, 2H), 2.57 (t, 2H), 2.33 (t, 2H), 2.27 (s, 3H), 1.87 (t, 2H).

1.2.2.5 Synthesis 4-(3-carboxypropyl)-4'-methyl-2,2'-bipyridine

The aldehyde from the previous step was dissolved in a minimum of acetone and a 1:1 molar ratio of $KMnO_4$ was added. The colour of the solution was dark purple upon the addition of the $KMnO_4$, and changed to brown as the reaction progressed.

The reaction was monitored using TLC with a 1:1 mixture of ethyl acetate/toluene as the eluent. When no migration of the compound was seen, the reaction was determined to be complete, at which point the acetone was removed *in vacuo* and the remaining solid was suspended in approximately 150mL of deionized water. The suspension was then heated until boiling to coagulate the manganese dioxide, then cooled to room temperature and eventually put in the fridge overnight.

The solid manganese dioxide was filtered out by gravity. The filtrate and eluate were then washed first with a saturated EDTA solution and then a sodium bicarbonate solution. The aqueous solution was then extracted with 2x100mL DCM to remove impurities.

The solution was then acidified using 1M HCl to a pH of 4.8. As the solution became more acidic, the colour of the solution turned pink. More EDTA was added to the solution, and

again it had a slight decolouring effect on the solution. At pH 4.8 the solution was extracted with 9x100mL DCM, and the organic layers were collected and dried over $MgSO_4$ and the solvent was removed *in vacuo*. It was important that the extraction was done at a pH of 4.8, as extractions at neutral and more acidic pH levels resulted in very low yields.

The product was purified by dissolving the sample in heated chloroform ($CHCl_3$), and adding hexanes dropwise until some precipitation was seen. Then, the solution was cooled to room temperature and refrigerated overnight. The crystals that formed were filtered out by suction. The yield of the crystals was 49%.

^{1}H NMR (300MHz, $CDCl_3$) δ 12.14 (s, 1H), 8.55 (d, 2H), 8.24 (s, 2H), 7.90 (t, 2H), 2.71 (t, 2H), 2.42 (s, 3H), 2.27 (t, 2H), 1.87 (p, 2H).

1.2.3 Synthesis of $[Co(bipy)_2Cl_2]Cl$

1.2.3.1 Materials

Methanol (Reagent grade) was purchased from Caledon Laboratories (Georgetown, ON). Chlorine gas (≥99.5%), potassium chloride (minimum 99.0%), 2,2'-dipyridyl (≥99%) and cobalt(II) chloride hexahydrate (98%) were purchased from Sigma-Aldrich (Oakville, ON). Argon gas (ultra high purity) was purchased from Praxair (Mississauga, ON).

1.2.3.2 Procedure

The synthesis of the cobalt bis(bipyridyl) was done according to the procedures described by Vlček.[38]

To start, potassium chloride (1.0g, 0.013mol) and 2,2'-bipyridyl (1.6g, 0.010mol) were dissolved in 50 mL of methanol in a two-necked round bottom flask. The KCl did not dissolve completely at room temperature. The solution was then refluxed under flowing argon at 80°C for one hour, at which point cobalt(II) chloride hexahydrate (1.0g, 0.0042mol) was added and the heat was turned off. Upon the addition of the $CoCl_2 \cdot 6H_2O$, the solution turned a brown colour.

The solution, with continuous stirring, was cooled to room temperature and placed in an ice bath. The argon gas flow was then replaced with chlorine gas flow. Under the chlorine gas,

the solution became purple in colour, and a green gas formed in the flask. The solution was kept in the ice bath for approximately 15 minutes.

The solution was then filtered by suction using a medium-grained sintered glass frit. The filtrate was collected in an Erlenmeyer flask and a purple precipitate was transferred to a small beaker.

The precipitate was dissolved in 50mL of 10^{-3} M hydrochloric acid by heating the solution to 90°C for five minutes followed by cooling to room temperature. The solution's colour at this point was dark purple. A 30mL portion of 4M HCl was then added to the solution, which was stored in a refrigerator overnight.

After no precipitate had formed, approximately half of the solvent was removed *in vacuo*. The solution was then placed back in the refrigerator and a small amount of gray precipitate formed. The precipitate was removed by suction filtration. Another quantity of the solvent was evaporated *in vacuo*, resulting in the precipitation of a light purple solid with a yield of 3.7%.

The solvent was then fully evaporated *in vacuo*. This resulted in the precipitation of a dark gray and a dark purple solid. The dark gray precipitate was easily dissolved in distilled water, leaving the dark purple precipitate to be filtered by suction. The purple precipitate had a yield of 72%.

^{1}H NMR (300MHz, D_2O) δ 9.87 (d, 1H), 9.12 (d, 1H), 8.70 (d, 1H), 8.64 (d, 1H), 8.57 (t, 1H), 8.54 (t, 1H), 8.51 (d, 1H), 8.38 (d, 1H), 8.18 (t, 1H), 8.11 (t, 2H), 8.05 (t, 1H), 7.41 (t, 1H), 7.30 (d, 1H), 7.26 (t, 1H), 7.09 (d, 1H)

1.2.4 Synthesis of $[Co(bipy)_2(bipy')]^{3+}$

1.2.4.1 Materials

Anhydrous ethanol was purchased from Commercial Alcohols Inc. (Brampton, ON). Silver triflate (99+%), tetrabutylammonium bromide (98+%) and ammonium hexafluorophosphate (95+%) were purchased from Sigma-Aldrich (Oakville, ON). Sodium chloride was purchased from BDH (through VWR, Mississauga, ON).

1.2.4.2 Preparation of $[Co(bipy)_2(bipy')]Br_3$ in ethanol

A sample of $[Co(bipy)_2Cl_2]Cl$ (150mg, 0.31mmol) was dissolved in 30mL of ethanol in a round bottom flask under a flow of argon gas. To dissolve the entire amount, heating to 95°C was required. After the complex had been dissolved, the solution was a transparent purple colour.

A 3:1 molar ratio of silver triflate (238.9mg, 0.93mmol) was then added to the solution and the solution was refluxed at 95°C overnight. If the solvent level was too low, more ethanol was added to the solution. Upon the addition of the silver triflate, a white/purple/grey precipitate formed in the solution. The vessel was covered in aluminum foil to minimize light exposure while the solution was refluxing overnight.

After refluxing, the solution was cooled and the precipitate was filtered out by suction using a medium-grained sintered glass frit. The precipitate was discarded and the filtrate was replaced in the round bottom flask. The solution was still a deep, transparent purple. A 1:1 mol ratio of bipy' was added to the solution. The solution was sealed under argon, and the flask was recovered with aluminum foil. The solution was stirred overnight under argon with no heating. Upon the addition of bipy', the solution turned a deep orange colour.

When the stirring was finished, a 3:1 molar ratio of tetrabutylammonium bromide (TBAB) was added to the solution. In some cases, the bromide salt of the product precipitated right away. The precipitate was filtered out by suction using a sintered glass frit. In other cases when no precipitation formed immediately, some of the solvent was removed *in vacuo*, and the solution was placed in the fridge until a precipitate was visible. The precipitate was filtered by suction using a glass frit. The yield was approximately 45%.

1.2.4.3 Sephadex column chromatography

Sephadex G-50 and Sephadex C-25 were purchased from Sigma, and were received as a dry powder. A 0.1M sodium chloride (NaCl) solution was used to suspend the Sephadex, and load the column. The $[Co(bipy)_2(bipy')]Br_3$ sample to be separated was dissolved in a minimum of 0.1M NaCl solution, and loaded onto the column. The elution was done first with 0.1M NaCl solution, which resulted in the formation of two orange bands. The first orange band was eluted

with a 0.1M NaCl solution, but a 3M NaCl solution was required to elute the second band. The fractions collected were approximately 1mL in volume, and were collected in Eppendorf tubes. The solvent was then removed *in vacuo*, and similar fractions were added together. In between runs, the Sephadex column was washed with 0.5M NaCl solution.

1.2.4.4 Preparation of $[Co(bipy)_2(bipy')](PF_6)_3$ in water

This procedure was also presented in Tariq Francis' Bachelor of Science in Chemistry Honours Thesis.[39] In 20mL of EDTA-treated deionized water, $[Co(bipy)_2Cl_2]Cl$ (0.30g, 0.63mmol) was dissolved, resulting in a light purple solution. The temperature of the water solution was raised to 60°C in order to dissolve the cobalt bis(bipyridyl) compound. The bipy' ligand (0.16g, 0.63mmol) was added to the solution, and the solution was allowed to cool to room temperature. During the reaction, the colour of the solution changed from purple to green and eventually to orange. After four hours, the solvent was evaporated in vacuo, leaving behind a deep orange paste. The paste was dissolved in a minimum of deionized water and ammonium hexafluorophosphate (0.58g, 3.6mmol) was added, resulting in an orange precipitate. The precipitate was filtered out by suction using a sintered glass frit, with a yield of 117%. The filtrate was left uncovered in a beaker, and over time orange crystals formed. The filtrate was left for two weeks and then the crystals were filtered out with a yield of 1%.

Another aqueous synthesis was attempted by dissolving $[Co(bipy)_2Cl_2]Cl$ (0.30g, 0.62mmol) in 50mL of deionized water in a beaker. To keep the reaction vessel at approximately 0°C, the beaker was placed in an ice bath. In a separate beaker, the bipy' ligand (0.16g, 0.63mmol) was dissolved in 20mL of deionized water. A temperature of approximately 45°C was needed in order to completely dissolve the bipy' in the water, after which it was added dropwise to the reaction solution while it was still warm. The reaction was left in the ice bath overnight, and the colour of the solution changed from purple to orange. The next day, ammonium hexafluorophosphate (0.31g, 1.9mmol) was added to the reaction solution, resulting in the precipitation of an orange solid. The precipitate was filtered out by suction using a sintered glass frit and washed with cold water, with a yield of 36%. The colour of the precipitate was pink/orange. Leaving the reaction solution to evaporate resulted in the formation of a flaky precipitate. The reaction solution was split into four samples, which were centrifuged at 3000

revolutions per minute for 10 minutes. The supernatant solution was removed, and the precipitate was dried in a desiccator. The yield of the solid was approximately 10%.

1.2.5 Electrochemistry

1.2.5.1 Materials

Concentrated sulfuric acid was purchased from Anachemia Science (Mississauga, ON). TRIS was purchased from BioShop Canada (Burlington, ON). The buffer solution used in the characterization of $[Co(bipy)_2(bipy')]Br_3$ was 25mM TRIS (pH adjusted to 8.2 with hydrochloric acid) and 100mM sodium chloride.

1.2.5.2 Metathesis of $[Co(bipy)_2(bipy')](PF_6)_3$ with tetrabutylammonium bromide (TBAB)

Since the hexafluorophosphate salt of the probe complex was not soluble in water, the probe complex was changed to a bromide salt by salt metathesis. The $[Co(bipy)_2(bipy')](PF_6)_3$ salt (52.4mg, 49.3μmol) was dissolved in a minimum of acetone, and three molar equivalents of TBAB (47.7mg, 148μmol) were added. The resulting orange precipitate (35.2mg, 40.6μmol) was filtered out of solution by suction using a sintered glass frit.

1.2.5.3 Electrochemical analysis

The gold electrodes were prepared by first polishing with alumina, and then etching with a 1M sulfuric acid solution prepared by diluting concentrated H_2SO_4 with deionized water. The etching was done by placing the Ag/AgCl reference, gold working and platinum auxiliary electrodes in the sulfuric acid solution, and cycling the potential as described in Table 1.2.

A solution of the redox label complex was prepared by dissolving the entire $[Co(bipy)_2(bipy')]Br_3$ sample from the metathesis step in 25mL of the buffer solution. This solution was transferred to a plastic vial into which the working, Ag/AgCl reference and platinum electrodes were placed. The sample was degassed with flowing argon before measurements were taken. The parameters used for cyclic voltammetry and square wave voltammetry are outlined in Tables 1.2 and 1.3.

Table 1.2. Cyclic voltammetry parameters used in the electrochemical characterization of $[Co(bipy)_2(bipy')]Br_3$.

	1M H_2SO_4 potential sweep	**$[Co(bipy)_2(bipy')]Br_3$ characterization**
Initial potential	0V	+0.4V
High potential	+1.6V	+0.4V
Low potential	-0.3V	-0.8V
Final potential	0V	+0.4V
Scan Rate	0.1V/s	0.1V/s

Table 1.3. Square wave voltammetry parameters used in the electrochemical characterization of $[Co(bipy)_2(bipy')]Br_3$.

Initial E	+0.4V
Final E	-0.8V
Increments of E	0.004V
Amplitude	0.025V
Frequency	15Hz

1.2.6 Conjugation of bipy' and $[Co(bipy)_2(bipy')](PF_6)_3$ to DNA

1.2.6.1 Reagents

Refer to Sections 1.2.2 and 1.2.4.4 for synthesis of bipy' and $[Co(bipy)_2(bipy')](PF_6)_3$. N,N-dimethylformamide (≥ 99.5%) and 1-ethyl-3-(3-dimethylaminopropyl) carbodiimide hydrochloride were ordered from Fluka Analytical (through Sigma-Aldrich, Oakville, ON). N,N-diisopropylethylamine (99.5%), diethylamine (99.5%), (Benzotriazol-1-yloxy)tripyrrolidino-phosphonium hexafluorophosphate (98%) and N-hydroxysuccinimide (98%) were ordered from Sigma-Aldrich (Oakville, ON). Ammonium hydroxide (28%) was purchased from Anachemia Science (Mississauga, ON).

1.2.6.2 DNA synthesis

DNA synthesis was performed using a BioAutomation MerMade 6 synthesizer (Irving, TX). The four phosphoramidites (dA-CE, Ac-dC-CE, dT-CE and dG-CE) and the amino modifier (5'-DMS(O)MT-amino-modifier C6) used for the synthesis of the DNA and anhydrous acetonitrile were purchased from Glen Research (Sterling, VA). Activator, deblock, capping, and oxidizer solutions used in the DNA synthesis were purchased from BioAutomation (Irving, TX). The DNA synthesis was initiated on MerMade 1000Å CPG 1μmol support columns (Glen Research). The support columns contained glass beads to which the first nucleotide at the 3' end of the sequence was attached. After synthesis, the solid support columns were deblocked immediately or stored under argon in the freezer.

1.2.6.3 DNA sequences

The DNA sequence used for the conjugation experiments discussed in Section 1.3.7 was 5'-CCT ATG ATA GCA TCG GTC-3'. The 5'-end of the DNA strand was modified with an amino-C6 modifier, making the working DNA strand 5'-H_2N-$(CH_2)_6$-CCT ATG ATA GCA TCG GTC-3'.

The DNA sequence used for the conjugation experiments discussed in Section 1.3.8 was 5'-AGA TCC GAT C-3'. The 5'-end of the DNA strand was modified with an amino-C6 modifier, making the working DNA strand 5'-H_2N-$(CH_2)_6$-AGA TCC GAT C-3'.

1.2.6.4 Deblocking the support-bound DNA sequences

After synthesis, the synthesized DNA was still bound to the solid supports inside the columns. The amino modifier at the 5' of the DNA was protected with a 4,4'-dimethoxy-4"-methylsulfonyl-trityl group which had to be removed prior to conjugation. The procedure that was followed is described by Michael Beking in his Honour's thesis.[40]

The solid support columns were mounted in a BioAutomation cleaving chuck (see Figure 1.7), which uses suction to draw liquids through the columns. First, the columns were treated with 300μL of anhydrous acetonitrile, and then with 3x300μL of 10% solution of diethylamine (DEA) in anhydrous acetonitrile. Each aliquot of DEA solution was allowed to mix with the solid support for approximately one and a half minutes. After washing with 2x300μL of

anhydrous acetonitrile, the column was then treated with 2x200μL of deblock solution. After washing with 300μL of anhydrous acetonitrile, conjugation experiments were performed immediately.

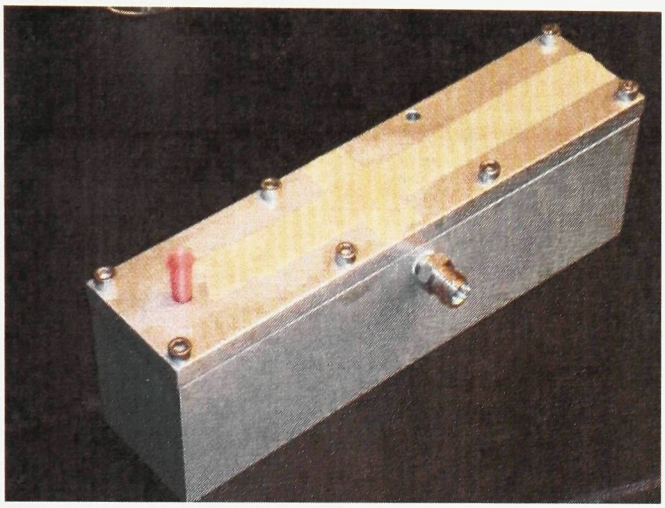

Figure 1.7. A BioAutomation cleaving chuck, with a 1μmol DNA synthesis column (red column) mounted in the top.

1.2.6.5 Activating bipy' and $[Co(bipy)_2(bipy')](PF_6)_3$ with PyBOP

Activation of the carboxylic acids was done before deblocking the amine group on the DNA (see Section 1.2.6.4) in order to perform the coupling reaction as quickly as possible after the anime group was deblocked.

For the experiments discussed in Section 1.3.7.2, a 1:1 molar equivalent of bipy' or $[Co(bipy)_2(bipy')](PF_6)_3$ to DNA (1μmol) was used. The samples were dissolved in a minimum of dimethylformamide (DMF) and mixed with diisopropylethylamine (6μmol) for approximately 10 minutes. To this solution, PyBOP (3μmol) dissolved in a minimum of DMF was added and the solution was shaken for thirty minutes. The total volume of the solution was kept below 300μL.

For the experiments discussed in Section 1.3.8, a 10:1 molar ratio of bipy' or $[Co(bipy)_2(bipy')](PF_6)_3$ to DNA (10μmol) was used. The amounts of DIPEA (60μmol) and PyBOP (30 μmol) were also increased. The solutions were mixed as described above.

1.2.6.6 Activating bipy' and $[Co(bipy)_2(bipy')](PF_6)_3$ with EDC and NHS

As described above, the activation of the carboxylic acids by EDC and NHS was done before deblocking the DNA so that the coupling reaction could be done immediately after the deblocking was completed.

A 110:1 molar excess of EDC to DNA (110μmol) was dissolved in 1mL of DMF under argon. To this solution, either bipy' or $[Co(bipy)_2(bipy')](PF_6)_3$ (10μmol) was added and the solution was mixed under argon for approximately 10 minutes. After the 10 minutes had passed, NHS (320μmol) was added to the solution and the solution was shaken under argon for approximately 30 minutes.

1.2.6.7 Conjugation of amino-modified DNA with activated ligands

After deblocking was completed, the glass beads were removed from the columns and collected in Eppendorf tubes. The activated bipy' or $[Co(bipy)_2(bipy')](PF_6)_3$ solution was then pipetted into the tubes, the solution was sealed under argon and the tube was covered with aluminum foil. The solution was shaken overnight.

After the shaking was complete, the tube was centrifuged at 13000rpm for 2 minutes so that the supernatant solution could be removed more easily. The beads were then washed with two 500μL aliquots of DMF, followed by centrifugation and removal of the supernatant. If it was necessary, any remaining DMF was evaporated *in vacuo*.

1.2.6.8 Cleavage and deprotection

To the glass beads, 1mL of 28% ammonium hydroxide solution was added and the solution was sealed under argon and left overnight at room temperature. The glass beads were removed from the ammonium hydroxide/DNA solution using a 0.45 μm nylon microfilterfuge (Rainin Instruments, Woburn, MA), and the filtrate solution was evaporated *in vacuo*, leaving only the DNA remaining in the Eppendorf tube.

1.2.7 Purification of the coupling reaction products by high performance liquid chromatography

Reverse-phase high performance liquid chromatography (HPLC) was performed on an Agilent 1200 Series HPLC, with a diode array detector. The column used was an Agilent Zorbax Extend-C18 column, with a particle size of 5μm and dimensions 9.4 x 250mm.

To prepare the mobile phase, acetonitrile (HPLC grade) was purchased from Fisher Scientific (Ottawa, ON), and ammonium acetate (NH_4OAc) was purchased from BDH (through VWR, Mississauga, ON). A 50mM NH_4OAc solution was prepared by dissolving 3.85g of NH_4OAc in 1L of deionized water. The solution was then filtered through a 0.22 μm cellulose acetate sterilizing filter and stored in polystyrene containers (Corning 431154 filter systems). The mobile phase used in the elution of the conjugated DNA samples is outlined below. The detector was set to monitor absorbance at 260nm and 290nm to detect the presence of oligonucleotides.

Table 1.4. Reverse-phase HPLC mobile phase program used to analyze conjugated DNA.

Time (min)	Fraction of acetonitrile (%)	Fraction of 50mM NH_4OAc (%)	Flow rate (mL/min)	Column temperature
0	5	95	2 mL/min	25°C
30	30	70	2 mL/min	25°C
40	100	0	2 mL/min	25°C

1.2.8 Purification of the coupling reaction products by polyacrylamide gel electrophoresis

1.2.8.1 Materials and apparatus

Urea (molecular biology grade), ammonium persulfate (electrophoresis grade), N,N,N',N'-tetramethylethylenediamine (>99%), acrylamide (DNA-sequencing grade), N,N'-methylenebisacrylamide, sodium dodecyl sulphate (BioUltraPure, electrophoresis grade) and tris(hydroxymethyl)aminomethane were ordered from BioShop Canada (Burlington, ON). Boric acid was purchased from BDH (through VWR, Mississauga, ON). Magnesium acetate tetrahydrate (minimum 98%) was purchased from Sigma-Alrich (Oakville, ON).

An acrylamide stock solution was prepared by dissolving 190g of acrylamide and 10g of *N,N'*-methylenebisacrylamide in 250mL of deionized water and heating the solution to 37°C.

The volume of the solution was then increased to 500mL with deionized water and filtered by gravity.

Polyacrylamide gel electrophoresis (PAGE) experiments were performed using a Hoefer 600X Chroma vertical electrophoresis system. The power supply used was a Fisher Scientific FB1000 Electrophoresis Power Supply. Gels were imaged using an Alpha Innotech AlphaImager® EC.

1.2.8.2 5x TRIS/Borate/EDTA (5x TBE) and elution buffer preparation

The 5x TBE buffer was prepared by dissolving TRIS (107.8g, 0.890 mol), boric acid (55.0g, 0.890mol) and EDTA (7.44g, 0.0200mol) in 2L of deionized water. The solution was then filtered by vacuum through a 0.22μm cellulose acetate sterilizing filter.

The buffer that was used to elute the DNA and conjugate molecules from the gel after PAGE had been performed comprised of 0.1% (w/v) sodium dodecyl sulphate (SDS), 0.5M ammonium acetate and 10mM magnesium acetate. The buffer solution was prepared by dissolving the components in deionized water and filtering through a 0.22μm cellulose acetate sterilizing filter prior to use.

1.2.8.3 PAGE gel preparation and electrophoresis

The gel solution was prepared by dissolving urea (31.5g) in 37.5mL of acrylamide stock solution and 15mL of 5x TBE buffer solution in a beaker. A magnetic stir bar was added to the solution and heated and stirred to 37°C until all of the solids had been dissolved. The solution was filtered while hot through a qualitative filter paper and left to cool.

While the buffer solution was cooling, a 10% solution of ammonium persulfate was prepared by dissolving 0.1g of ammonium persulfate in 1mL of deionized water. When the gel solution was cool, 450μL of the ammonium persulfate solution and 35μL of N,N,N',N'-tetramethylethylenediamine (TEMED) were added and the solution was swirled. Before the solution had a chance to polymerize, the gel was cast and left to set for approximately 30 minutes. After the gel had polymerized, it was run using 1x TBE buffer (prepared by diluting 400mL of the 5x TBE to 2L using deionized water) without samples for approximately 20 minutes at a constant current (25mA).

While the gel was "pre-running", the DNA samples were prepared by dissolving the DNA in a minimal amount of deionized water (at most, 15μL). The volume of water used to dissolve the DNA was matched with the same volume of formamide (Sigma-Aldrich) and heated to 55°C for five minutes.

After the gel was ready the samples were loaded and the gel was run at a constant current (25mA) for the determined amount of time. For specific run times, please see the Section 1.3.8.1. After the electrophoresis was complete, the gel was imaged and the desired bands were cut out of the gel. The bands were then cut further so that they would fit into an Eppendorf tube, and 1mL of the elution buffer was added to each tube. The tubes were then incubated (Labnet Mini Incubator) at 37°C overnight to elute the DNA and conjugates from the gel.

After elution was complete, the solid gel pieces were removed by filtration using Rainin Microfilterfuges (0.45μm nylon-66). The filtration was done by centrifuging the solution in the microfilterfuges at 13000 revolutions per minute (rpm) for 4 minutes. After filtration, the solution was evaporated off *in vacuo*.

1.2.8.4 Ethanol precipitation

In order to purify the DNA from gel impurities and salt from the elution buffer, ethanol precipitation was used. The DNA sample was dissolved in a minimum (no more than 100μL) of deionized water. Then, 1mL of cold anhydrous ethanol was added to the solution. If no precipitation was seen, 25μL of a 3M sodium chloride solution was added. The solution was then placed under dry ice for 30 minutes, and centrifuged at -9°C for 30 minutes using a Sorvall Legend 21R Microcentrifuge (Thermo Scientific) at 10000rpm. The solution was then decanted off and the precipitated DNA was dried *in vacuo*.

1.3 Results and Discussion

1.3.1 Justification of the redox-active label selection

The need for a redox-active label with a low redox potential in the proposed electrochemical sensor design arises from the requirement to reduce the creation of false positive signals that may occur in aptamer-based electrochemical sensing. These false positive signals are based on the observation that DNA was attracted to a gold electrode surface if the electrode's potential was over +450mV[33] or +400mV[41] against a silver wire electrode. If the redox-active label tethered to the 5'-end of the aptamer strand requires a more positive potential at the electrode in order to perform electron-transfer with the label, it may result in the attraction of the DNA to the electrode. If this were to occur, it would bring the label in contact with the electrode surface, creating an unwanted positive signal.

The results of previous studies using other redox labels may have suffered for these reasons. In a study by Xiao *et al.*,[21] methylene blue was covalently attached to the aptamer for thrombin. The binding of the aptamer to thrombin would create a distance between the label and the electrode, stopping the electron transfer and reducing the voltammetric signal (see Figure 1.4a in the Introduction). However, as can be seen by the voltammogram in the same figure, the signal in the presence of thrombin does not decrease the voltammetric response of the sensor significantly, which ideally should approach a current of zero in the presence of the target. One reason for this may be that methylene blue, although meant to be covalently bound to the DNA, can also bind externally to single-stranded DNA and also adsorb onto the gold surface.[42] The interaction of the methylene blue with points on the aptamer strand closer to the electrode would create a voltammetric response even in the absence of the target, and may be the reason for the large response in the presence of the analyte. In a study by Radi *et al.*,[22] the redox-active label covalently attached to DNA was ferrocene, which in aqueous solution had a redox potential of approximately 0.15-0.2V against a Ag/AgCl reference electrode (see Figure 1.4b in the Introduction). In the presence of the analyte, the redox label was brought closer to the electrode, and the electron transfer created a voltammetric signal. However, in the absence of the analyte, a response was still observed. This may have been due to the fact that ferrocene required a potential from the electrode that was high enough to attract the DNA to the surface, which would

have brought the label close enough to communicate with the electrode, creating a background signal.

The primary reason for developing a modified cobalt tris(bipyridyl) compound in this sensor design was that the reported redox potentials of $[Co(bipy)_3]^{3+}$ in aqueous solutions have been lower than +450mV against a silver wire. As a result, this compound may accommodate scanning electrochemical analysis at potentials that will not result in the attraction of the DNA for the electrode. When implemented, a detection method may be found that can almost entirely eliminate a voltammetric response in the absence of the target. Another reason for using the proposed label complex is that electrocatalysis could be used to create another electron transfer system in the sensor design, which would as a result reduce or oxidize the label complex back to its original state, enhancing the signal and increasing the sensitivity of the detector.

1.3.2 Synthesis of 4-(3-carboxypropyl)-4'-methyl-2,2'-bipyridine (bipy')

The synthesis of the modified bipyridyl ligand was performed as described by Della Ciana et al.,[37] with slight modifications that will be discussed. The series of reactions to synthesize bipy' is shown in Scheme 1.3.

Scheme 1.3. Overall synthesis of bipy' based on the method reported by Della Ciana et al.[37]

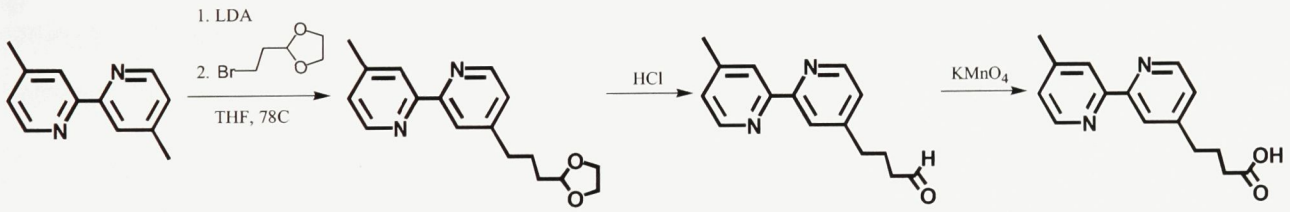

1.3.2.1 Synthesis of 4-[3-(1,3-dioxolan-2-yl)propyl]-4'-methyl-2,2'-bipyridine

In the paper on which this synthesis was based,[37] *n*-butyllithium was used to lithiate 4,4'-methyl-2,2'-bipyridine in order to deprotonate the methyl group(s) on the bipyridyl to allow the reaction with an electrophile, in this case 2-(2-bromoethyl)-1,3-dioxolane. Lithium diisopropylamide (LDA) was used in this experiment, since *n*-butyllithium is also a nucleophile. LDA is not known as a nucleophile, and as a result there would be less chance for side reactions.

The products of this reaction were the mono- and bis-dioxolane forms of the bipyridine. Also, unreacted bipyridine starting materials were present in the final solution. As a final product, a mono-acid product was desired, as a redox label with two carboxylic acid groups may form peptide bonds with more than one aptamer strand during conjugation. In order to purify mono-dioxolane from the product, a silica gel column was used. Prior to loading the column with the product, the column was pretreated with a 10% triethylamine (TEA) solution. In silica-based chromatography, compounds can be adsorbed to silanol groups present in the columns, which can lead to a much longer retention of the compounds.[43] This retention could increase the band width of the products as they move through the column, which would reduce the resolution between the compounds and reduce the yield of the desired pure product. TEA is a silanol blocker, and so pretreating the column with TEA before separation was done to maximize the yield of the mono-dioxolane product.

Elution from the column was monitored by silica thin layer chromatography (TLC) using a 30:70 solution of ethyl acetate to hexanes, which was the same solution used for elution from the column. The unreacted starting material eluted from the column first, followed by the mono-dioxolane product and then the bis-dioxolane product. From the TLC results, it was found that the starting material had a retention factor (R_f) value of 0.81, while the mono-dioxolane and bis-dioxolane products had R_f values of 0.57 and 0.24, respectively. TLC was used in order to determine which eluted fractions contained which product, and the combined fractions were then analyzed by nuclear magnetic resonance (NMR) spectroscopy to confirm the structure.

The NMR spectrum for the mono-dioxolane product is shown in Figure 1.8. The peak corresponding to H8 was used as a reference, and the integration of the peak corresponding to the methyl group (H3) was used to evaluate the products in the samples. In relation to peak 8, if the integration was higher than three, starting material was still present in the sample. If the integration was lower than three, there was some bis-dioxolane product present in the sample. An NMR spectrum of the bis-dioxolane product can be seen in Figure A-1.1 of the Appendix. In that spectrum, the integration of the peak corresponding to H3 was much lower in relation to H8, showing that there was more bis-dioxolane product in the sample than mono-dioxolane.

Figure 1.8. ^{1}H NMR spectrum (300 MHz, $CDCl_3$) and peak assignments of 4-[3-(1,3-dioxolan-2-yl)propyl]-4'-methyl-2,2'-bipyridine.

The yield of pure mono-dioxolane product isolated by silica gel chromatography was 44%, which was lower than the reported yield.[37] In another synthesis trial, a silica gel column was used that was not pre-treated with the 10% TEA solution. The column separation provided a pure mono-dioxolane product, however the yield of this process was 37%. These results indicated that the TEA pre-treatment could increase the amount of isolated mono-dioxolane product.

Pure, isolated dioxolane product was preferred for use in the next step in the reaction series, however a mixture of the mono-dioxolane product with unreacted starting material was preferred to a mixture of the mono-and bis-dioxolane products, since the starting material would not be affected by the next reaction, and could possibly be removed more easily than a bis-aldehyde product.

1.3.2.2 Synthesis of 4-(3-formylpropyl)-4'-methyl-2,2'-bipyridine

The next step in the reaction series was the acid hydrolysis of the mono-dioxolane reagent to form an aldehyde product. Upon the adjustment to a basic pH level, the colour of the

solution changed to pink. This pink colour was determined to be the result of the formation of an iron tris(bipyridyl) compound, since iron was likely present in the sodium carbonate and sodium bicarbonate used to make the solution basic. Coordination of the bipyridyl ligand to iron may have created complications in the extraction of the bipyridyl at the end of the reaction, so the iron contamination had to be removed. This was done by saturating the sodium carbonate or sodium bicarbonate solutions with ethylenediaminetetraacetic acid (EDTA). EDTA coordinates to iron as a hexadentate ligand, and is preferred to the coordination of the bipyridine. When EDTA was included in the solution, the pink colour was much less intense, indicating that the iron tris(bipyridyl) complex was less abundant. For fear of losing desired product, a comparison of the extractions performed from an iron-contaminated sample and an iron-neutralized sample was not performed, but it may provide insight as to whether the EDTA step was necessary.

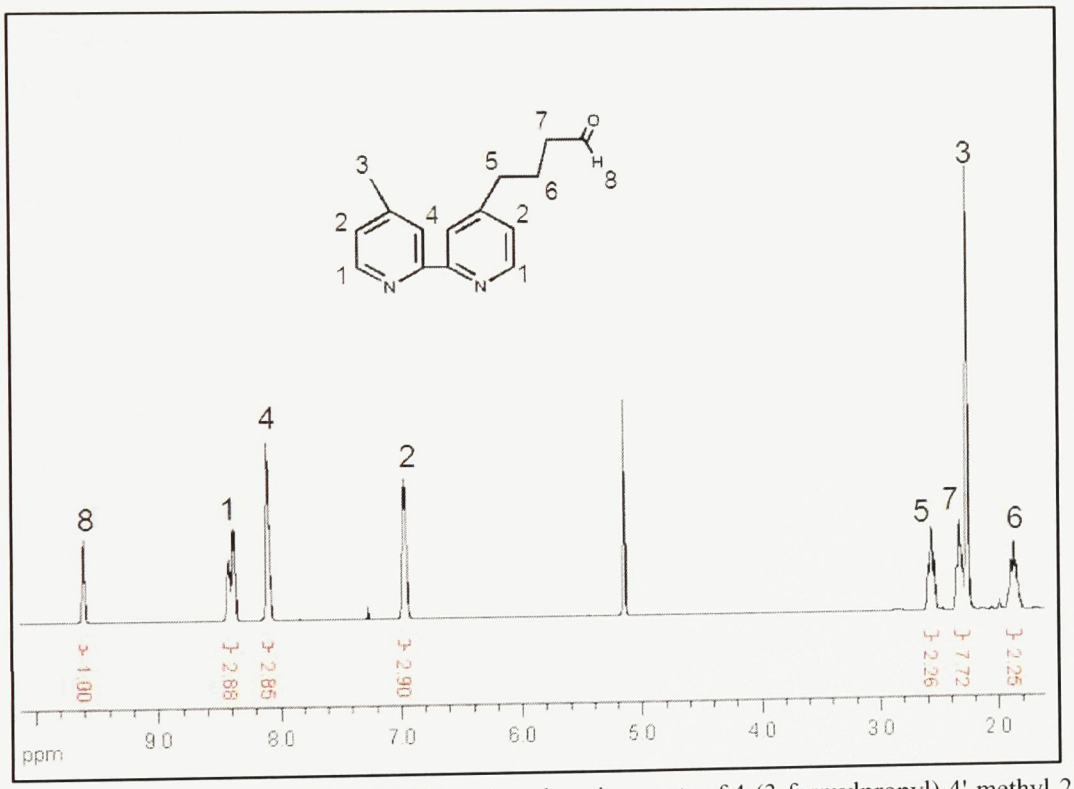

Figure 1.9. ^{1}H NMR spectrum (300 MHz, $CDCl_3$) and peak assignments of 4-(3-formylpropyl)-4'-methyl-2,2'-bipyridine.

The yield of this reaction step was 95%, which is comparable to the reported yield.[37] The structure of the aldehyde product was confirmed by proton NMR, shown in Figure 1.9. The high integrations of the aromatic and methyl peaks with respect to the peak corresponding to the aldehyde proton (H8) indicated that there was still dimethyl starting product in the sample. The

peak at approximately 5.2ppm corresponded to dichloromethane in the deuterated chloroform ($CDCl_3$) NMR solvent, showing that the product was not completely dry when the NMR was performed.

1.3.2.3 Synthesis of 4-(3-carboxypropyl)-4'-methyl-2,2'-bipyridine

The last step in the synthesis of bipy' was the oxidation of the aldehyde reagent to the carboxylic acid product using potassium permanganate. To monitor the progress of the reaction, samples of the reaction solution were taken and analyzed by TLC using a 1:1 ethyl acetate to toluene solution as the eluent. When no migration of the spot from the reaction was observed, the reaction was deemed to be complete.

Prior to the liquid/liquid extraction of the desired carboxylic acid, the pH of the solution was made basic and a liquid/liquid extraction was done in order to remove some of the impurities in the solution. A proton NMR spectrum was taken of this extract and is included in the Appendix. The spectrum showed the presence of primarily the 4,4'-dimethyl-2,2'-bipyridyl starting material.

The pH of the aqueous solution was then lowered to 4.8. This pH level was found to be crucial to the recovery of the desired ligand. Extraction at a higher pH extracted only the original starting material, as described above. Extraction at a lower pH resulted in the extraction of little to no ligand. Yields for extractions attempted at pH levels below 4.8 were around 1%.

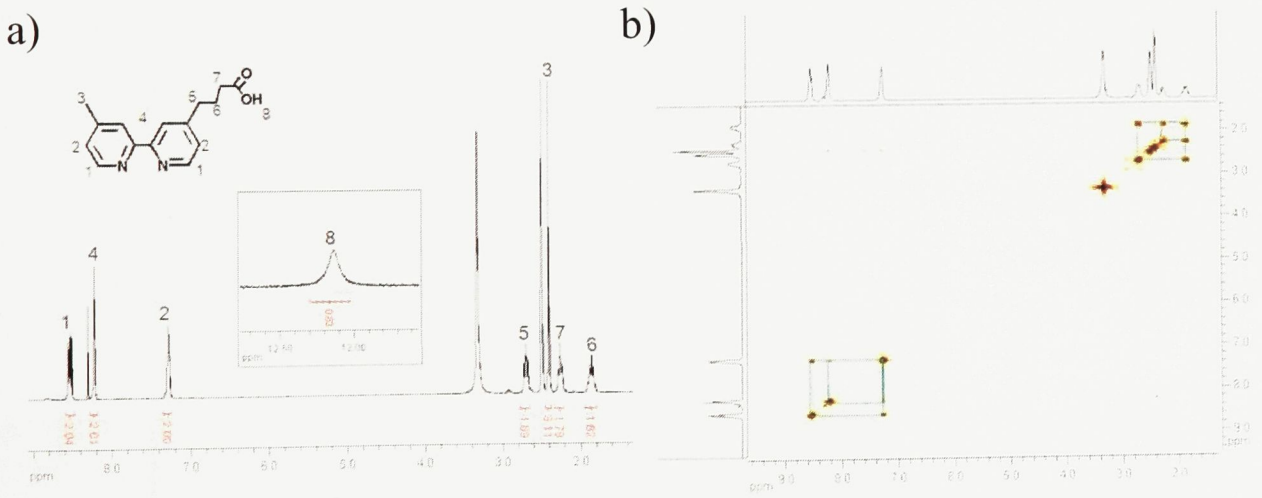

Figure 1.10. ^{1}H NMR spectrum (300 MHz, DMSO-d_6) and peak assignments of 4-(3-carboxypropyl)-4'-methyl-2,2'-bipyridine. a) One-dimensional ^{1}H NMR of the aromatic and aliphatic regions, with the carboxylic acid peak inset. b) The two-dimensional COSY spectrum of the aromatic and aliphatic regions.

Recrystallization of the product extracted at a pH of 4.8 resulted in the formation of beige crystals, with a yield of 49%. This yield was similar to the yield of 52% that had previously been reported.[37] This resulted in an overall yield of 17%, which gave 2.32g of product. The step that reduced the yield was the first reaction, most likely due to the need for column chromatography. The product was characterized by one- and two-dimensional proton NMR, as well as electrospray-ionization mass spectrometry. The NMR results are presented in Figure 1.10.

The integration of the proton NMR showed six protons in the aromatic region and 9 protons in the aliphatic region, which was consistent with the structure of the desired product. From the two-dimensional proton (COSY) spectrum, it was seen that there was a weak correlation between the peaks at 7.3ppm and 8.2ppm, which would only be observed for the protons at H2. As a result, identification of the aromatic proton peaks was made possible. In the aliphatic region, the COSY spectrum also made the assignment of the proton peaks possible. The COSY spectrum showed a strong correlation of the triplets at 2.7ppm and 2.3ppm to the pentet at 1.8ppm, which would only occur if the peaks at 1.8ppm corresponded to H6. The protons at H5 are at a higher chemical shift than the protons at H7 due to deshielding effects from the pyridine ring. A weak correlation was also observed between the methyl peak at 2.4ppm and the peaks corresponding to H2 and H4, which was also consistent with the structure of the desired product.

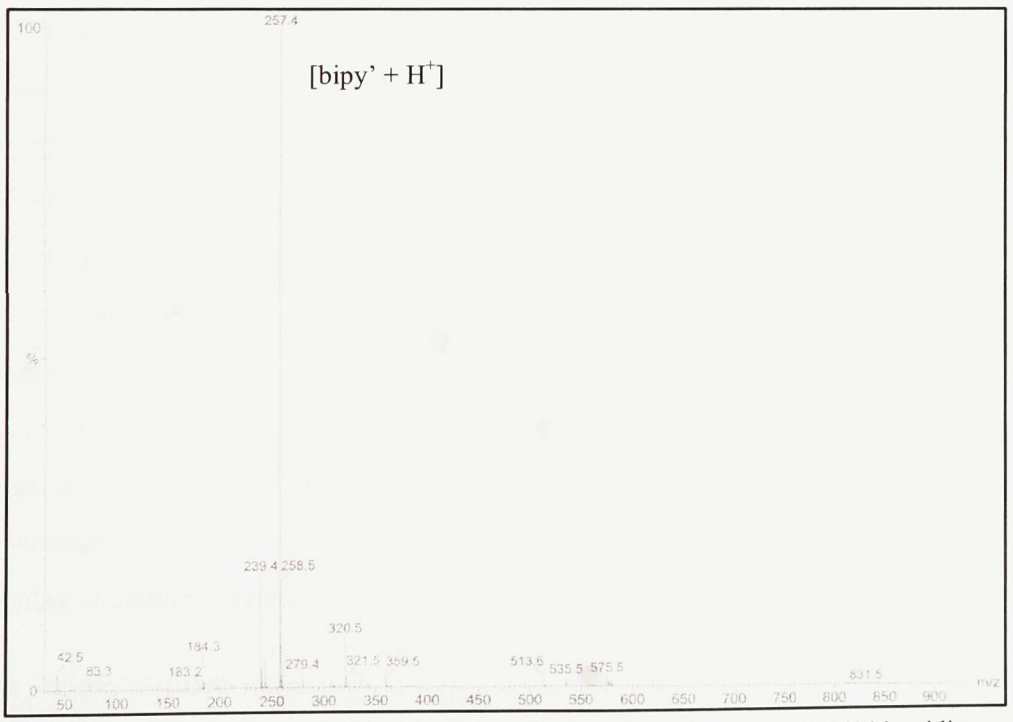

Figure 1.11. Electrospray mass spectrum of 4-(3-carboxyl)-4'-methyl-2,2'-bipyridine.

Electrospray mass spectrometry was also used to characterize the product, and is shown in Figure 1.11. The peak at a mass/charge ratio of 257.4 corresponds to the mass of [bipy' + H^+]$^+$, providing even more evidence that the desired bipy' product had been synthesized. The small peak at 513.6 may have corresponded to the dimerization of bipy'.

1.3.2.4 Stability of the ligand in acidic solution

When it was discovered that the bipy' ligand could not be extracted at a pH lower than 4.8, a solution that had been abandoned from an earlier extraction was adjusted to a pH of 4.8 using a concentrated sodium carbonate solution. The solution had been sitting in the fume hood for approximately 5 months, and when measured, its pH was 0.6. After adjusting fhe pH of the solution, liquid/liquid extraction was performed with 5x100mL of dichloromethane. The product was recrystallized from dichloromethane using hexanes, and beige crystals were collected. Proton NMR showed that the recrystallized product had the peaks corresponding to the desired product (refer to Figure A-1.3 in the Appendix). The yield of the product was 47%, although from the integration of the NMR spectrum it appeared as though some of the dimethyl starting material was still present in the sample.

1.3.3 Synthesis of $[Co(bipy)_2Cl_2]Cl$

The synthesis of $[Co(bipy)_2Cl_2]Cl$ from cobalt(II) chloride and 2,2'-bipyridyl was performed as previously described.[38] The product of the reaction was typically a purple powder, although crystals were previously isolated and analyzed.[39] The analysis of these crystals showed a symmetrical structure, and was reflected in the proton NMR spectrum. Proton NMR spectra of the powder product, shown in Figure 1.12, was much more complex, although the structure of the desired bis(bipyridyl) cobalt product was deduced. The proton NMR showed an integration of 16 aromatic protons, which was consistent with the desired product. The shifts of these peaks also corresponded to previously reported proton shifts.[44] With help from the two-dimensional proton spectrum (refer to Figure A-1.4 in the Appendix), it was found that eight protons correlated strongly with one other proton, while eight protons correlated strongly to two protons, which was also consistent with the desired structure.

Due to the similar nature of the bipyridyl ligands bound to the cobalt centre, it was difficult to assign protons for each NMR peak. However, the two protons with chemical shifts

above 9ppm most likely belonged to the protons closest to the chlorine atoms, as they would be the most deshielded. This knowledge, with help from the two-dimensional correlation spectrum, allowed a rough assignment of the rest of the protons in the NMR spectrum. All of the protons that belonged to the same pyridine rings as the identified protons also had higher shifts, which indicated that they were also deshielded by the chlorine atoms. The lowest shifts in the spectrum (between 7 and 7.5ppm) belonged to the two adjacent protons on the inside of the pyridine rings positioned away from the chlorine atoms. The outer two protons on those pyridine rings showed higher shifts, likely due to deshielding effects from the nitrogen atoms.

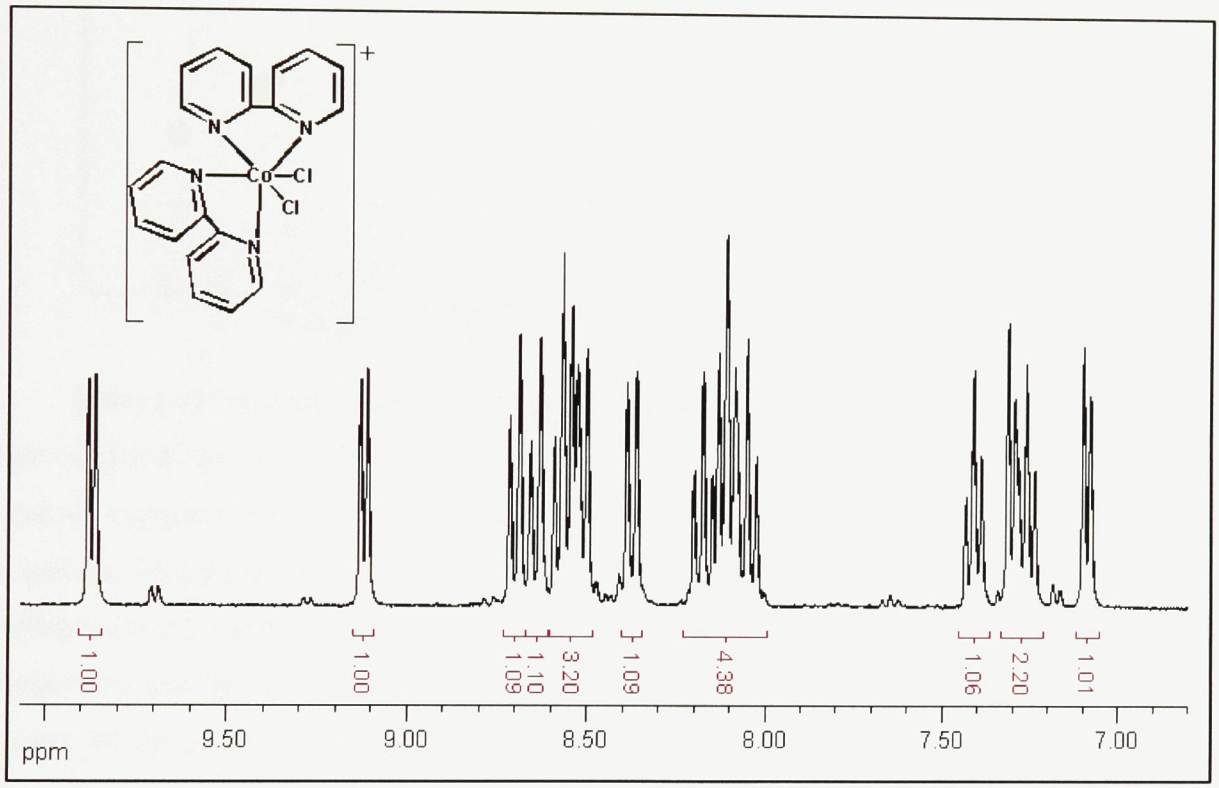

Figure 1.12. ^{1}H NMR spectrum (300 MHz, D_2O) of $[Co(bipy)_2Cl_2]Cl$.

Electrospray mass spectrometry was also used in order to confirm the presence of the desired bis(bipyridyl) product. The peak at a mass/charge ratio of 441.3 corresponded to $[Co(bipy)_2Cl_2]^+$, and the peaks at 406.3 and 371.3 correspond to the compound after losing one and two chlorine atoms, respectively. The peak at 291.2 could not be identified. The mass/charge ratio of $[Co(bipy)Cl_2]^+$ would be 286.0, but its relationship to the peak at 291.2 is unclear.

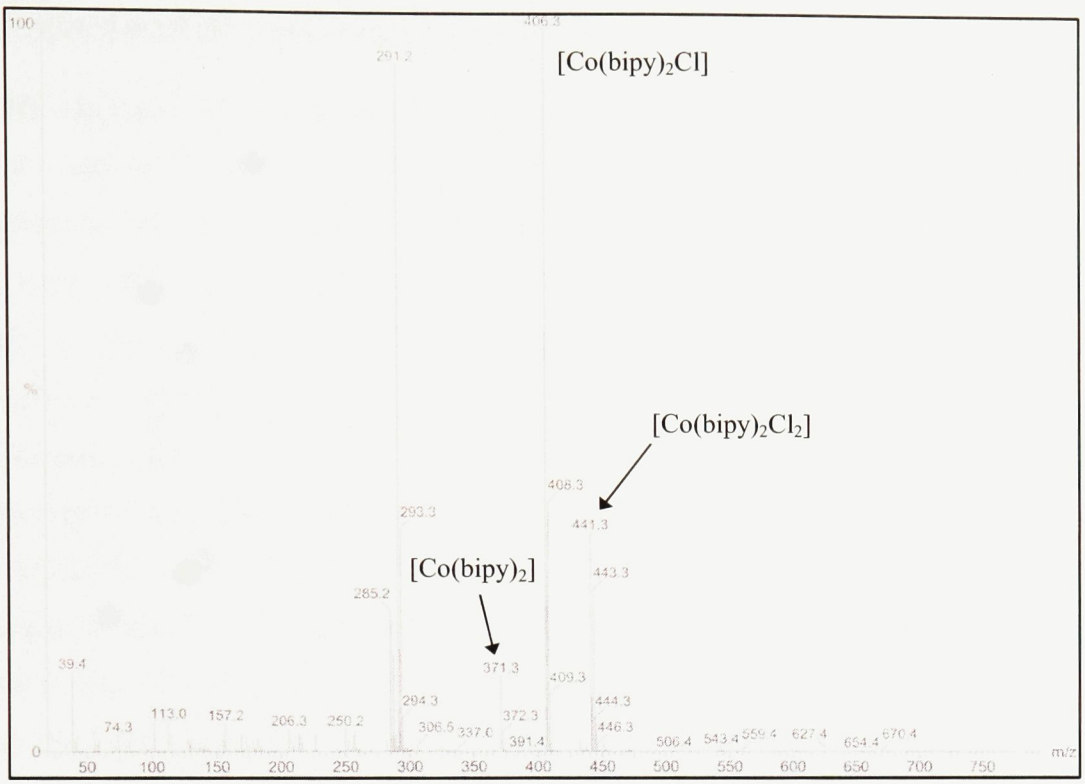

Figure 1.13. Electrospray mass spectrum of $[Co(bipy)_2Cl_2]Cl$.

During the synthesis of the bis(bipyridyl) precursor, a small amount of green product was observed along with the major purple product. When a metal spatula was used to transfer the precursor complex, the green product would also form if the precursor was left in contact with the spatula. This finding was not uncommon, and has been reported in published literature. In the $[Co(bipy)_2Cl_2]Cl$ synthesis paper by Vlček,[38] a green product along with the desired purple product was precipitated. This was at first believed to be the *trans*-isomer of the bis(bipyridyl) product, while the *cis*-isomer was the purple precipitate. However, it was shown that what was believed to be the *trans*-isomer was actually a mixture of cobalt tris(bipyridyl) mixed with $CoCl_4^{2-}$ and Cl^- ions.[45]

It should be noted that the method used to synthesize $[Co(bipy)_2Cl_2]Cl$ can be potentially dangerous. During one experiment, after the addition of the chlorine gas a release of pressure occurred, in which one of the rubber stopcocks came off the roundbottom flask, releasing chlorine gas into the surrounding area. Such an incident was also reported in a letter to the editor of the Chemistry & Industry journal, in which the reaction vessel was shattered and the chlorine gas was ignited.[46] Extreme care should be taken when performing this reaction.

1.3.4 Preparation of $[Co(bipy)_2(bipy')]Br_3$ in ethanol

The synthesis of the redox label complex was first attempted in a similar fashion to a published method.[47] This method involved the addition of silver triflate after the $[Co(bipy)_2Cl_2]Cl$ had been dissolved, in order to precipitate out the chlorine ligands from the bis(bipyridyl) precursor in the form of silver chloride (AgCl). This would allow bipy' to coordinate to the cobalt in the vacancies left by the removal of the chlorine. During the experiments, the addition of the silver triflate resulted in the immediate precipitation of a white solid. This precipitation occurred so quickly that it was unsure if the solid was precipitated AgCl or undissolved silver triflate. For this reason, after the precipitate had been removed it was left in a vial exposed to light. Silver chloride is known to photodecompose into elemental silver and chlorine gas, resulting in a purple colour. Over time, the colour of the precipitate went from bright white to a dull purple-gray colour, confirming that the precipitate was silver chloride. An infra-red spectrum of the precipitate also produced no peaks, confirming the absence of silver triflate, whose bonds produce several absorbance bands in the IR spectrum.

The vacancies created by the removal of the chlorine atoms would then allow the coordination of the bipy' ligand to cobalt by simply adding the two in solution, allowing enough time for the proper dative covalent bonds to form. The precipitation of the label complex from ethanol was done by adding tetrabutylammonium bromide (TBAB) to form a bromide salt that was insoluble in ethanol. A three-fold molar equivalent of TBAB was added, since the label complex (as well as cobalt tris(bipyridine)) had oxidation states of three, which would require the formation of a tribromide salt. In many cases, the addition of a three-fold molar equivalent of TBAB did not result in any precipitation from the solution, since the complex was still soluble. A combination of evaporating the solvent *in vacuo* and refrigerating the sample helped to precipitate a solid out of the solution. The addition of more TBAB to the solution also helped in the formation of the precipitate, although this created problems with impurities that will be described below.

After filtering the precipitate, the solid was analyzed by proton NMR, shown in Figure 1.14a. The desired label complex would integrate to a total of 22 aromatic protons, and 9 aliphatic protons. The integration of the NMR in Figure 1.14a resulted in six aromatic protons and the desired 9 aliphatic protons. The integration of this spectrum indicated that the primary

constituent of the precipitate was the bipy' ligand, which had six aromatic protons and nine aliphatic protons. One explanation for this result is that the majority of the product from the reaction was unreacted bipy' starting material. This is a logical explanation, although there were some reasons that this might not be the case, one being that the product was easily dissolved in deuterated water before the NMR analysis was done. During the synthesis of bipy', the NMR analyses of the ligand were conducted in deuterated chloroform or dimethyl sulfoxide since bipy' was sparingly soluble in D_2O. As well, comparing the proton NMR of the product to the one for the bipy' ligand (Figure 1.10), there is a slight change in the chemical shift of one of the aromatic proton environments. In the bipy' spectrum, the shift representing two protons at 8.2ppm was shifted to approximately 7.5ppm in the proton spectrum of the reaction product. This may have been the result of the formation of an iron tris(bipy') complex, if there was an iron contamination while the reaction was taking place. In Figure 1.14a, a small peak at 8.2ppm was observed, which may have been from unreacted bipy' ligand, since it is a match with the shift in the bipy' spectrum. However, chemical shifts of protons vary depending on the solvent used, and the change in chemical shift may also have been simply the result of using a different solvent to perform the NMR analysis. An effort to eliminate the possibility of iron contamination will be discussed in a later section.

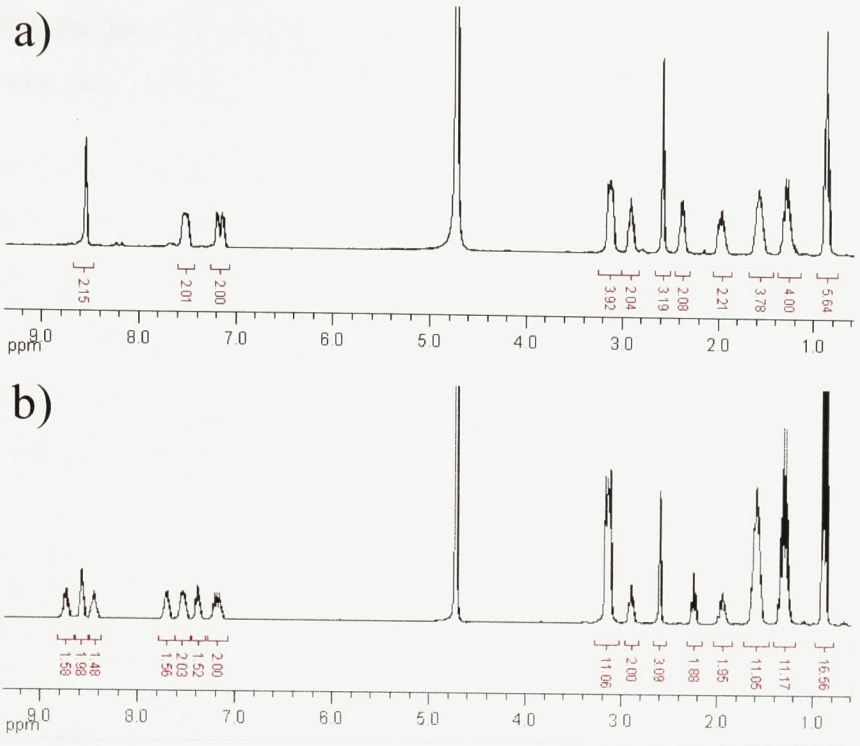

Figure 1.14. ^1H NMR spectra (300MHz, D_2O) of $[Co(bipy)_2(bipy')]Br_3$. a) The reaction crude product. b) Combined Sephadex G-50 fractions of the second separated band.

The proton NMR also showed a considerable contamination of tetrabutylammonium cation (TBA^+) in the sample. TBA^+ in proton NMR would produce three peaks for the $-CH_2-$ chain proton environments, and one $-CH_3$ group. The CH_2 peaks appeared at 3.2ppm, 1.6ppm and 1.3ppm in the spectrum, and the CH_3 peak appeared at 0.9ppm. It was feared that this

contamination would interfere with the general characterization of the label complex, so attempts were made to remove this contamination with Sephadex.

Electrospray mass spectrometry characterization of the reaction products also showed a compound with the mass of TBA^+ in the sample, with a peak at a mass/charge ratio of 242.5 being the predominant peak in all samples submitted. This impurity made the visualization of the other components of the sample more difficult, as their relative intensity was so low that possibly important minor peaks were less distinguishable from the baseline noise. No peaks that pertained to the desired $[Co(bipy)_2(bipy')]Br_3$ compound could be deduced from the other peaks present in the MS results.

1.3.4.1 Sepahadex purification of the bromide salt product

Sephadex is an ion exchange separation column material, and it was used in this experiment to try to isolate the desired $[Co(bipy)_2(bipy')]^{3+}$ product after the ethanol reactions. In the reaction product, the major impurities were unreacted bipy' ligand and tetrabutylammonium, from the precipitation of the bromide salt. Since the cobalt tris(bipyridyl) complex would have a positive charge of either 2+ or 3+ due to the oxidation state of the cobalt center, it would migrate at a different speed from the bipy' ligand or tetrabutylammonium in cation exchange.

Sephadex G-50 was used to make small columns, and a 0.1M NaCl solution was used as the eluent in order to slow the elution of the product components and create the proper separation between them. During the elution of the products, two bands formed. The first band was typically bright orange to red in colour, and eluted out of the column using the 0.1M NaCl solution as the eluent. The second band was orange in colour, and a stronger eluent of 3M NaCl was used to elute it from the column. After both bands were collected they were analyzed by proton NMR. The proton spectrum of the first band was similar to the overall spectrum depicted in Figure 1.14a, with an integration of six aromatic protons and nine aliphatic protons, and the presence of tetrabutylammonium. The proton NMR spectrum of the second band is shown in Figure 1.14b. In this spectrum, four more peaks appeared in the aromatic region of the spectrum. These protons corresponded to the protons on the unmodified bipyridine ligands. The shifts of these protons were divided into four distinct environments, which was different from the multiple environments shown in the proton NMR of the $[Co(bipy)_2Cl_2]Cl$ precursor (see Figure

1.12). There were also changes in the shifts of the proton environments, which may have been the result of the dissociation of the chlorines and the formation of a bond with a bipy' ligand. These four environments, when their integrations were observed separately, were equal in magnitude, which was consistent with the protons of the bipyridine ligands. However, when compared to the rest of the spectrum, their integration was less than it would be in the characterization of a pure redox label compound.

In $[Co(bipy)_2(bipy')]Br_3$, the unmodified bipyridine protons should give a total integration of 16 protons, or 4 protons in each environment. In the spectrum however, the relative integration was much less, at approximately 1.5 at each environment. This observation may have been the result of many situations. One possible source of the peaks may have been unreacted cobalt bis(bipyridyl) precursor. This was a possibility, since the NMR spectrum also suggested the presence of unreacted bipy' ligand in the sample. If this was the case, however, the chemical shifts of the protons seen in the spectrum should be like the ones seen in Figure 1.12, but they were quite different in the observed spectrum. Also, the colour of the product was distinctly orange, and no purple was seen in the product. Another possible reason for the difference was the formation of a mono(bipyridyl) cobalt complex, with the other four ligands being either chlorine or water. The last possibility is that the peaks were from the formation of the desired redox label, but it was much less abundant than the bipy'-based impurity. However, since a proton NMR of a pure redox label product was not done in D_2O, this possibility was not tested.

Despite the success in the separation of two compounds using Sephadex G-50, the presence of TBA^+ was seen in all of the fractions that were collected. This was most likely because Sephadex G-50 is not an ion exchange medium. The G-series of Sephadex is the matrix that can be modified with charged functional groups, which can then be used for ion exchange. When this was discovered (the bottle in the lab had been simply labelled 'Sephadex'), a separation column was prepared with Sephadex C-25, which is designed for cation exchange chromatography.

The separation using the new Sephadex proceeded similarly to the previous separation, with the first band being eluted with 0.1M NaCl and the second band with 3M NaCl. The proton NMR spectra of the bands were also identical to the spectra seen from the first separation, with

three aromatic environments seen in the first band and seven observed in the second band. However, in these spectra no peaks for TBA^+ were observed. From this experiment, it was concluded that the C-series of Sephadex was able to remove the TBA^+ contamination from the reaction product, but isolation of a pure redox label was still a problem.

1.3.5 Synthesis of $[Co(bipy)_2(bipy')](PF_6)_3$ in water

Once it was determined that purification and crystallization of the redox label complex was difficult to perform from ethanol, the decision was made to attempt the synthesis in water, using a bulkier counter-ion (ammonium hexafluorophosphate, $(PF_6)^-$) to perhaps facilitate the formation of crystals from the aqueous solution. The procedure was based on an aqueous synthesis of $[Co(bipy)_3]Cl_3$ that was previously published.[48] The method of complex precipitation was modified from the published method, and EDTA was added to the water, in order to eliminate the possibility of contamination from iron.

The addition of the EDTA may have resulted in unwanted reactions, however, and it was believed that the solution's colour change to green observed before the usual orange colour was due to the formation of a Co(EDTA) complex.[39] However, this may not have been the problem, since the colours of Co^{2+}(EDTA) and Co^{3+}(EDTA) have been reported as pink and blue-violet, respectively.[49]

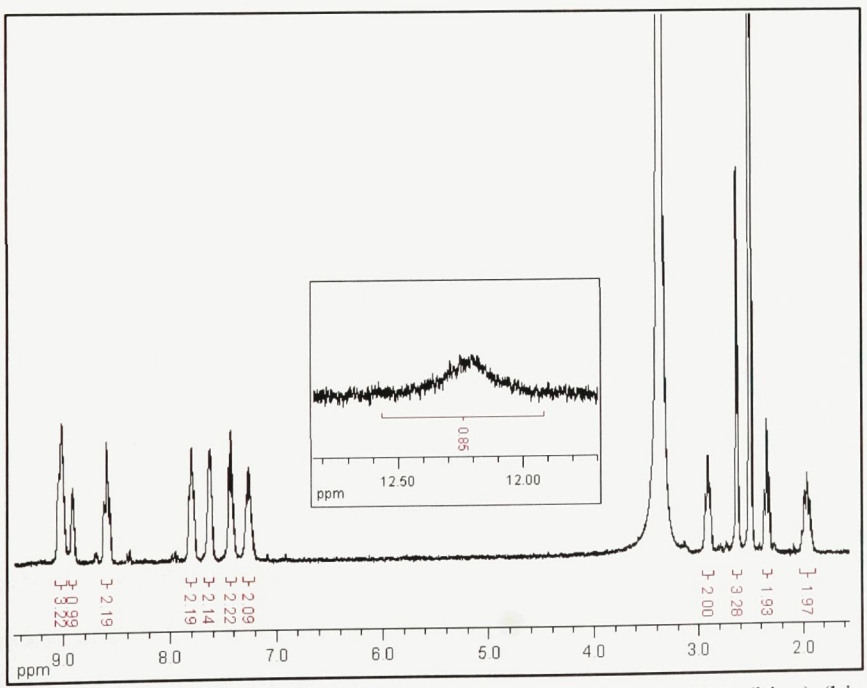

Figure 1.15. ^1H NMR (300MHz, DMSO-d_6) of the initial precipitation of $[Co(bipy)_2(bipy')](PF_6)_3$.

Immediately upon the addition of ammonium hexafluorophosphate to the reaction solution, an orange solid precipitated. This solid was filtered from the solution and analyzed by proton NMR, as illustrated in Figure 1.15. The integration of the spectrum showed that there was a relatively low integration for the aromatic protons compared to the aliphatic protons, with the aromatic protons integrating to 14 when 22 protons were expected.

One encouraging observation from the proton NMR was the fact that the peaks that correlated to the unmodified bipyridines occupied only four proton environments, whereas in the proton spectrum for the $[Co(bipy)_2Cl_2]Cl$ precursor there were many more proton environments observed. This change may have been due to the replacement of the chlorine atoms on the cobalt center by bipy', which may have created a better symmetry of the environments for the unmodified bipyridine ligands. Since the NMR spectra were taken in different solvents, however, this could not be a definitive answer.

Using a two-dimensional proton NMR spectrum, the aromatic proton peaks at 8.9ppm, 7.6ppm and 7.2ppm were assigned to the bipy' ligand, and the peaks at 9.0ppm, 8.6ppm, 7.8ppm and 7.4ppm were assigned to the unmodified bipyridine ligands of the complex. Upon closer inspection, a shoulder on the higher-shift side on the peak at 9.0ppm also correlated to the bipy' ligand, bringing its integration to six protons, which was expected. The integration of the unmodified bipyridine ligands, however, was half of what it should have been. These results indicated that there was an excess of unreacted bipy' ligand present in the solid product.

Attempts were made to try to recrystallize and purify the desired complex from the reaction product, and are described elsewhere.[39] These attempts involved recrystallizing the label complex from acetone or acetonitrile using hexanes, or removing the impurity with solvents such as warm water or isopropanol. However, no crystallization was achieved, and all resulting proton NMR spectra showed spectra similar to the original, indicating that the purification was not successful.

1.3.5.1 Formation of $[Co(bipy)_2(bipy')](PF_6)_3$ crystals

After filtering out the original product synthesized in the previous section, the filtrate was collected in a beaker and left to evaporate in the fume hood. After some time, it was discovered that a small amount of orange crystals had formed in the bottom of the beaker. These crystals

were filtered out of the solution and analyzed by proton NMR, as is shown in Figure 1.16. The integration of the peaks in the spectrum revealed 22 protons in the aromatic region and 7 in the aliphatic region. One of the $-CH_2-$ peaks was masked by an acetone peak at approximately 2.1ppm and as a result was difficult to integrate, so it was concluded that all nine aliphatic protons were accounted for in the spectrum.

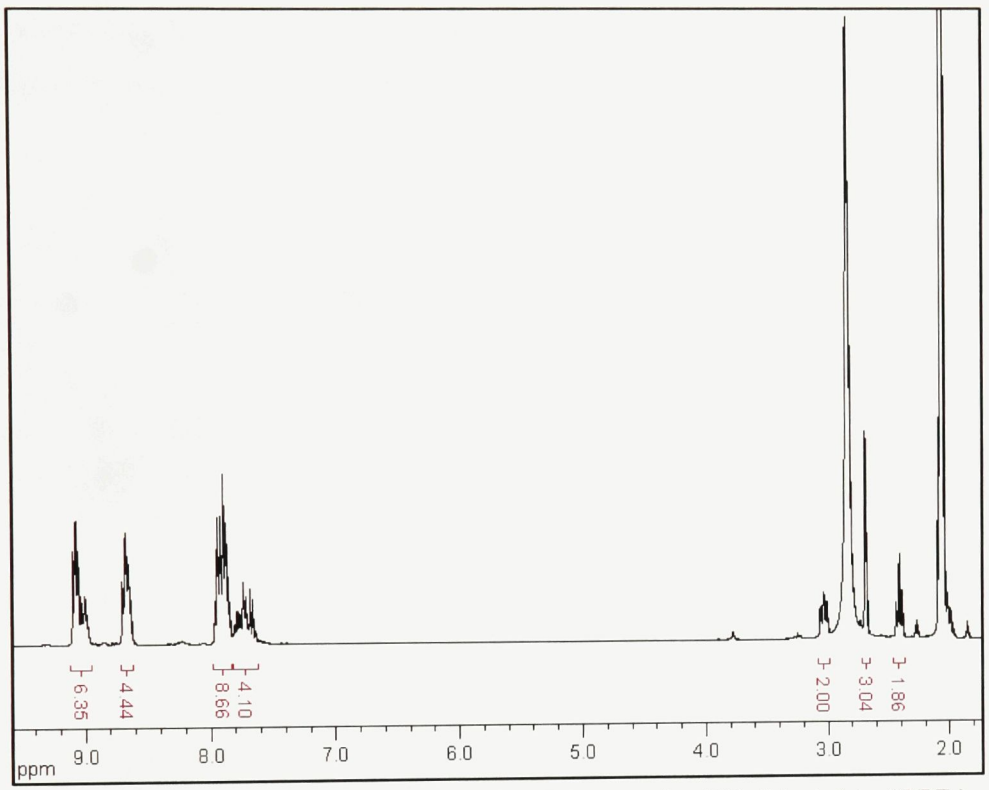

Figure 1.16. ^1H NMR (300MHz, acetone-d_6) of the crystals of $[Co(bipy)_2(bipy')](PF_6)_3$.

The COSY spectrum, shown in Figure 1.17, was used to assign the chemical shifts to specific areas of the bipy and bipy' ligands. In the aliphatic region of the spectrum (Figure 1.17a), the correlations of the peaks matched those of the bipy' ligand, with the peaks at 2.0, 2.4 and 3.0ppm corresponding to the $-CH_2-$ groups in the butyl chain, and the peak at 2.7ppm corresponding to the 4'-methyl protons. The aromatic region (Figure 1.17b) was more complicated, but strong correlations were found between the peaks at 9.1, 8.6 and 7.9ppm, indicating that these protons were from the unmodified bipyridine ligands, since the proton arrangement of bipy' did not allow the strong correlation between three protons (see Figure 1.17d). On closer inspection, the multiplet peak at 7.9ppm could be divided into two halves, one half at 7.9ppm and the other half at 7.8ppm. These two halves also appeared to correlate to each other, although this observation was rendered more difficult by the resolution of the spectrum.

From these observations, the protons on the unmodified bipyridine ligand were assigned, as shown in Figure 1.17c.

To help assign the protons in the bipy' ligand, a weak correlation was observed between the peaks at 9.0ppm and 7.7ppm. The large multiplet at 7.7ppm, like with the peak at 7.9ppm mentioned previously, could be divided into two halves, with one peak at 7.7ppm and the other at 7.6ppm. From the COSY spectrum, it appeared as though the two halves interacted with each other. These observations allowed the assignment of the protons, seen in Figure 1.17d.

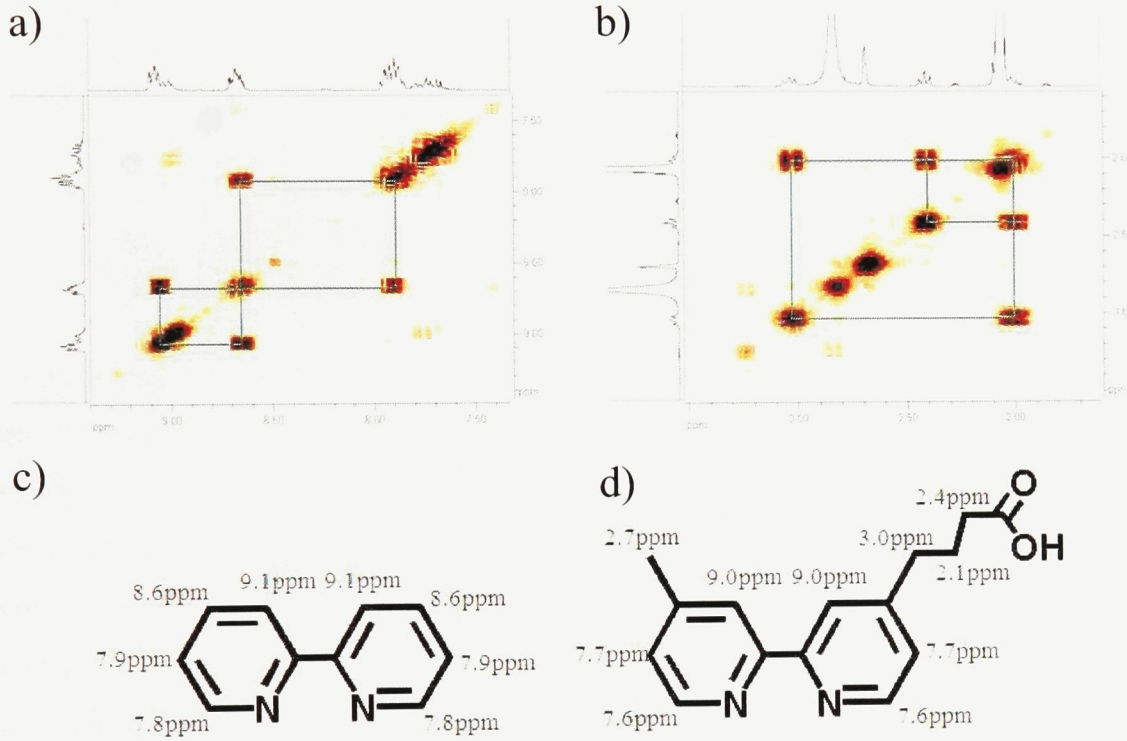

Figure 1.17. ^{1}H NMR COSY (300MHz, acetone-d_6) spectra of the $[Co(bipy)_2(bipy')](PF_6)_3$ crystals. a) Correlations (green boxes) of the chemical shifts in the aromatic region. b) Correlations (green boxes) of the chemical shifts in the aliphatic region. The determined chemical shifts of protons in the c) 2,2'-bipyridine and the d) 4-(3-carboxypropyl)-4'-methyl-2,2'-bipyridine ligands are also shown.

A sample of the $[Co(bipy)_2(bipy')](PF_6)_3$ crystals was also sent for electrospray mass spectrometry characterization. The resulting spectrum is shown in Figure 1.18. From the spectrum, some peaks were found to correspond to possible mass/charge values from the label complex ($M = [Co(bipy)_2(bipy')]^{3+} = 627.6$ g mol^{-1}). The peak at 917.2 matched the mass of $[M + 2(PF_6)^-]^+$, while the peak at 470.3 matched the mass/charge ratio of $[M + 2(PF_6)^- + Na^+]^{2+}$, suggesting that the crystals were the desired label complex.

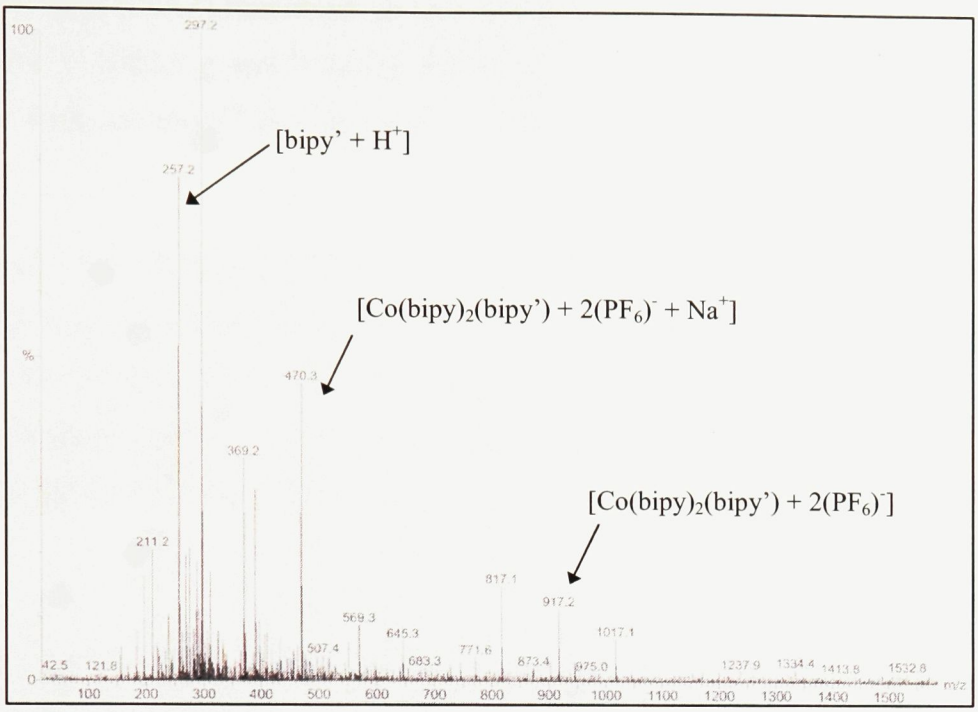

Figure 1.18. Electrospray ionization mass spectrum of $[Co(bipy)_2(bipy')](PF_6)_3$.

Other peaks that may have corresponded to parts of the redox label complex, but not the complex as a whole, were also identified. The peak at 257.2 matched the m/z of $[bipy' + H^+]^+$, which was possible since one of the nitrogens in the bipy' ligand may have become protonated during the MS analysis process. The peak is fairly abundant in the spectrum, and there are a few possible reasons for this. One possibility is that the peak comes from unreacted bipy' in the crystal product, which may be supported by the peak at 369.2 that is close to the mass of $Co(bipy)_2$ (MW = 371.3g mol^{-1}). There was also a peak at 371.2 (not shown in the figure), which was even closer to the precursor's molecular mass, although this assignment does not account for the charge on the cobalt center. Another possible reason for the abundance of the peak was the degradation of the label complex during the MS analysis. The most abundant peak in the spectrum was the peak at 297.2, which may have been due to the bipy' ligand being derivatized during a reaction or during the MS process, or even to an impurity in the sample. However, a compound that corresponds to the peak has not yet been identified.

The pronounced peaks on either side of the peak at 917.2 may also be atributed to two separate processes. The peak at 817.1 may correspond to $[M + (PF_6)^-]^{2+}$ that was derivatized with an ethoxide group, which may have been possible since the MS sample was prepared by dissolving the label complex crystals in ethanol. The peak at 1017.1 may have been the result of

the carboxylic acid (COO^-) functional group coming off the bipy' ligand from the $[M + 3(PF_6)^-]$ complex (MW = 1062.5 g mol^{-1}) during MS analysis. It has been reported in studies that the CO_2^- groups from aromatic[50] and aliphatic[51] compounds can be lost during mass spectrometric analysis.

In a UV-Vis spectroscopy study of $[Co(bipy)_3]^{2+}$,[52] an absorption maximum was found at 454nm, with a molar extinction coefficient of $50M^{-1}$ cm^{-1}. This absorbance was found to correspond to a d→d transition in the cobalt center. This value was used for comparison to a basic UV-Vis study performed on the $[Co(bipy)_2(bipy')](PF_6)_3$ crystals that were synthesized. According to the Beer-Lambert law, the absorbance (A) of an analyte is based on the equation

$$A = \varepsilon cl,$$

where ε and c are the molar absorption coefficient and concentration of the analyte, respectively, and l is the path length of the light through the sample. By analyzing the absorbance of a known concentration of $[Co(bipy)_2(bipy')](PF_6)_3$ in acetonitrile, an absorbance maximum was found at 453nm. The molar extinction coefficient at this band maximum was calculated to be $47M^{-1}$ cm^{-1}, very close to the value observed for cobalt tris(bipyridine). This was a desirable outcome since it was hoped that the modifications of bipy' did not highly effect the characteristics of the cobalt center. Although repeated analyses would give a reproducible outcome as to the absorption activity of the complex, this study provided evidence that the replacement of 2,2'-bipyridine with bipy' did not have a great effect on the cobalt center.

The studies performed on the crystals provided evidence that the desired complex had been synthesized by the reaction, and that the effect of the modified ligand may not have altered the characteristics of the cobalt tris(bipyridyl) complex in an undesirable way. However, this product was formed by chance, and its yield was very low (a few milligrams), and at the present a method to synthesize a greater amount of the label complex is a challenge.

1.3.5.2 Effect of reaction temperature on the synthesis of $[Co(bipy)_2(bipy')](PF_6)_3$

The observations made during the successful (although low-yield) synthesis of $[Co(bipy)_2(bipy')](PF_6)_3$ suggested that the redox label could be synthesized in an aqueous medium with no added reagents. As a result, the synthesis was retried at 0°C in the hopes that any unwanted side-reactions would be less favoured. Also, the EDTA was omitted in this reaction, to further simplify the conditions and to avoid possible unwanted coordination with cobalt. Upon the addition of NH_4PF_6, a precipitate formed. The precipitate was orange in colour, and proton NMR analysis showed integration values similar to those shown in Figure 1.15. As with the previous experiment, after the precipitate was filtered out, the filtrate was left to evaporate in the fume hood. As some of the filtrate evaporated, flakes began to form in the solution. The flakes were removed from the solution by centrifuging the filtrate and decanting the supernatant. The flakes were then dried in a desiccator.

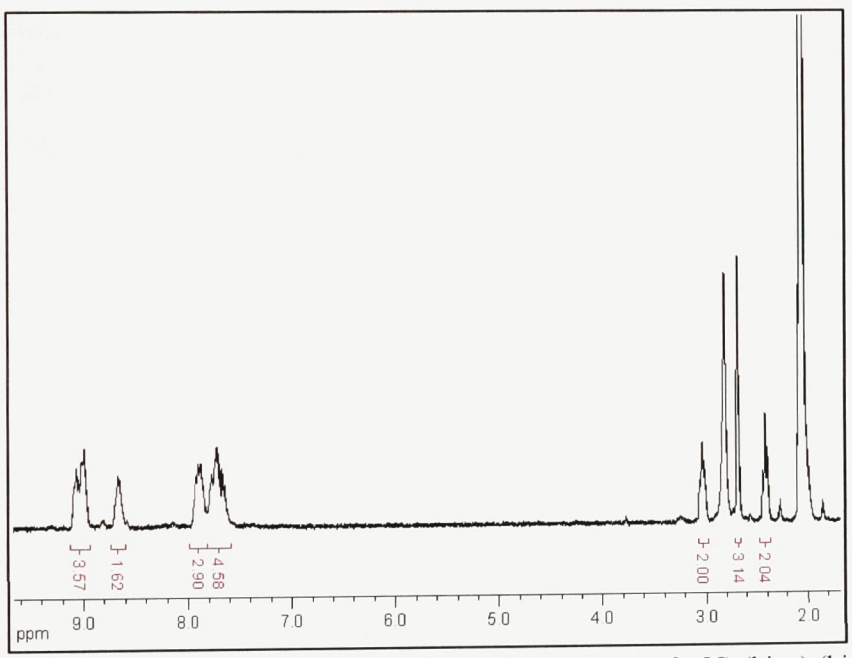

Figure 1.19. ^1H NMR (300MHz, acetone-d_6) of flakes formed in the filtrate of a $[Co(bipy)_2(bipy')](PF_6)_3$ reaction product. The reaction is described in Section 1.3.5.2.

The proton NMR spectrum of the flakes is shown in Figure 1.19. It was hoped that the flakes would provide the same spectrum as the crystals, shown in Figure 1.16. From the analysis of the spectrum, it was found that the integration of the aromatic region of the spectrum was too low relative to the integration of the aliphatic region. The peaks that pertained to the protons of the bipy' ligand also had a higher integration relative to the unmodified bipyridine protons,

signifying that there was an excess of unreacted bipy'. Allowing more of the filtrate to evaporate did not result in the formation of any crystals. The characterization of the flakes showed that the desired product had been synthesized, but impurities were also a considerable product.

The reaction was also performed at 75°C, as was described elsewhere.[39] Similar results to those above were observed, and purification attempts were again unsuccessful in attaining the desired integration in the proton NMR.

Finding a reaction method that could be used to synthesize the pure redox label on a large scale was not accomplished in this study, although the isolation and characterization of crystals allowed proton NMR and mass spectrometry characteristics to be identified. It was determined that the desired $[Co(bipy)_2(bipy')](PF_6)_3$ complex was being synthesized, but impurities made definitive characterization spectra difficult to attain. Synthesis of the label complex was also attempted at controlled pH levels. NMR characterization of the product of a synthesis performed at a pH of 4.8 showed a greater presence of the desired label complex; however, more study is necessary in order to confirm these results. Conjugation experiments were performed with the reaction products of the aqueous syntheses, on the expectation that the probe complex would be able to couple with DNA even in the presence of minor impurities.

1.3.6 Electrochemical characterization of $[Co(bipy)_2(bipy')]Br_3$

To assess the suitability of the redox label for its implementation in the electrochemical sensor design, its redox potential was measured using cyclic voltammetry and square wave voltammetry. The desired result was a redox potential that was similar to the $[Co(bipy)_3]^{3+}$ / $[Co(bipy)_3]^{2+}$ potential that was previously reported, or one that was more suitable than that of ferrocene.

For simplicity, an aqueous electrolyte buffer was prepared to use in the experiments. This required the salt metathesis of $[Co(bipy)_2(bipy')](PF_6)_3$ to $[Co(bipy)_2(bipy')]Br_3$ in order to make the complex water-soluble. After the metathesis product was filtered and dried, the yield of the metathesis was approximately 80%.

The cyclic voltammetry experiments showed a reversible reduction/oxidation process that had a redox potential of $E_{1/2} = 0.022 \pm 0.007$mV against a Ag/AgCl reference electrode. Square wave voltammetry analysis resulted in a redox potential of 0.016mV against a Ag/AgCl electrode. This value showed an improvement over ferrocene, which had a reported redox potential of 0.16V against a Ag/AgCl electrode in a 0.1M solution of NaF.[53]

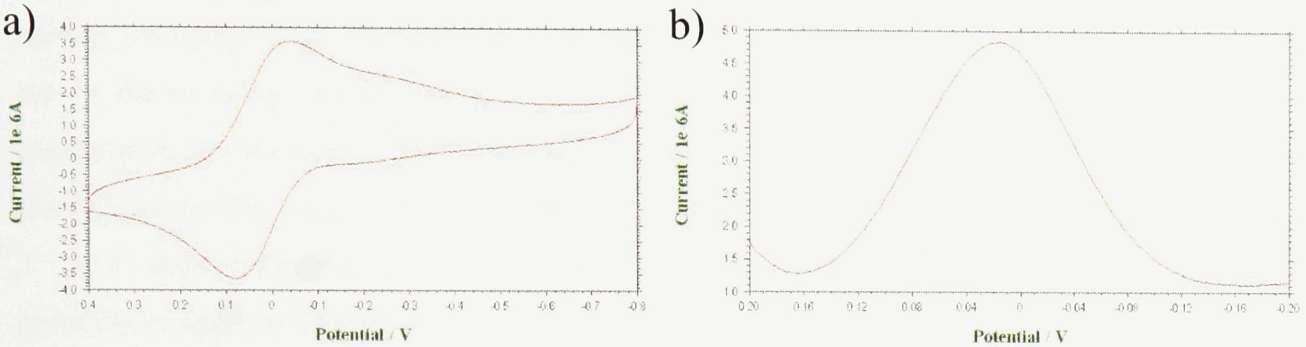

Figure 1.20. a) Cyclic voltammetry and b) square wave voltammetry electrochemical analyses of $[Co(bipy)_2(bipy')](PF_6)_3$, using Ag/AgCl as a reference electrode. The electrolyte buffer used was 25mM TRIS-HCl (pH 8.2) and 100mM NaCl.

The electrochemical study of $[Co(bipy)_2(bipy')]^{3+}$ conducted in this report was preliminary, so more analysis, particularly study of a purer sample, would be needed in order to fully assess the suitability of the label complex for the sensor design. However, the preliminary results showed promise that use of this complex in the sensor would be able to improve the signal-to-noise ratio.

Another advantage of implementing a cobalt tris(bipyridyl) complex in this sensor is the potential for electrocatalysis, in which a compound can be added in solution that will also transfer electrons with the redox-active label. This coupling of the electrode reduction and oxidation of the compound with a chemical reaction to convert the species back to its original state can create an electrocatalytic cycle, which would enhance the observed electrochemical signal.[54] Although electrocatalysis was not tested with the modified cobalt tris(bipyridyl) label produced in this project, further study may show that electrocatalysis can add signal enhancement to an advantageous redox potential to produce a highly desirable redox-active label for use in an electrochemical sensor.

1.3.7 Redox label and bipy' conjugation to DNA

Covalent binding of the redox label to the DNA aptamer is preferred to ionic or non-specific binding for a number of reasons. First, a 1:1 ratio of label-to-DNA is guaranteed after covalent attachment and purification, which will allow more reproducibility in the results, as labelling by non-specific interactions adds a degree of uncertainty to the preparation of the sensor. Secondly, since aptamers have specific structural responses to their targets, redox labels can be placed on specifically designated spots on the aptamer, in order to ensure that no signal is observed in the absence of the target, and an efficient electron transfer pathway is established in the presence of the target. The attachment of the label on the aptamer does not have to be on the 5'- or 3'-ends of the aptamer; amine-modified bases can be purchased to attach the label at any point in the aptamer strand.[55]

1.3.7.1 Two different approaches to conjugation of the label to DNA

In an attempt to find the most efficient mode of label-DNA attachment, two different methods were used. The first method was tethering the redox label itself to DNA. Since mass spectrometry results had shown that the desired label was in the product, it would have been available to attach to DNA in a peptide coupling reaction. Although purification of the probe molecule was not easily done from the product, attaching the probe to DNA would facilitate another way of isolating and characterizing it. The other approach was to tether bipy' to the aptamer first, and reacting the bipy'-DNA conjugate with $[Co(bipy)_2Cl_2]Cl$ in order to have the fully-formed label bound to DNA as a result.

Each of these approaches provides their own advantages and disadvantages. Advantages of tethering the redox label as a whole to DNA are that it could be done in one step, and since the DNA is bound to a solid support, the reaction solution could be removed and the support-bound DNA could be washed easily and without the need for extensive cleanup. On the other hand, the need of a harsh base to cleave the DNA from the support may result in the degradation of the compound. This problem could be solved by coupling the bipy' ligand to the DNA first, then cleaving the bipy'-DNA conjugate from the solid support and reacting it with $[Co(bipy)_2Cl_2]Cl$. The bipy'-DNA bond may be more stable to the ammonium hydroxide needed to cleave the DNA off the glass beads than the bonds of the bipyridine ligands, and allow the formation of the

label complex after the conjugate is cleaved. However, this requires finding the correct conditions for the reaction of the $[Co(bipy)_2Cl_2]Cl$ precursor, and isolating the desired conjugate from the unreacted reagents would require extra purification steps.

Scheme 1.4. Redox label-DNA conjugation by tethering bipy' first and reacting with $[Co(bipy)_2Cl_2]Cl$.

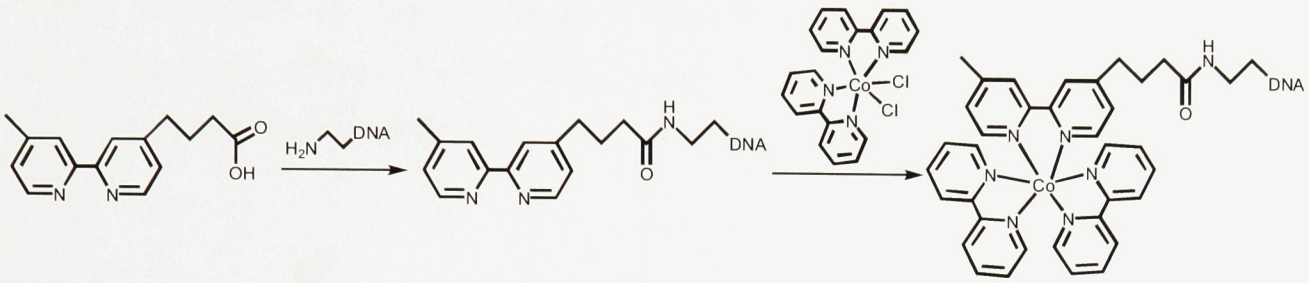

Scheme 1.5. Redox label-DNA conjugation by tethering $[Co(bipy)_2(bipy')](PF_6)_3$ to DNA.

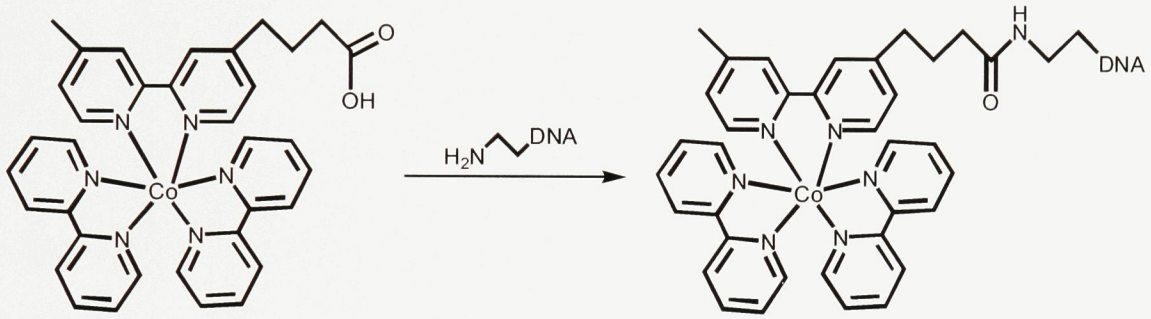

1.3.7.2 Early conjugation attempts using PyBOP

The first attempts at DNA conjugation with bipy' and the redox label were done using the PyBOP method described in Section 1.2.6.2. The DNA sequence used was a random 18-base DNA sequence. With the C6 amino-modifier, the overall DNA sequence was 5'-H_2N-$(CH_2)_6$-CCT ATG ATA GCA TCG GTC-3'. The molecular weight of the H_2N-DNA was calculated with Oligocalc[56] as being 5653.6 g mol^{-1}, and the molecular weights of the bipy' and label-DNA conjugates were calculated as being 5891.9 and 6263.2 g mol^{-1}, respectively.

The validity of the conjugation was verified by mass spectrometry. The phosphate groups that comprise a part of the DNA backbone are negatively charged; the charge of a DNA strand could vary from single- to multiple-charged strands, with strands of the same sequence having different charges. This results in a complex mass spectrum. However, by running a convoluted mass spectrum through a computer program that assigns charges to specific MS peaks, a

deconvoluted spectrum can be determined. An example of a convoluted and deconvoluted mass spectrum is shown in Figure 1.21. The label that each peak in the spectrum are given is in the format (mass/charge – charge – peak ID). As an example from Figure 1.21a, the reading (821.7 -9 A) means that the peak at a mass/charge ratio of 821.7 corresponds to a DNA strand 'A' with a charge of -9. This peak is derived from the same DNA strand as the peaks at 739.3, 924.3 and 1056.5. When all of these peaks are multiplied by their charges, they give the large peak in the deconvoluted mass spectrum at 7403.3. Thus the full molecular weight of the DNA strand can be determined using mass spectrometry.

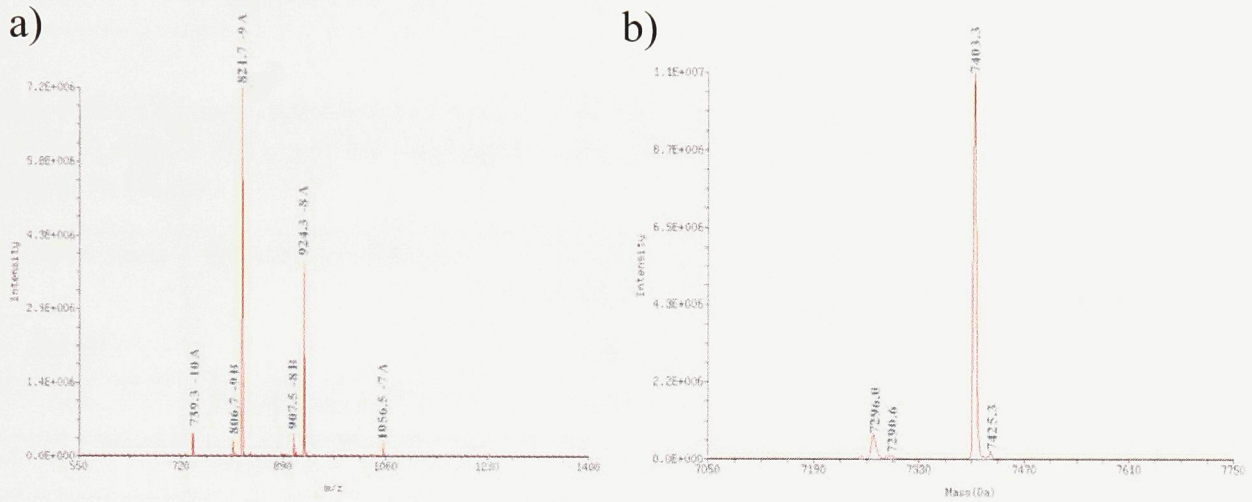

Figure 1.21. Examples of a) convoluted and b) deconvoluted mass spectra of a nucleic acid strand. The calculated mass of the nucleic acid was 7402.8 g mol^{-1}.

The first series of conjugation attempts was performed using the same procedure as has been reported for the coupling of a bipy'-modified ruthenium complex to DNA in the literature (see Section 1.2.6.2).[57] After cleaving the DNA from the beads, high-performance liquid chromatography (HPLC) was used to attempt to separate the bipy'- and probe-conjugated DNA from the unconjugated DNA. As well as monitoring at 260nm, which is the maximum absorbance wavelength of DNA, the spectrum was also monitored at 290nm. This was done in order to track the DNA signal more accurately at higher concentrations, since for concentrated samples the diode array detector would quickly saturate at 260nm, but the value at 290nm would be relatively smaller since it is shifted from the maximum absorbance. The MS results for the first bipy' and label conjugation attempts are listed in Tables 1.5a and 1.5b. From the tables, it was observed that the bipy'-DNA conjugation attempt using PyBOP was unsuccessful, while the

results for the label-DNA conjugation attempts showed peaks that indicated that bipy' had been tethered to the DNA.

Table 1.5a. ESI mass spectrometry results of HPLC fractions collected from a bipy'-DNA conjugation experiment using PyBOP, the procedure of which is outlined in Section 1.2.6.2.

Retention time (min)	Spectrum reference	Calculated molecular weight ($g\ mol^{-1}$)	Observed molecular weight ($g\ mol^{-1}$)	Desired conjugate observed
9	Appendix, A-1.5.1	5891.9	5696.6	None
11	Appendix, A-1.5.2	5891.9	5758.2	None

Table 1.5b. ESI mass spectrometry results of HPLC fractions collected from a $[Co(bipy)_2(bipy)'](PF_6)_3$-DNA conjugation experiment using PyBOP, the procedure of which is outlined in Section 1.2.6.2.

Retention time (min)	Spectrum reference	Calculated molecular weight ($g\ mol^{-1}$)	Observed molecular weight ($g\ mol^{-1}$)	Desired conjugate observed
5.5	Appendix, A-1.6.1	6263.2	5696.3	None
11	Appendix, A-1.6.2	6263.2	5696.3	None
17	Appendix, A-1.6.3	6263.2	5892.4	bipy'-DNA

The most encouraging result from this trial is the MS result from the fraction collected at 17 minutes from the HPLC separation of the redox label-DNA conjugation attempt (Table 1.5b). The mass spectrum showed a peak at 5892.4, which is in agreement with the molecular weight of the bipy'-DNA conjugate. The bipy'-DNA peak was also the most abundant peak in the mass spectrum by far, indicating the HPLC had succeeded in isolating the bipy'-DNA conjugate. However, upon closer inspection of the other two HPLC fractions collected from the same run, peaks corresponding to a bipy'-DNA were also seen, with the 5.5 minute fraction showing a peak at 5891.7 and the spectrum of the 9 minute fraction displaying a peak at 5893.2. Despite the evidence that the fraction at 17 minutes appeared to demonstrate that HPLC could isolate bipy'-conjugated DNA, the conjugate was still eluting throughout the entire HPLC program. These results indicated either that isolation could not be performed by HPLC, or possibly that only the isolation of the bipy'-DNA could not be done successfully (see Section 1.3.7.5).

Subsequent bipy'-DNA conjugation attempts using PyBOP for coupling also failed, which may indicate that PyBOP was not a useful reagent for bipy'-DNA conjugation experiments. However, if this were true, a bipy'-DNA conjugate should not have been seen in the MS results from the label-DNA conjugation attempts. Subsequent label-DNA tests sent for MS evaluation also showed peaks for the bipy'-DNA conjugate and no label-DNA conjugate. One possible explanation for these observations is that the presence of the redox label (or one of the impurities) in solution facilitated the tethering of bipy' to DNA, a factor which was not present in a solution of bipy'. A more likely scenario is that the label-DNA conjugate was being formed by the conjugation reaction, but degradation in either the isolation of the DNA conjugate after the reaction, or in the mass spectrometer, resulted in a formed peak for bipy'-DNA.

1.3.7.3 bipy'-DNA conjugation with EDC and NHS

Since it was believed that PyBOP was not functional in the conjugation reactions of the bipy' ligand and DNA, alternative reagents were used in an attempt to complete the conjugation successfully. In the conjugation attempts with EDC and NHS, a different reaction scheme was followed, and a much higher molar ratio (11:1 of bipy' to DNA) was used. Also, since EDC did not readily dissolve in dimethylformamide, a larger volume had to be used. This was not desirable, since the larger reaction volume may have led to a lower efficiency of the conjugation reaction, but the problem may have been corrected by the molar excess of the reagents.

The mass spectrometry results from a crude bipy'-DNA sample (the sample was not purified after cleaving and deprotection by HPLC or any other method), are shown in Figure 1.22. The expected molecular weight of the bipy'-DNA conjugate was 5891.9, as mentioned above (Section 1.3.7.2). In the deconvoluted mass spectrum, a peak at 5890.6 was observed, which indicated the presence of a bipy'-DNA conjugate in the sample.

This result showed that a bipy'-DNA conjugate could be produced when EDC and NHS were used to form the intermediate. No peak corresponding to the molecular weight of the amino-modified DNA (5653.6 g mol^{-1}) was observed, although a peak at 5695.7 was fairly predominant. This peak was observed in most mass spectrometry results, and may have corresponded to the amino-modified DNA and an acetyl group, although the source of the acetyl group was uncertain. Some of the other peaks in the spectrum may have been the results of

impurities, or sodium (MW = 23 g mol^{-1}) or potassium (MW = 39 g mol^{-1}) ions binding to the negatively-charged phosphate functional groups in the backbone of the DNA.

Since the presence of bipy'-DNA in the sample had been determined, the sample was then used for the next step, which was reacting the bipy'-DNA conjugate with the cobalt bis(bipyridyl) chloride precursor.

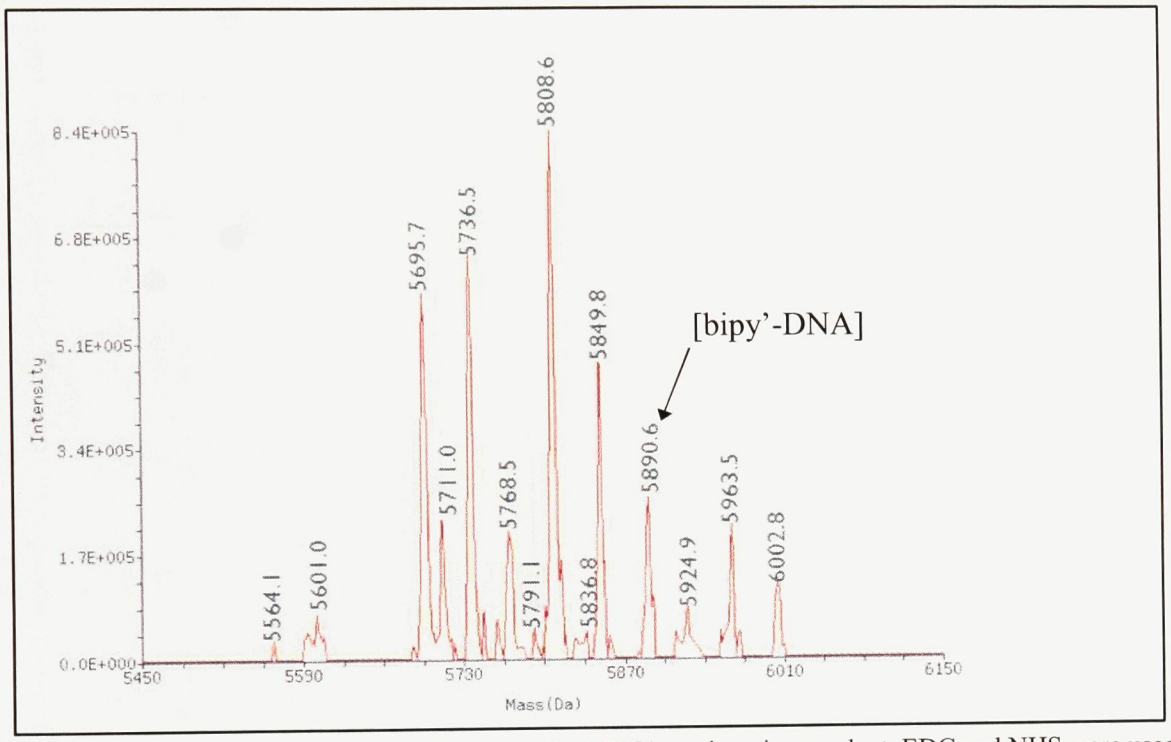

Figure 1.22. Deconvoluted mass spectrum of a crude bipy'-DNA conjugation product. EDC and NHS were used in the peptide coupling reaction.

1.3.7.4 Reacting bipy'-DNA with $[Co(bipy)_2Cl_2]Cl$

It was believed, since the redox label was synthesized by simply dissolving the cobalt bis(bipyridyl) precursor in water and then adding the bipy' ligand, that dissolving the bis(bipyridyl) precursor in aqueous solution and then adding the bipy'-DNA conjugate might result in the formation of the completed redox label tethered to the DNA strand. If the mass spectrum of this product showed a peak corresponding to a label-DNA conjugate, it could be concluded that the conditions under which the conjugation was performed, or under which the conjugate was isolated (concentrated NH_4OH), resulted in the degradation of the $[Co(bipy)_2(bipy')]^{3+}$ complex. This would prove that degradation of the label complex in mass spectrometry was not a problem. The difficulty associated with this reaction was that it was done

after the DNA was cleaved off the glass beads, which made the removal of the unreacted bis(bipyridyl) precursor more difficult. The mass spectrometry result of the product is shown in Figure 1.23. No peak corresponding to the redox label-DNA conjugate (calculated molecular weight: 6263.2 g mol^{-1}) was observed, but a peak corresponding to the bipy'-DNA conjugate was present in the spectrum.

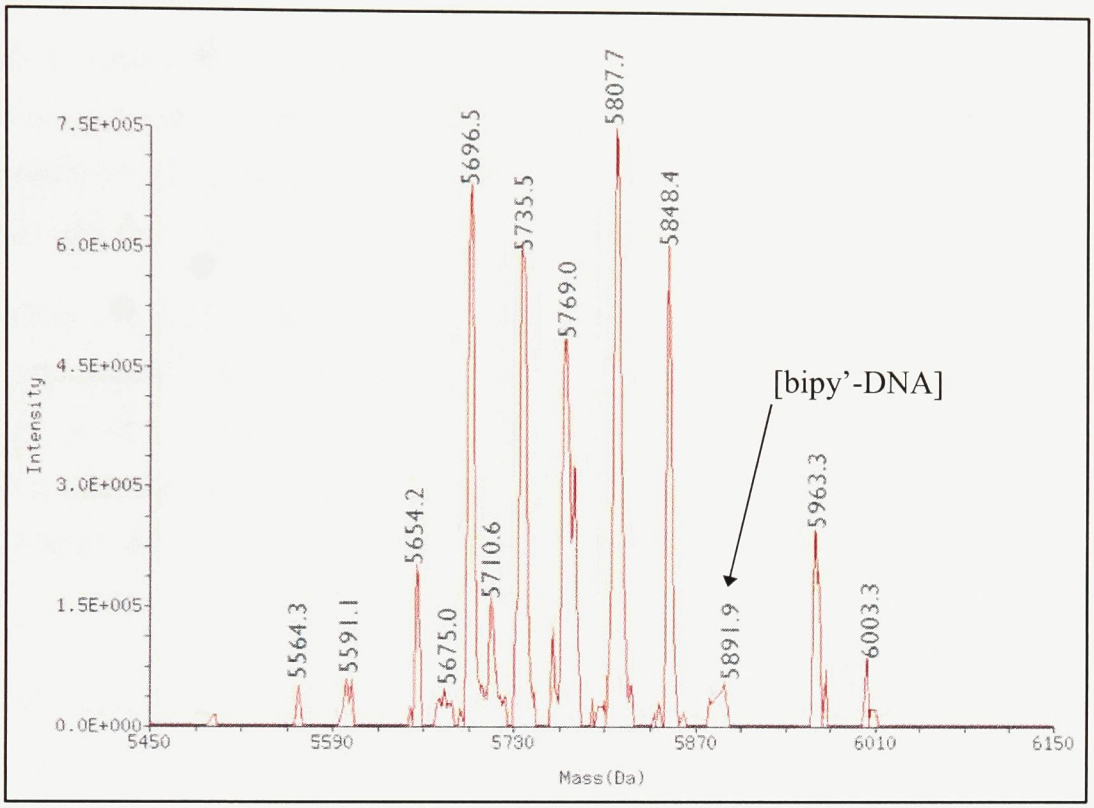

Figure 1.23. Deconvoluted mass spectrum of a crude product of the reaction between the bipy'-DNA conjugation product and $[Co(bipy)_2Cl_2]Cl$ in aqueous solution.

It was also observed that the bipy'-DNA conjugate peak in the mass spectrum was much smaller than it was in the previous sample. Since the bipy'-DNA used to react with the cobalt bis(bipyridyl) precursor was from the same sample that provided the mass spectrum in Figure 1.22, the peak should have been more intense than the peak that was observed. This may have simply been due to variation between the sample that was sent for analysis and the sample that was used for the reaction, as the relative intensities for the other major peaks in Figure 1.23 are different from those in Figure 1.22. Another possible reason that the peak was relatively lower may be that the bipy'-DNA was reacted with the cobalt bis(bipyridyl) complex, which lowered the abundance of bipy'-DNA in the product. However, the relative intensity of the peak is the

only evidence that this reaction may have occurred, since no peaks corresponding to a label-DNA conjugate were visible in the mass spectrum.

1.3.7.5 High-performance liquid chromatography (HPLC) of the peptide coupling reaction products

From the MS results, it was determined that HPLC was not effective at isolating the bipy'-DNA conjugated from label-DNA conjugates or unconjugated DNA, since a peak corresponding to bipy'-DNA was found in all three fractions from a $[Co(bipy)_2(bipy')]^{3+}$ and DNA peptide coupling product (refer to Section 1.3.7.2). However, the HPLC analyses did provide results that were not explored entirely, but which may prove to be important.

From the HPLC collection run for the first label-DNA coupling reaction (Section 1.3.7.2), the sample that gave a retention peak at 17 minutes was predominantly the bipy'-DNA conjugate, as was shown by the mass spectrometry results. This peak was also seen in a subsequent label-DNA conjugation attempt, for which an MS analysis of the crude showed a peak at 5890.9, which indicated the presence of a bipy'-DNA conjugate.

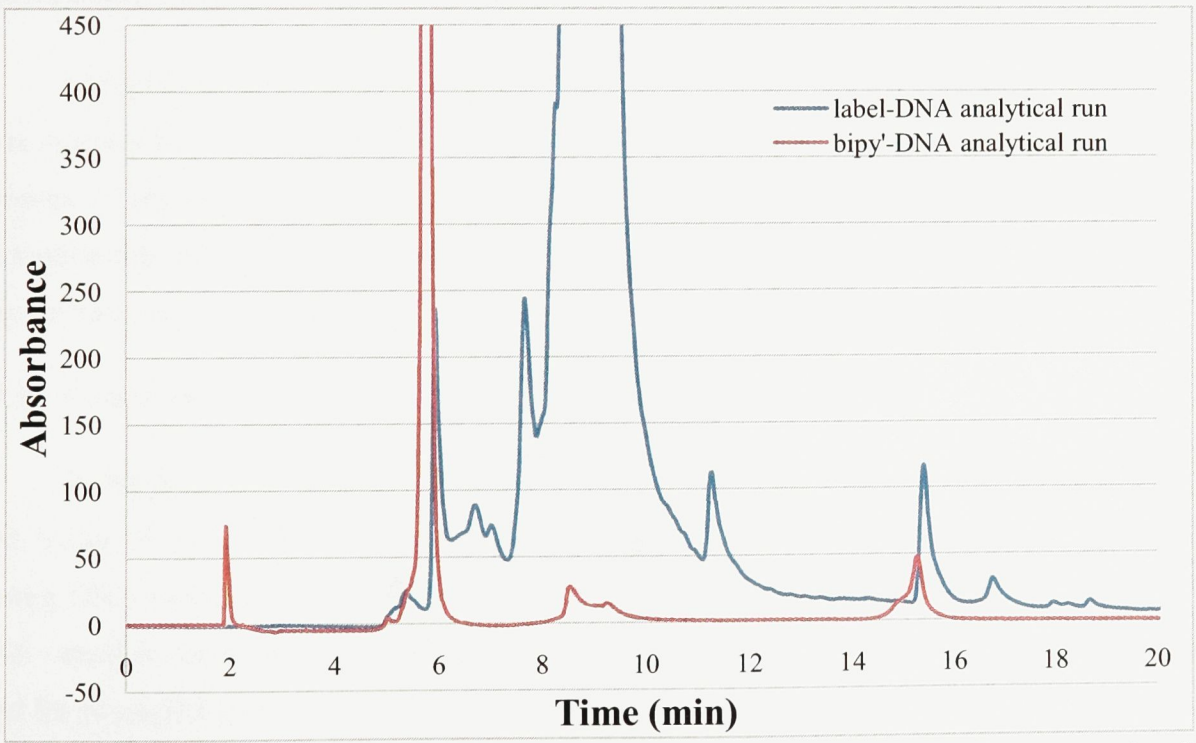

Figure 1.24. Diode array detector signals observed at 260nm from reverse-phase HPLC, elution program described in Section 1.2.7. The red line represents the product of a bipy' and DNA coupling reaction using EDC and NHS (see Section 1.3.7.3). The blue line represents the product of a redox label and DNA coupling reaction using PyBOP.

HPLC analysis was used to characterize all of the crude conjugation products for the early peptide coupling reaction attempts. It was found that the HPLC analysis of bipy' and DNA coupling attempts under the same mobile phase conditions did not display a peak with a retention time at 17 minutes. This was also true for an HPLC analysis done of a bipy'-DNA product for which the presence of bipy'-DNA was confirmed by MS (see Section 1.3.7.3). An overlaid graph of the diode array detector responses at 260nm for a label-DNA analytical run and a bipy'-DNA analytical run is shown in Figure 1.24.

Since the label-DNA sample produced a peak at 17 minutes that was determined to contain primarily bipy'-DNA, the same peak should also have appeared in the HPLC for a bipy'-DNA sample that contained the bipy'-DNA conjugate. However, as seen above, this was not the case. This could suggest that the peak at 17 minutes in the label-DNA coupling samples was the desired label-DNA conjugate. However, this compound may have degraded into predominantly the bipy'-DNA conjugate during the mass spectrometry analysis and as a result a label-DNA peak was not observed in the mass spectra. The peaks in both samples that eluted at approximately 15 minutes were found to not contain DNA, and may have been caused by unreacted bipy' ligand.

Unfortunately, the only method used to characterize the sample eluted at 17 minutes was mass spectrometry, so it could not be determined that the peak was conclusively a label-DNA complex. Considering the observations from the implementation of polyacrylamide gel electrophoresis (PAGE) discussed later (see Section 1.3.8.1), analysis of the fraction by PAGE may be more helpful in the identification of compounds present in the sample.

1.3.8 Conjugation of bipy' and the redox label to shorter DNA strands

In the hopes of being able to synthesize complete DNA strands with a higher yield, the next series of conjugation attempts was done using a shorter amino-modified DNA strand. During DNA synthesis, the addition of each nucleotide is not 100% efficient, so the longer the DNA strand is, the lower the yield of the complete strand. The sequence of the new DNA strand used for conjugation was 5'-H_2N-$(CH_2)_6$-AGA TCC GAT C-3'.

Another unique aspect of the conjugation attempts performed was that after the peptide coupling reactions, cleaving of the DNA from the beads was done at room temperature, whereas

previously cleaving had been done at 55°C. Differences resulting from changing the temperature at which the DNA was cleaved from the solid support could be noted by visual observation of the glass beads. The bipy' ligand was mostly colourless, but $[Co(bipy)_2(bipy')]^{3+}$ had a bright orange colour. After peptide coupling with the redox label, the glass beads changed colour to orange. This orange colour persisted, even after washing with dimethylformamide. Cleaving with ammonium hydroxide (NH_4OH) at 55°C resulted in the beads turning purple, while cleaving with NH_4OH at room temperature resulted in clear beads. The orange colour on the beads may have been the result of successfully conjugated label molecules on the support-immobilised DNA, or by non-specific affinity of the label molecule to the glass beads. While the cause of the purple colour on the beads after heated cleaving was not studied, one possibility would be the non-specific binding of $[Co(bipy)_2Cl_2]^+$ to the glass beads, since the colour of the complex was purple. This would indicate that the redox labelled DNA decomposed to $[Co(bipy)_2Cl_2]^+$ when heating was used during the cleaving procedure. This may be another reason that only a bipy'-DNA conjugate was observed when the conjugated product was analyzed by MS (see Section 1.3.7.2), but more study is required to validate this hypothesis.

Conjugation of the bipy' ligand and redox label using EDC and NHS was done in the same manner as the previous experiments. For the experimental coupling of the label to DNA using PyBOP, however, a molar excess of 10:1 of label to DNA was used, compared to the 1:1 molar ratio used previously. This was done to see if the yield of the conjugated product could be increased.

1.3.8.1 Polyacrylamide gel electrophoresis (PAGE)

Another difference between this series of peptide coupling experiments and previous experiments was the use of PAGE to attempt to isolate bipy'- or label-DNA conjugates from the crude coupling reaction products. Since the bipy'-DNA conjugate would be more massive than the DNA itself, and the label-DNA conjugate even more massive, it was hoped that the migration of these conjugates through the gel would be slower than the unconjugated DNA. Then, cutting out the correct band from the gel, and eluting the DNA from the gel would produce the isolated desired product.

A PAGE gel with a high acrylamide content was used, since relatively short DNA strands were used in the coupling reactions. Higher acrylamide content slows the migration of the molecules, which gives the molecules more time in the gel, and results in better separation. In order to determine the correct length of time for the electrophoresis process to get the best separation between sample contents while avoiding having them running off the end of the gel, a gel was run with fractions of the amine-modified DNA injected at different times during the process. The reference DNA sample was synthesised with the same sequence as the DNA strand used in the coupling experiments, and was also used as a control sample for the PAGE separations of the coupling products. From the gel shown in Figure A-1.7 in the Appendix, it was determined that running the gel for 1.5 hours would allow adequate separation of the products, while eliminating the possibility of losing the products off the end of the gel. The gel from this experiment also showed two bands, the lower one corresponding to the DNA strand without the amine modifier, and the higher one corresponding to the desired amine-modified DNA strand.

1.3.8.2 Electrophoresis of the coupling reaction products

It should be stated that the samples in a gel migrate from the top to the bottom, so smaller molecules migrate faster, and their bands will appear lower than the bands of larger molecules. Before the samples were loaded into the gels, they were heated to 55°C with formamide for five minutes. Also, the gels were prepared with a high urea content. This was done in order to ensure that the DNA was unstructured during its migration through the gel. The formation of a two-dimensional conformation by the DNA would change its overall size, and therefore affect its migration through the cell. For the migration of the DNA through the gel to be uniform, denaturing of the DNA was desired.

A PAGE gel imaged under UV light is shown in Figure 1.25. In this gel, a bipy'-DNA conjugate that was reacted with $[Co(bipy)_2Cl_2]Cl$ products (lane d), as well as the conjugate products label-DNA coupled using EDC/NHS and PyBOP (lane b, and c, respectively), were compared to a control sample of unconjugated amine-modified DNA (lane a). This gel is from an analytical run, and samples collected for MS analysis were loaded with a greater concentration of the samples, in order to elute and desalt a large enough sample to send for analysis. From the image, three main areas were targeted for analysis. The first was the band that appeared above the amine-DNA band in the control lane, which appeared in lanes c and d. Both of the bands

were collected and sent for mass spectrometry (red rectangle). The second area was the band below the unmodified DNA band in the control sample, which was present in lanes b, and c (yellow rectangle). The third area was the lowest band in lane d, which migrated much lower than any component of the control sample (blue rectangle).

From lanes c and d, the top bands (red rectangle) were cut out, eluted, ethanol precipitated, quantified and sent for analysis by mass spectrometry. The molecular weight of the amine-modified DNA strand was calculated as being 3191.0 g mol^{-1}, and the molecular weight of the bipy'-DNA and label-DNA conjugates were calculated as being 3429.3 g mol^{-1} and 3800.6 g mol^{-1}, respectively. For the PyBOP conjugation attempt (lane c), the abundant peak was 3232.4, which correlated to the amine-modified DNA plus an unknown factor that had a mass of 41 g mol^{-1}. This may correspond to an acetyl group. The other major peak appeared at 3428.9, which corresponded to the bipy'-DNA conjugate. A small peak at 3428.9 was also observed in the mass spectrum for the sample sent from lane d, indicating that this band contained the bipy'-DNA conjugate. However, the presence of peaks with masses of 3232.4 g mol^{-1} also indicated that this method may not have been completely efficient at separating the conjugated and unconjugated DNA in the products from each other. It was still unclear whether the peak at 3428.9 for the PyBOP coupling sample was due to the decomposition of the label complex during the conjugation reaction, gel procedures, or decomposition during mass spectrometry analysis. The peak at 3428.9 in the bipy'-DNA and cobalt bis(bipyridyl) reaction product may have been due to an incomplete or unsuccessful reaction, or decomposition similar to the label-DNA coupling product.

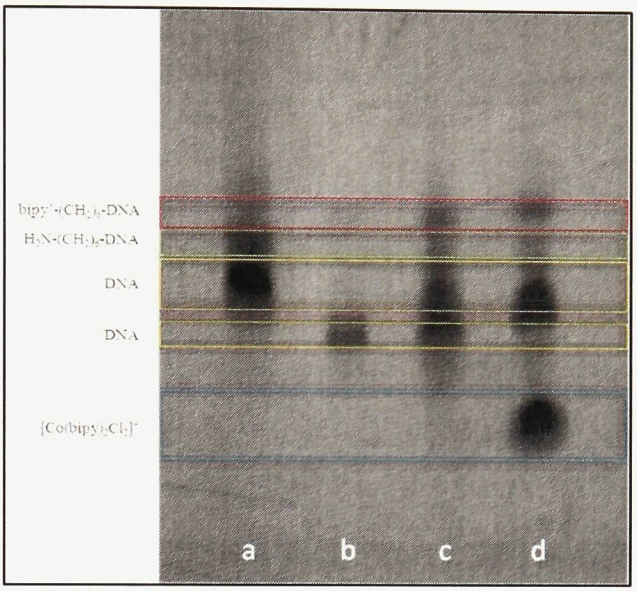

Figure 1.25. PAGE results for bipy' and label conjugation products, containing an amine-modified 10-nucleotide DNA control sample (lane a), label-DNA conjugation with PyBOP product (lane b), label-DNA conjugation attempt with EDC/NHS (lane c), and bipy'-DNA conjugate and $[Co(bipy)_2Cl_2]Cl$ reaction (lane d). Bands of interest are also indicated by rectangles and identified on the left-hand side (see text for details).

The easiest band to identify was the band from the third area. This band, from observation under natural light, was purple in colour. When the eluted samples were analyzed by UV-Vis spectroscopy, no absorbance at 260nm was observed, indicating that no DNA was present in the sample. These observations led to the conclusion that this area was unreacted $[Co(bipy)_2Cl_2]^+$ which, despite the unfavourable positive charge was able to migrate through the gel faster than any nucleic acid. This observation introduced the possibility that the influence of the label tethered to the DNA may make the conjugate migrate faster through the gel.

The bands in the third area in lanes b and c migrated slightly further than the DNA in the control sample that had not been amine-modified. A collection gel was run to isolate these two bands, and they were sent for mass spectrometry. It was hoped that the results would show that these bands belonged to the label-DNA conjugate, and that they migrated further because of the influence of the label on the DNA. Unfortunately, the MS spectra of the samples that were sent only showed peaks that corresponded to unconjugated DNA. The fast migration of the $[Co(bipy)_2Cl_2]^+$ molecule was most likely due to its small size compared to the DNA molecules, despite the fact that its charge was unfavourable for migration.

1.3.9 Summary of peptide coupling reactions and separation techniques

From the mass spectrometric results of multiple conjugation attempts using different methods and reagents, it can be concluded that the conjugation of bipy' and the redox label $[Co(bipy)_2(bipy')](PF_6)_3$ to DNA was partially successful. The conjugation of bipy' to DNA was possible using EDC and NHS as activating reagents, and was confirmed by mass spectrometry. The conjugation of the redox label to DNA was partially successful, as mass spectrometry showed that a bipy'-DNA conjugate resulted from this coupling reaction. A coupling reaction of the redox label and DNA was attempted with EDC and NHS as activating reagents, with negative results. An attempt to react the bipy'-DNA conjugate with $[Co(bipy)_2Cl_2]Cl$ also gave negative results, although more work involving reaction conditions would be needed to determine the feasibility of this approach.

The HPLC results showed that it was not efficient at separating bipy'-DNA conjugates, as a mass spectrometry peak corresponding to bipy'-DNA was shown in several fractions collected over a twelve minute time frame during one HPLC run. PAGE was also used, and was

able to separate out bipy'-DNA conjugates from the products of different conjugation experiments. However, this separation was not able to completely isolate the conjugated product from the unconjugated DNA in the sample.

Although the synthesis of a bipy'-DNA conjugate was confirmed, it was still unclear as to whether the conjugation of the redox label to DNA was possible. Mass spectrometry results from many label-DNA conjugation attempts showed the formation of bipy'-DNA, but it is unclear whether this was the result of reagent degradation during the peptide coupling reaction, the result of degradation during the HPLC or PAGE separation techniques, or the result of degradation during mass spectrometry. It may also be that a bipy' impurity in the redox label starting material conjugated to the DNA, and there was no tethering of the label. More study will be needed to identify the source of these results with certainty.

1.4 Conclusions

For the proposed electrochemical biosensor to operate successfully according to the design, the synthesis of a redox-active label complex that had a low redox potential was essential to avoid the creation of a false-positive response during the sensing of the analyte. For this reason, a label complex based on $[Co(bipy)_3]^{3+}$ was chosen.

Reactions done to synthesize $[Co(bipy)_2(bipy')]^{3+}$ were attempted under varying conditions. Synthesis experiments showed that the aqueous synthesis was more successful at producing the desired complex, however impurities present in the product made it difficult to characterize the label complex without interference. However, the formation of a small amount of crystals allowed some NMR, mass spectrometry and UV-Vis absorbance characteristics of the complex to be observed. Electrochemical measurements of the label complex indicated that it would be electrochemically suitable for the aptamer-based sensor design.

Coupling of the label complex to DNA was also attempted, and it was found that although a label-DNA conjugate was not confirmed, the reaction resulted in the coupling of bipy' to the DNA. It is uncertain as to whether this label complex degradation occurred during the coupling reaction, the cleaving/deprotecting procedure, or mass spectrometry analysis. More study will be needed in order to determine the reason for the degradation of the label molecule. The ligand bipy' was also successfully coupled to DNA on its own, but the outcome of a subsequent reaction with cobalt bis(bipyridine) to form the full redox label complex tethered to DNA was not successful, possibly due to the same reasons listed above.

These experiments have indicated that $[Co(bipy)_2(bipy')]^{3+}$ was successfully synthesized and demonstrated characteristics suitable for use in the design of an aptamer-based biosensor due to its low redox potential and potential ability to bind to DNA. However more research, particularly into the process of the coupling of the label complex to DNA, will be required in order to fully assess the suitability of the compound for use in an electrochemical sensor.

1.5 References

(1) O'Sullivan, C. K. *Anal. Bioanal. Chem.* **2002**, *372*, 44-48.

(2) Palchetti, I.; Mascini, M. *Analyst* **2008**, *133*, 846-854.

(3) Tuerk, C.; Gold, L. *Science* **1990**, *249*, 505-510.

(4) Luzi, E.; Minunni, M.; Tombelli, S.; Mascini, M. *TrAC, Trends Anal. Chem.* **2003**, *22*, 810-818.

(5) Willner, I.; Zayats, M. *Angew. Chem. Int. Ed.* **2007**, *46*, 6408-6418.

(6) Jenison, R. D.; Gill, S. C.; Pardi, A.; Polisky, B. *Science* **1994**, *263*, 1425-1429.

(7) Kleinjung, F.; Klussman, S.; Erdmann, V. A.; Scheller, F. W.; Fürste, J. P.; Bier, F. F. *Anal. Chem.* **1998**, *70*, 328-331.

(8) Hermann, T.; Patel, D. J. *Science* **2000**, *287*, 820-825.

(9) Jayasena, S. D. *Clin. Chem.* **1999**, *45*, 1628-1650.

(10) Stojanovic, M. N.; de Prada, P.; Landry, D. W. *J. Am. Chem. Soc.* **2001**, *123*, 4928-4931.

(11) Drake, T. J.; Tan, W. *Appl. Spectrosc.* **2004**, *58*, 269A-280A.

(12) Tyagi, S.; Kramer, F. R. *Nat. Biotechnol.* **1996**, *14*, 303-308.

(13) Li, Y.; Zhou, X.; Ye, D. *Biochem. Biophys. Res. Commun.* **2008**, *373*, 457-461.

(14) Ravera, M.; Bagni, G.; Mascini, M.; Osella, D. *Bioinorganic Chemistry and Applications* **2007**, 91078.

(15) Sassolas, A.; Leca-Bouvier, B. D.; Blum, L. J. *Chem. Rev.* **2008**, *108*, 109-139.

(16) Ahmed, M. U.; Hossain, M. M.; Tamiya, E. *Electroanalysis* **2008**, *20*, 616-626.

(17) Kerman, K.; Kobayashi, M.; Tamiya, E. *Meas. Sci. Technol.* **2004**, *15*, R1-R11.

(18) Li, F.; Chen, W.; Tang, C.; Zhang, S. *Talanta* **2008**, *77*, 1-8.

(19) Lee, J.-G.; Yun, K.; Lim, G.-S.; Lee, S. E.; Kim, S.; Park, J.-K. *Bioelectrochemistry* **2007**, *70*, 228-234.

(20) Millan, K. M.; Mikkelsen, S. R. *Anal. Chem.* **1993**, *65*, 2317-2323.

(21) Xiao, Y.; Lubin, A. A.; Heeger, A. J.; Plaxco, K. W. *Angew. Chem. Int. Ed.* **2005**, *44*, 5456-5459.

(22) Radi, A.-E.; Sánchez, J. L. A.; Baldrich, E.; O'Sullivan, C. K. *J. Am. Chem. Soc.* **2006**, *128*, 117-124.

(23) Staros, J. V.; Wright, R. W.; Swingle, D. M. *Anal. Biochem.* **1986**, *156*, 220-222.

(24) Pierce Biotechnology. *EDC*. **2008**. *http://www.piercenet.com/Objects/View.cfm?type=ProductFamily&ID=02030312* (accessed 11/27, 2008).

(25) Berkman, C. *Organic synthesis in drug discovery*. **2006**. *http://userwww.sfsu.edu/~cberkman/640_org_synth_drug_discov_1.pdf* (accessed 11/27, 2008).

(26) Coste, J.; Le-Nguyen, D.; Castro, B. *Tetrahedron Lett.* **1990**, *31*, 205-208.

(27) Raymond, S.; Wang, Y.-J. *Anal. Biochem.* **1960**, *1*, 391-396.

(28) Solomon, E. P.; Berg, L. R.; Martin, D. W. *Biology*, 5th ed.; Harcourt College: Orlando, FL, 1999; p 311.

(29) Kaplan, B. *Anal. Chim. Acta* **1998**, *372*, 161-172.

(30) Ferapontova, E. E.; Olsen, E. M.; Gothelf, K. V. *J. Am. Chem. Soc.* **2008**, *130*, 4256-4258.

(31) Li, Y.; Qi, H.; Peng, Y.; Yang, J.; Zhang, C. *Electrochem. Commun.* **2007**, *9*, 2571-2575.

(32) Davis, F.; Higson, S. P. J. *Biosens. Bioelectron.* **2005**, *21*, 1-20.

(33) Kelley, S. O.; Barton, J. K.; Jackson, N. M.; McPherson, L. D.; Potter, A. B.; Spain, E. M.; Allen, M. J.; Hill, M. G. *Langmuir* **1998**, *14*, 6781-6784.

(34) Widrig, C. A.; Chung, C.; Porter, M. D. *J. Electroanal. Chem* **1991**, *310*, 335-359.

(35) Hiramatsu, Y.; Okamoto, K.-I.; Hidaka, J.; Einaga, M. *Inorg. Chim. Acta* **1984**, *82*, L13-L15.

(36) Benko, J.; Vollárová, O.; Gritzner, G. *Phys. Chem. Chem. Phys.* **2001**, *3*, 1471-1478.

(37) Della Ciana, L.; Hamachi, I.; Meyer, T. J. *J. Org. Chem.* **1989**, *54*, 1731-1735.

(38) Vlček, A. A. *Inorg. Chem.* **1967**, *6*, 1425-1427.

(39) Francis, T. *Development of a Cobalt Reporter Probe Complex for Use in Electrochemical Aptasensing*, Carleton University, Ottawa, ON, 2008.

(40) Beking, M. *Development of Aptamer-Gadolinium Conjugates as MRI Contrast Agents*, Carleton University, Ottawa, ON, 2008.

(41) Ceres, D. M.; Barton, J. K. *J. Am. Chem. Soc.* **2003**, *125*, 14964-14965.

(42) Yau, H. C. M.; Chan, H. L.; Yang, M. *Biosens. Bioelectron.* **2003**, *18*, 873-879.

(43) Park, J. H.; Ryu, Y. K.; Lim, H. J.; Lee, H. S.; Park, J. K.; Lee, Y. K.; Jang, M. D.; Suh, J. K.; Carr, P. W. *Chromatographia* **1999**, *49*, 635-642.

(44) Ghosh, S.; Barve, A. C.; Kumbhar, A. A.; Kumbhar, A. S.; Puranik, V. G.; Datar, P. A.; Sonawane, U. B.; Joshi, R. R. *J. Inorg. Biochem.* **2006**, *100*, 331-343.

(45) Berka, L. H.; Gagne, R. R.; Philippon, G. E.; Wheeler, C. E. *Inorg. Chem.* **1970**, *9*, 2705-2709.

(46) Dollimor, L. S.; Gillard, R. D. *Chem. Ind. (London)* **1973**, 377.

(47) Wang, X.-L.; Chao, H.; Hong, X.-L.; Liu, Y.-J.; Ji, L.-N. *Transition Met. Chem.* **2005**, *30*, 305-311.

(48) Grassini-Strazza, G.; Sinibaldi, M.; Messina, A. *Inorg. Chem.* **1980**, *44*, L295-L297.

(49) Eberhardt, M. K. *Reactive Oxygen Metabolites: Chemistry and Medical Consequences;* CRC Press: Boca Raton, FL, 2001; p 89.

(50) Hutchinson, M. J.; Young, P. Y.; Hewitt, S. A.; Faulkner, D.; Kennedy, D. G. *Analyst* **2002**, *127*, 342-346.

(51) Johnson, S. K.; Houk, L. L.; Johnson, D. C.; Houk, R. S. *Anal. Chim. Acta* **1999**, *389*, 1-8.

(52) Palmer, R. A.; Piper, T. S. *Inorg. Chem.* **1966**, *5*, 864-878.

(53) Bond, A. M.; McLennan, E. A.; Stojanovic, R. S.; Thomas, F. G. *Anal. Chem.* **1987**, *59*, 2853-2860.

(54) Zhang, J.; Wang, L.; Pan, D.; Song, S.; Fan, C. *Chem. Comm.* **2007**, 1154-1156.

(55) Glen Research. *Products for DNA Research*. **2008**. *http://www.glenresearch.com/* (accessed December 18, 2008).

(56) Kibbe, W. A. *Nucleic Acids Res.* **2007**, *35*, W43-W46.

(57) Augustyn, K. E.; Stemp, E. D. A.; Barton, J. K. *Inorg. Chem.* **2007**, *46*, 9337-9350.

Chapter 2

Development of an aptamer-based fiber optic surface plasmon resonance sensor

2.1 Introduction

2.1.1 Surface plasmon resonance

Surface plasmon resonance (SPR) is an electromagnetic oscillation that occurs at the interface of two materials with dielectric constants of opposite signs, an example being a metal and a dielectric. This phenomenon consists of the excitation of longitudinal oscillations of electrons in metals at the metal/dielectric interface with the help of light. If a beam of light passes through a medium of higher refractive index towards a thin gold film at an angle equal to or greater than the critical angle, total internal reflection will occur. Under total internal reflection, when the light's angle of incidence reaches the resonance angle (θ) optical energy is transferred to the surface of the metal and excites a charge density oscillation that can span 100 nanometres above and below the metal surface.[1] This effect is known as the surface plasmon resonance. The SPR condition depends on the incident angle, wavelength of light, and the dielectric constants of the two layers.[2]

The most popular and commercially available configuration of SPR is the Krestchmann, or prism, configuration, in which a thin metal film is deposited directly on the base of a dielectric prism.[2] For use in biosensing, the gold layer is positioned between the prism and the sample to be analyzed. The popular metal choices for SPR biosensors are gold and silver. The use of gold increases sensitivity to refractive index changes, while using silver results in a better signal-to-noise ratio, however silver has a lower chemical stability than gold.[2] The wavelength or angle at which resonance can occur depends on the refractive index at the interface of the metal and the sample.[2] A change in composition at the metal/sample interface results in a change of the refractive index and therefore causes a change in the angle of the SPR, known as an SPR shift.[1] This shift is directly related to the adsorption of the analyte in the sample to the metal surface.[1]

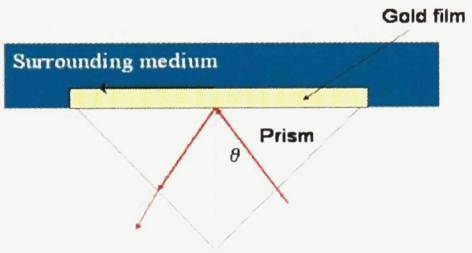

Figure 2.1. The Krestchmann configuration for exciting SPR waves.[21]

The label-free sensing capabilities of SPR have predictably resulted in considerable interest in the field of biosensing. Label-free detection, in which the DNA strand does not need to be modified with a dye or any other molecule, is desirable for sensors since it makes the construction of the sensor simpler and less costly. SPR imaging has been used successfully in the

detection of DNA-DNA[3] and DNA-protein[4] interactions, and even conformational changes in immobilized proteins.[5] In another study, complementary DNA was labelled with gold nanoparticles, which enhanced the SPR signal when the complementary strand was hybridized with an immobilized DNA aptamer. This configuration was used for the detection of adenosine using a DNA aptamer.[6] With the addition of adenosine, the angle shift in the surface plasmon was decreased, since the binding of the aptamer to its target prevented the hybridization of the DNA complement to the aptamer, and therefore the enhancement by the gold nanoparticles was not observed. These analyses showed that SPR could be used to monitor biomolecular interactions, and set an encouraging precedent for the detection of targets using aptamers.

2.1.2 Optical fibers

Optical fibers are thin strands of glass or plastic that are designed to transmit light from a transmitter to a receiver. The typical fiber consists of three regions: the core, the cladding and coating. The core is in the centre of the fiber, and is the region in which the light is transmitted. The cladding region surrounds the core region of the fiber, and is designed to reflect light back in to the core. The final region is the coating, or buffer, which protects the inner regions of the fiber from moisture and abrasion, and also strengthens the fiber as a whole.[7]

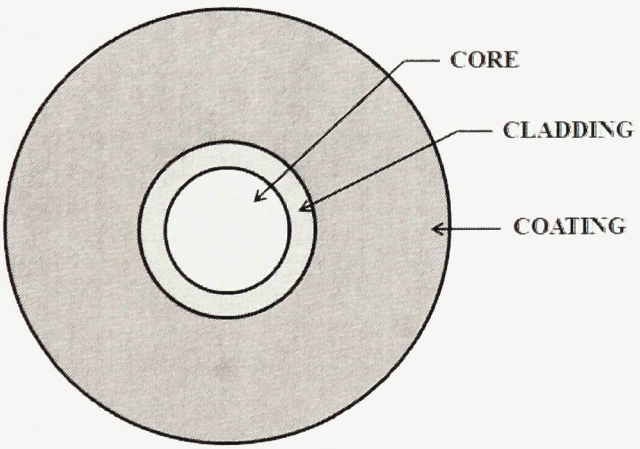

Figure 2.2. Cross section of an optical fiber.[7]

The optical fiber operates on the principal of total internal reflection. In the fiber, the core region has a higher index of refraction than the surrounding cladding region. When light is passed from a medium of higher refractive index to lower, the critical angle at which the light travels parallel to the interface (Θ_c) can be calculated from Snell's Law:

$$\Theta_c = \sin^{-1}\left(\frac{n_2}{n_1}\right) \tag{2.1}$$

where n_1 represents the medium with the higher refractive index and n_2 represents the medium with the lower refractive index. If the angle of incidence is larger than the critical angle, total internal reflection can occur.[7] Therefore, if the angle of incidence of the light introduced into the core region of the fiber is larger than the critical angle, the light would be reflected through the fiber with a low rate of loss. Most fibers are composed of nearly pure silica, and the refractive indices of the regions can be adjusted using dopants.[8] Popular dopants used to increase the refractive index of silica are GeO_2, P_2O_5, TiO_2 and Al_2O_3. Dopants used to reduce the refractive index are B_2O_3 and F.[9]

2.1.2.1 Optical fibers in sensing

The development of optical fiber sensors owes much to the physical properties of the fibers. The fact that optical fibers are small, lightweight, inexpensive, durable and immune to electromagnetic interference makes them desirable for sensing in many fields.[10] Optical fiber sensors can be divided into two categories: intensity attenuation sensors and interferometric sensors. In intensity attenuation sensors, environmental variations (such as temperature change) alter the optical characteristics of the fiber, which in turn changes the intensity of the light passing through the fiber. In interferometric sensors, the phase of the light passing through the fiber can be modulated by outside influences, and differences between the modulated phase and the initial phase can be detected.[10]

2.1.2.2 Surface plasmon resonance sensors using optical fibers

At the metal-dielectric interface, a surface plasmon can be excited when the wavevector of the light that is parallel to the interface matches that of the surface plasma wave (SPW), and couples with it.[11] Since surface plasma waves cannot be excited by light that is directly incident at the interface, the light must be passed through a medium of higher refractive index than that of the dielectric medium at the interface in order to enhance its wavevector.[11] This can be done with the help of a waveguide surrounded by a medium with a lower refractive index. As the light propagates through the waveguide, a small amount of the optical energy propagates through the surrounding medium in the form of an evanescent wave. The evanescent wave can be used to

excite a surface plasma wave at the outer or inner surface of the metal film.[11] An optical fiber, which transmits light in a core with a higher refractive index than the surrounding cladding mode, is therefore a form of waveguide, and provides the means to excite surface plasma waves if the fiber is coated with a thin metal layer.

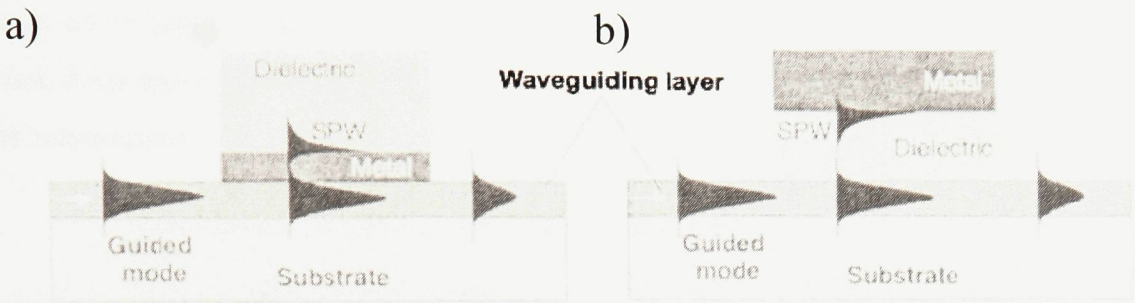

Figure 2.3. The excitation of surface plasma waves by optical waveguides. a) Excitation at the outer surface of the metal layer, and b) excitation at the inner surface of the metal layer.[11]

In surface plasmon resonance (SPR) sensors, the sensitivity of the propagation constant of a surface plasma wave to changes in refractive index is exploited in order to measure changes in the refractive index brought about by different factors. A change in the propagation constant of the SPW results in a change of the characteristics of the light wave that interacts with the SPW.[11] There are many ways of detecting changes in the light interacting with the SPW, such as angular, wavelength, intensity, polarization and phase modulation.[11] The type of modulation to be analyzed can be determined before experimentation, and is an important decision in the design of SPR sensor analyses.

2.1.2.3 Fiber Bragg gratings and tilted fiber Bragg gratings

Since their introduction by Ken Hill of the Canadian Communication Research Centre in 1978,[12] fiber Bragg gratings (FBGs) have drawn considerable attention in both the fiber optic communications and sensing fields. FBGs are periodic refractive index (RI) perturbations that can be imprinted in the core of fibers.[13] In the field of sensing, they have become reliable sensors in the measurement of load, strain, temperature and vibration,[14] and provide many advantages compared to other fiber optic sensing methods since they can be directly written into the interior of the fiber without affecting its external characteristics, and can be produced at low cost.[15] Also, and perhaps most importantly, the measurements from FBG sensors are based on wavelength,

which is an absolute measurement and not dependent on a consistent output from the light source.[16]

FBGs can be formed in fiber core modes using two intersecting high-powered UV radiation beams. The periodic index differences form partially reflective planes, which can reflect a set of beams from a broadband light shone through the core mode. The reflected beams interfere destructively with each other,[15] unless they are the specific Bragg wavelength, λ_B, given by the relationship

$$\lambda_B = 2n\Lambda \tag{2.2}$$

where n is the average refractive index of the FBG, and Λ is the period of the grating. Beams that satisfy this relationship are reflected by the grating in phase, while some beams that do not satisfy the relationship pass through the grating.[16] From the stated relationship, changes in the fiber grating can be measured as a shift of the Bragg wavelength, and external forces such as strain or temperature can be observed using the reflected or transmitted light spectra.[14]

A major form of fiber Bragg gratings in biosensing is long-period fiber gratings (LPFGs), which are manufactured with periods between 100μm to 1mm, three to four orders of magnitude longer than traditional grating periods.[13] LPFGs allow the coupling of the core mode to the cladding mode (see Figure 2.4a), and as a result change the expression of the resonance condition to

$$\lambda = (n_{\text{eff-core}} - n_{\text{eff-cladding}})\Lambda \tag{2.3}$$

where $n_{\text{eff-core}}$ is the average RI in the core mode, and $n_{\text{eff-cladding}}$ is the RI of the cladding mode. The increased field intensity in the cladding mode makes $n_{\text{eff-cladding}}$ sensitive to changes of the RI in the medium surrounding the fiber, and changes in the external RI can affect the wavelength of the reflected beam.[13] Biomolecular interactions taking place on the external surface of the fiber can effectively change the surrounding RI, producing a measurable change in the reflected beam. The sensitivity of LPFG sensors can be improved by etching the cladding material down,[17] but despite this LPFG biosensors still do not compete with the detection limits of other forms of optical biosensors.[13]

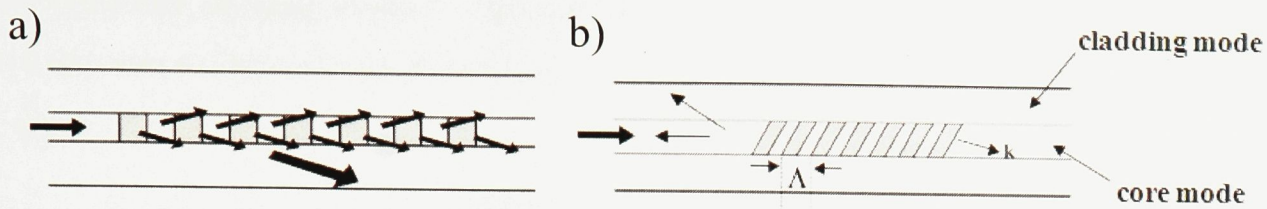

Figure 2.4. Different types of fiber Bragg gratings used for external RI monitoring. a) Long-period fiber gratings, and b) tilted fiber gratings.[17]

Another type of fiber grating that allows the coupling of light from the code mode to the cladding mode are tilted fiber Bragg gratings (TFBGs). TFBGs are types of short-period fiber gratings, with the grating planes slanted with respect to the fiber axis (see Figure 2.4b).[18] The tilts of the fiber gratings allow the coupling of the forward propagating core modes to the backward propagating cladding modes and the backward propagating core modes.[17] The resonance wavelength at the *i*th cladding mode (λ_{clad}^{i}) can then be calculated by

$$\lambda_{clad}^{i} = \frac{(n_{eff}^{i}+n_{clad}^{i})\Lambda}{cos\theta} \tag{2.4}$$

where n_{clad}^{i} is the effective index of the ith cladding mode, n_{eff}^{i} is the effective index of the core mode at λ_{clad}^{i}, and Λ and θ are the period and internal tilt angle of the tilted grating, respectively.[19] TFBGs provide some advantages over other techniques used for external RI sensing, such as fiber etching and LPFGs. These advantages include higher sensitivity to changes in RI without the need for etching, and lower cross sensitivity to external perturbations such as temperature and bending.[20]

In this experiment, the evanescent waves formed in the cladding mode using TFBGs were used to excite surface plasma waves in gold-coated optical fibers. TFBGs are used to couple the core mode to several cladding modes, each of which strikes the cladding-metal boundary at a different angle of incidence (see Figure 2.5a).[21] Light shone through the core mode of the fiber is coupled to the cladding modes using the tilted gratings, which then couple to the surface plasma wave if the correct polarity and periodicity requirements are met. When a cladding mode couples with an SPR, it experiences a loss in intensity compared to the other modes. Figure 2.5b shows a typical transmission spectrum of a gold-coated TFBG optical fiber, with the resonances labelled λ_p corresponding to wavelengths that are able to excite the surface plasmon. These wavelengths experience more loss than the other wavelengths in the spectrum.[21] From equation (2.4), it can be shown that the effective index of the SPR will have an effect on the resonance wavelengths of

the perturbed cladding modes.[21] The sensitivity of this system to external refractive index changes was determined to be 454 nm/unit.[21]

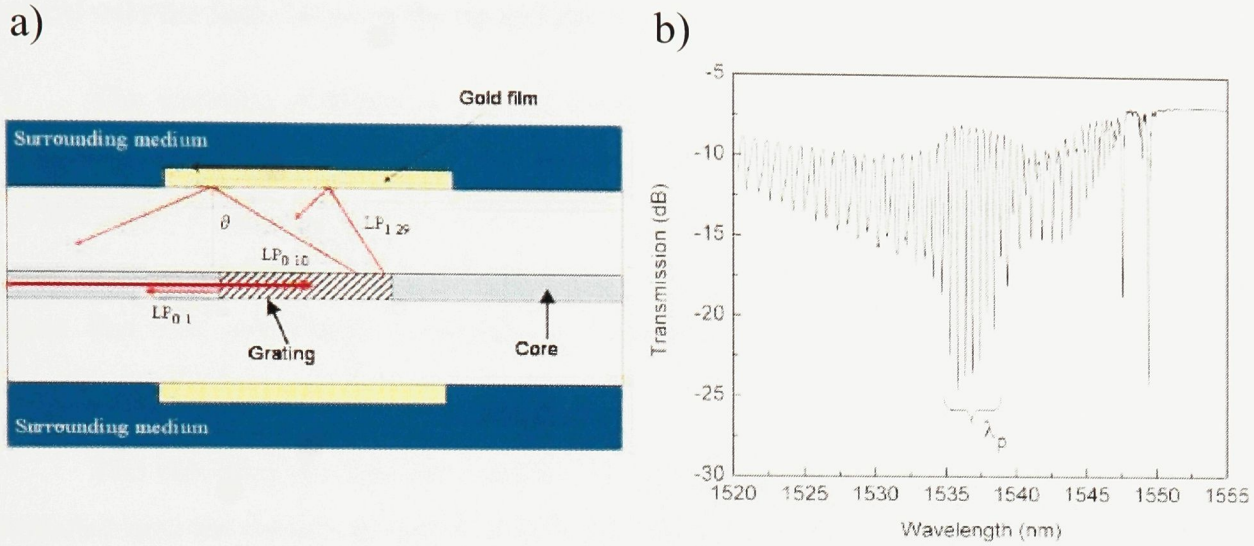

Figure 2.5. a) The optical fiber sensor setup, showing the excitation of SPR waves with fiber modes from a tilted FBG, and b) a transmission spectrum of a TFBG optical fiber coated with 20nm of gold and immersed in a sucrose solution with n_D=1.4378.[21]

2.1.3 Atomic force microscopy

Since its invention in 1986,[22] the atomic force microscope (AFM) has become arguably the most versatile piece of equipment in the scanning probe microscope (SPM) family, which generate images based on interactions between a sharp probe and a surface.[23] Characterization of a surface by AFM is based on the deflection of a laser by a cantilever attached to the tip as it follows the contours of the surface, which is then detected by a photodiode detector (see Figure 2.6). This setup allows AFM to characterize surfaces in three dimensions accurately on the nanometre scale,[24] and measure the force between tip and surface in the piconewton scale.[25]

There are three major elements that work to make the microscope: the tip, the scanning platform, and the detection mechanism. The AFM tip is a sharp spike that is mounted to the end of a cantilever, both of which are made from silicon or silicon nitride in order to prevent wear. The force from the bending of the cantilever (F) as it acts on a surface follows Hookes' Law,

$$F = -kd \tag{2.5}$$

where k is the force constant of the cantilever (which can also be described as its spring constant) and d is its displacement. Typically, the cantilever has a low force constant in order to have more control over the force between the tip and the sample.[23]

The scanning platform is very important to the AFM setup, since measurements over such small areas require the accurate placement of the tip over the sample.[23] A piezoelectric ceramic is used for the platform, since potentials applied on the x,y and z axes of the ceramic result in its expansion and a resulting motion of the sample along the three axes. It has been found that this movement is capable of sub-nanometre motion,[25] and that this motion is reproducible.[23]

The detection mechanism consists of a laser and a photodiode detector. The laser is projected onto the cantilever, which is deflected by the cantilever as it bends while traversing the surface. The photodiode detector is divided into four quadrants (see Figure 2.6) in order to monitor the vertical motion of the tip as well as any lateral (twisting) motion.[23]

There are three different modes of scanning using AFM: non-contact, contact and tapping. In non-contact mode, the tip is held above the surface at a distance of a few nanometres, and is given a small oscillation. When the distance between the tip and the surface is reduced by a feature on the surface, the oscillation of the cantilever is deviated by the van der Waals force that acts on it. The deviation in oscillation can then be used to form a map of the surface. In contact mode, the tip is brought into contact with the sample and a set force is applied to the sample by the tip. The tip is then moved over the sample, with the cantilever bending in order to maintain the force between the tip and the surface. In tapping mode, the tip is given a controlled oscillation amplitude, and is brought near the surface so that it makes contact with the surface with a frequency of around 50-500 kHz. Raises and recesses in the surface change the amplitude of the cantilever's oscillation, and these changes can be used to characterize the features of the surface.

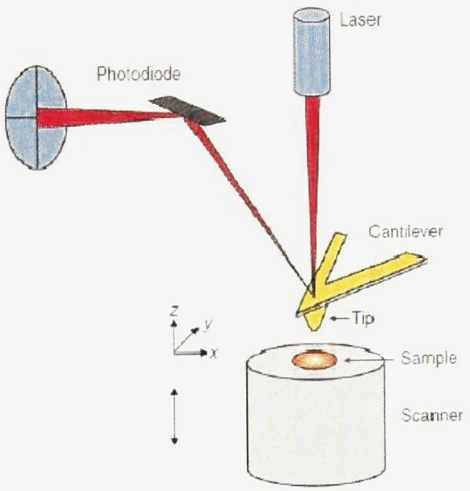

Figure 2.6. Schematic diagram of atomic force microscopy.[25]

The use of atomic force microscopy in biological applications has grown considerably in the last decade. Reviews by Hansma,[26] Dufrêne,[27] and Müller and Dufrêne[28] describe the use of AFM to characterize membrane proteins, live cells and DNA deposited on surfaces. Studies summarized in the reviews were also able to observe interactions between biomolecules, such as inhibitor binding on proteins, biomolecular changes brought about by environmental changes, as well as DNA-protein interactions. Aptamer-thrombin interactions have been studied by AFM in studies by Rinker *et al.*[29] and Liu *et al.*,[30] which used AFM to confirm aptamer-thrombin binding, and by Basnar *et al.*,[31] which used an aptamer-modified AFM tip to probe the force required to separate the aptamer-protein complex.

2.1.4 Confocal laser scanning microscopy

Confocal laser scanning microscopy (CLSM or confocal microscopy) is a powerful form of scanning optical microscopy that allows the collection of sharp, well-resolved images from selected levels within thick, three-dimensional objects.[32] A major advantage that confocal microscopy provides is the elimination of out-of-focus blur, which is caused by the bleeding of photons from above and below the focal plane of the image and which degrades the quality of the image by reducing contrast and sharpness.[33] This blurring is a major problem in the imaging of complex and thick tissues,[32] and frozen tissue imaging using conventional immunofluorescence microscopy was usually limited to a maximum thickness of 10μm to reduce its effects.[33] By using a confocal aperture, light from areas above or beyond the focal plane of the image are reduced, increasing the signal-to-noise ratio and facilitating the collection of three dimensional images.[34]

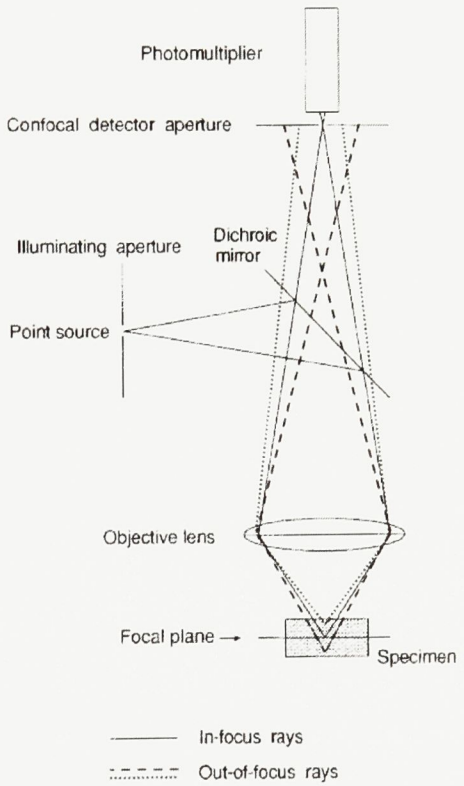

Figure 2.7. Schematic diagram of a confocal laser scanning microscope.[35]

The principle of CLSM is shown in Figure 2.7.[35] The laser light used to excite the sample is shone from the illuminating aperture through an excitation filter (not shown) and is deflected by the dichroic mirror towards the sample. The light is then focused by the microscope's

objective lens to a focal point within the specimen. The light emitted by the sample, from the focal plane as well as the light not in the plane, is then collected by the objective lens and passes through the dichroic mirror and an emission filter towards the photomultiplier tube detector. Light emitted from above (represented as ····· in the figure) and below (represented by - - - - - -) the in-focus plane are not allowed to pass through the confocal aperture, and as a result are prevented from reaching the detector. The light detected, as a result, is achieved almost exclusively from the in-focus plane (represented by a straight line).[33] In confocal microscopy a photodetector, such as a photomultiplier tube, is used to capture a digital image of the sample. This also provides an advantage over traditional fluorescence microscopy since capturing microscope images while reducing out-of-focus fluorescence on conventional epifluorescence microscopes was often impossible.[36]

A major use of confocal fluorescence microscopy has been to image biological samples, and the imaging of the components of plant[32] and animal[37] cells is extensively studied. It has also been shown that confocal microscopy could be used for other biological and non-biological purposes. Some applications of CLSM include the use of confocal microscopy in a fluorescent sensor for free Cd^{2+} in living cells,[38] and monitoring the entry of fluorophore-modified peptides into cells.[39] CLSM was also used to show protein binding to alkanethiols on gold,[40] and to study drying dynamics in porous media.[41] Since fluorescence microscopy has been used previously in the analysis of fluorophore-tagged thiols deposited on surfaces,[42,43] confocal microscopy is a good candidate to confirm the attachment of thiolated aptamers to the surface of a gold-plated fibre.

2.1.4.1 Cyanine 3

The sulfoindocyanine dye 1-(e-carboxypentynyl)-14-ethyl-3,3,34,34-tetramethylindocarbocyanine-5,54-disulfonate (Cyanine 3, Cy3) was first synthesized in 1993[44] and is now used widely in fluorescent biological experiments, either on its own or for fluorescence resonance energy transfer (FRET) experiments with Cy5. The excitation maximum wavelength of Cy3 is 550nm, and its emission wavelength is 570nm. The sulfonate groups of Cy3 make it water soluble,[45] giving it an advantage over other water-insoluble dyes. The N-hydroxysuccinimide (NHS) group in the structure also allows Cy3 to be bound easily to primary amines, such as NH_2-modified DNA strands. Other advantages of Cy3 are that it is pH

insensitive and shows less aggregation in labelling conditions,[44] and it is stable against photobleaching, compatible with many green lasers and readily available commercially.[46] The fluorescence intensity of Cy3 has been shown to increase when it was attached to DNA strands,[47] making an even more desirable dye to use for biological applications. Cy3 has been used in experiments to study DNA structure,[48] as well as DNA-protein[49] and protein-protein interactions.[50]

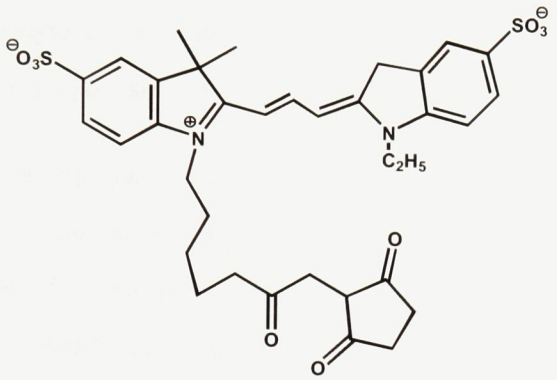

Figure 2.8. Structure of Cy3.

2.1.5 Ellman's reaction

Ellman's reaction was developed in order to quantify the amount of sulfhydryl (-SH) groups in tissues.[51] When 5,5'-dithiobis-(2-nitrobenzoic acid) (DTNB, Ellman's reagent) is reacted with a thiol, it is cleaved according to the reaction:

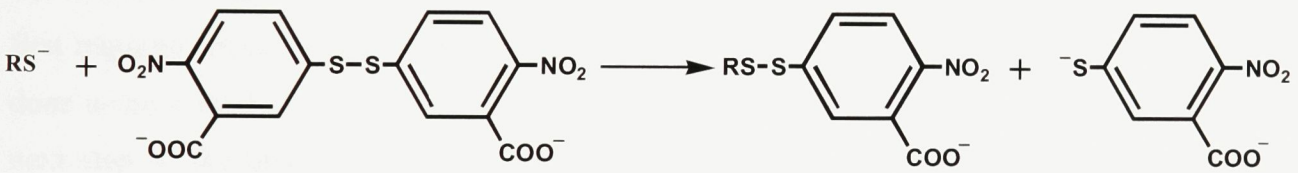

The formation of the product 2-nitro-5-thiobenzoate (TNB) results in a yellow colour. Pure TNB^{2-} has a molar extinction coefficient at 412nm (ε_{412}) of 14100 $M^{-1}cm^{-1}$,[52] therefore the presence of thiol groups can be monitored easily by measuring the absorption at 412nm using a spectrophotometer. The thiol groups can also be quantified, since the molar extinction coefficient of TNB is known.

2.1.6 Sensor design

The biosensor design for this project consists of an optical fiber with a tilted fiber Bragg grating written into its core and a thin layer of gold deposited on the surface of the cladding (see Figure 2.5a). The gold layer is deposited on the glass fiber, providing the necessary metal-dielectric interface required to excite the plasmon waves. It was found that depositing a gold coating thickness of 20-25 nm by sputtering was the most effective for the sensor.[21] At smaller thicknesses, the plasmon resonance becomes difficult to observe, while larger thicknesses limit the extension of the resonance into the surrounding medium.

The Bragg gratings in the fibers used for the sensing experiments were tilted at an angle of 10°, which allows the excitation of SPR in aqueous solutions. A tilt of 10° of the Bragg grating allows the spectrum of propagating cladding modes to reach a range of 100nm. This is useful since the resonances needed to excite SPR in aqueous media occur approximately 70nm away from the Bragg resonance. The Bragg resonance is the longest wavelength resonance on the spectrum (see Figure 2.5b), and is used as a reference for the shorter cladding resonance wavelengths in case of changes of temperature or strain during the experiment. During the experiments, transmission spectra are measured, and changes in the spectra are directly related to changes of the SPR due to external RI changes.

During the experiment, the changes in SPR are expected to be affected by the biomolecular interaction of an aptamer and its target on the gold-coated optical fiber surface. The first requirement is the attachment of the aptamer to the gold-coating on the fiber. This can be done using a thiol-modified aptamer sequence, as described in Chapter 1, Section 1.1.7.2. The next step of the procedure would be exposing the immobilized aptamer to a solution of the aptamer's target. Both steps of the biosensing procedure involve the immobilization of biological material on the surface of the fiber, which will change the effective refractive index at the surface and alter the propagation of the surface plasma wave during both steps. By monitoring the resonance spectra transmitted through the fiber, changes in the SPR in the surface can be monitored, and comparisons to the original spectra can be used to confirm the presence of the analyte. This, in effect, creates a lightweight, portable biomolecular probe that can be used in aqueous media. The versatility of the probe is also an advantage of this design. The tilt angles of the Bragg gratings can be changed, so that the probe could be used in media with differing

refractive indices. For example, tilt angles of 3.5° were used to excite SPR in media that provided an external RI of 1.42 to 1.45.[21] The versatility of the probe towards different targets is also an advantage; DNA aptamers have been selected for a variety of targets, as described in Chapter 1, Section 1.1.1.

In order to ensure that any changes in surface plasmon resonance measured during the experiments are due to the attachment and binding of the aptamer sequences and targets, physical characterization methods will also be used. These characterizations will be used to show that the conditions used in the experiments allow the attachment of the DNA aptamer to the gold-coated fiber, as well as allow the binding of the thrombin target to the surface-immobilized aptamer.

2.2 Experimental procedure

2.2.1 Optical fibers

The preparation of the optical fibers and tilted Bragg gratings was done by Yanina Shevchenko and Albane Laronche in supervisor Jacques Albert's Laboratory for Laser Induced Photonics Structures, Carleton University, Ottawa. Procedures used for fiber preparation were learned by communication with the members of the laboratory, as well as Yanina Shevchenko's Master's thesis[53] and Optics Letters journal artcle.[21]

2.2.1.1 Writing the tilted Bragg gratings in the fibers

The optical fibers used in the experiments were commercially available standard single mode telecommunications fibers (Corning SMF-28). These fibers had a core diameter of 8.2μm and a cladding diameter of 125.0 ± 0.7 μm.[54]

Prior to writing the Bragg gratings, the fiber was placed in a chamber under hydrogen for 14 days. This allowed the fibers to absorb the hydrogen to increase their photosensitivity, and the absorption was aided by a pressure of 2500 psi in the chamber. After the 14 days had passed, the coating of the fiber was removed and the cladding was rinsed with methanol.

The Bragg gratings were written into the core of the fiber using a side-writing technique, in which a single laser beam (a KrF excimer laser at 248 nm) was shone through a phase mask in order to create an interferometric pattern (see Figure 2.9). The phase mask and fiber were placed within 100 μm of each other, and the tilt of the Bragg gratings was created by rotating the phase mask and fiber with respect to the incident laser beam. From Figure 2.9, it can be seen that the tilt angle of the Bragg gratings can be changed with the angle at which the phase mask is rotated relative to the fiber.

After the Bragg gratings were written into the fibers, the gratings were stabilized by annealing using a heating gun for less than one minute. The fibers were then placed in an oven set at 120° and left for 12 hours.

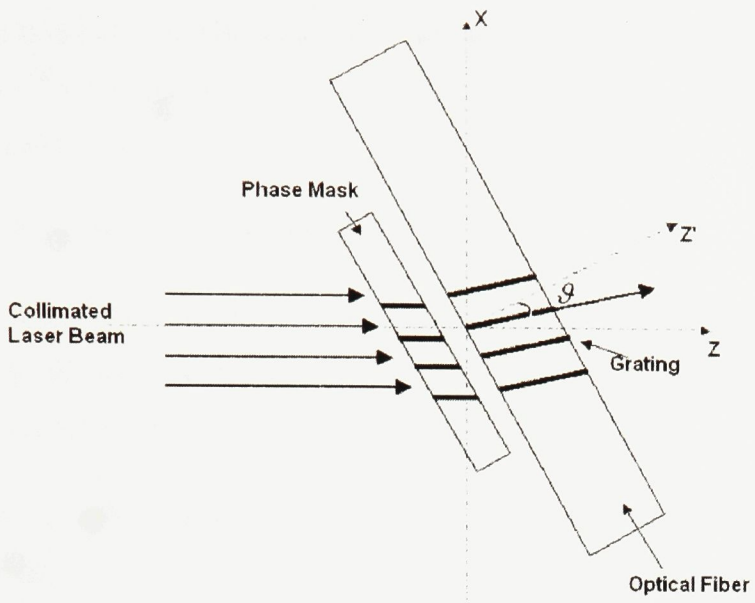

Figure 2.9. Schematic diagram of the side-writing technique.[53]

2.2.1.2 Gold plating the fibers

The gold coating was deposited on the surface of the fiber using the sputtering method (employing a Polaron E5100 sputter coater). Sputtering was done at a pressure of 0.1 Torr, with a high voltage ranging from 2.2 – 2.5 kV and a sputter current from 18 – 20 mA. The deposition was conducted in two steps: one side of the fiber was sputter coated for one minute, and then the fiber was rotated 180° and the other side of the fiber was coated for one minute. It was found that one minute of coating gave the desired 20 – 25 nm thickness of goal on the fiber.[21]

2.2.2 DNA sequences and proteins

All DNA sequences were ordered from Alpha DNA (Montreal), and were received as HPLC-purified, lyophilized dry samples. Human α-thrombin was ordered from Haematologic Technologies Inc. (Vermont, USA), and was received dissolved in a 50:50 solution of glycerine and water.

The DNA sequence used in the surface plasmon resonance imaging and atomic force microscopy was 5'-GGT TGG TGT GGT TGG-3', the 15-nucleotide aptamer for thrombin. This sequence was ordered with a 5'-thiol-C6 modifier, making the overall sequence of the DNA 5'-HS-$(CH_2)_6$-GGT TGG TGT GGT TGG-3'.

The DNA sequence used for confocal microscopy was the 15-nucleotide aptamer for thrombin as mentioned above. The aptamer strand possessed the 5'-thiol-C6 modifier, as well as a Cyanine 3 ($Cy3^{TM}$) dye modifier at the 3' end, making the overall sequence 5'-HS-$(CH_2)_6$-GGT TGG TGT GGT TGG-Cy3-3'.

2.2.2.1 DNA and thrombin solution preparation

Sodium dihydrogen-phosphate (99%), sodium phosphate dibasic (≥99%) and magnesium chloride (~325 mesh) were purchased from Sigma-Alrich (Oakville, ON). Sodium hydroxide was purchased from BDH (through VWR, Mississauga, ON).

The DNA buffer solution was prepared with 5mM phosphate (pH 7.0), 100mM magnesium chloride ($MgCl_2$) and 50mM sodium chloride (NaCl). The pH of the DNA buffer was adjusted with an aqueous sodium hydroxide (NaOH) solution when needed. The protein buffer solution was prepared with 50mM tris(hydroxymethyl)aminomethane (Tris, pH 7.4), 1mM MgCl2, 140 mM NaCl and 5mM potassium chloride (KCl). The pH of the protein buffer was adjusted with a 1M hydrochloric acid solution when needed. All buffer solutions were prepared in beakers, filtered through a 0.22μm cellulose acetate sterilizing filter and stored in polystyrene containers (Corning 431154 filter systems).

2.2.3 Ellman's test

DTNB (5,5'-dithio-bis(2-nitrobenzoic acid)) was purchased from Sigma-Aldrich (Oakville, ON).

This test was performed using the thiol-modified DNA sequences. A 30μM solution of the DNA was prepared using the DNA buffer. This solution was then mixed in equal parts with a 30μM solution of DTNB in DNA buffer solution. The reaction mixture was then left for two hours.

UV-visible spectroscopy was performed on a Cary 300 Bio system, monitoring the absorbance at wavelengths between 200 and 800nm. The results were analyzed to compare the reaction solution before and after the test.

2.2.4 Surface plasmon resonance (SPR) measurements

SPR experiments were performed in collaboration with Yanina Shevchenko, a Ph.D. candidate from Dr. Jacques Albert's optics laboratory at Carleton University, Ottawa. During the experiments, the light source that was used was a JDS Uniphase broadband source and the detector was an Ando AQ6317B optical spectrum analyzer.

For the SPR experiments, one end of the fiber was connected to a white light source, while the other end was connected to an Optical Spectrum Analyzer. The grating-inscribed area of the fiber was mounted on a plastic platform which had a section cut out to hold the DNA and protein solutions (see Figure 2.10). The cut-out section of the platform held approximately 500μL of solution. During the experiment, the cut-out section of the platform was covered with a glass slide, in order to prevent the evaporation of the buffer solution. The fibers were fixed to the platform using a UV-sensitive epoxy to prevent the displacement of the sensor during the experiments.

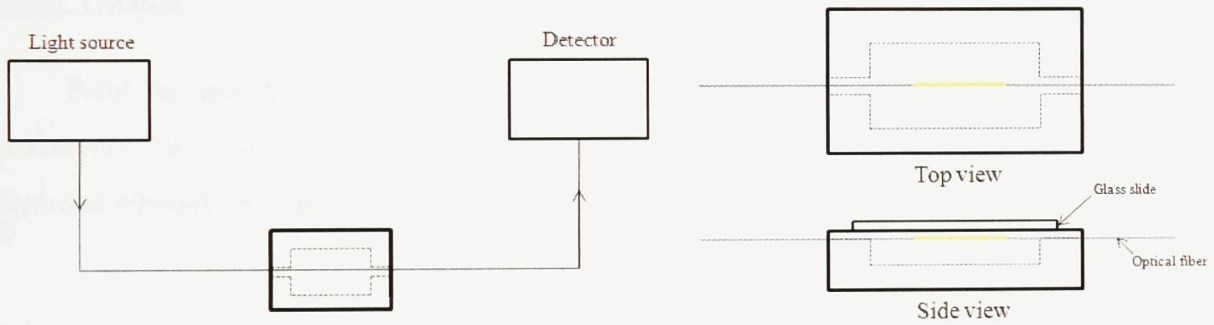

Figure 2.10. Diagram of the experimental setup, and a top and side view of an optical fiber mounted on the plastic platform.

2.2.4.1 Thiolated aptamer deposition

After the fiber was fixed in place on the platform, the cut-out section of the platform was filled with DNA buffer and a resonance spectrum was collected to act as the reference spectrum. The buffer solution was then removed, and the section was then filled with a 15μM solution of 5'-thiol-C6 modified aptamer for thrombin. Transmission spectra were collected automatically every minute during the entire experiment. DNA deposition times were varied, and are described in the Results section. After the DNA deposition was complete, the fiber was rinsed with deionized water several times before the protein solution was added.

2.2.4.2 Thrombin binding on an aptamer-immobilized fiber

A 30μM solution of thrombin was prepared using human α-thrombin and the protein buffer that was prepared as described in Section 2.2.2.1. This solution was used to fill the cut-out section of the platform and surround the aptamer-immobilized fiber. Transmission spectra were collected at one-minute intervals throughout the experiment.

2.2.5 Confocal microscopy

All confocal microscopy images were collected on a Zeiss LSM510 with a Plan-Acochromat 63x/1.4 Oil Dic objective with LP950 filter, with an excitation wavelength of 550nm and an emission wavelength of 570nm. All of the samples were mounted on microscope slides with a solution of 50% glycerol in water, and covered with 1.7μm thick cover slides. Images were collected with the help of Ann-Fook Yang and Denise Chabot at Agriculture Canada, Ottawa.

Prior to using the gold-coated optical fibers for any control or DNA deposition experiments, the glass tubes and the gold-coated ends of the fibers were rinsed first with anhydrous ethanol and then the DNA buffer.

Figure 2.11. Diagram of a gold-plated optical fiber placed in Cy3 solution.

2.2.5.1 Control samples

A Cy3-positive control slide was prepared by drying several drops of a solution of Cy3 on a slide, and was imaged as mentioned previously. A Cy3-negative control slide was prepared by drying several drops of the DNA buffer solution (as prepared in Section 2.2.2.1) on a slide, and was imaged as mentioned previously.

Background signal from unwanted Cy3 bound non-specifically to the fiber was observed by submerging a gold-plated optical fiber in a glass tube filled with a 15μM solution of Cy3 dye in DNA buffer (see Figure 2.11) for 20 hours. The fiber was rinsed with DNA buffer prior to mounting on a microscope slide.

2.2.5.2 Dye-tagged thiolated DNA deposition

The 5'-thiol-C6 and Cy3-3' modified aptamer for thrombin was dissolved in DNA buffer to make a 45μM solution. This solution was used to fill a glass tube, in which the gold-plated optical fiber was submerged (see Figure 2.11). The fiber was left in the solution for amounts of time that varied based on the experiment being conducted. The fiber was rinsed with DNA buffer before mounting on the microscope slide.

2.2.6 Atomic force microscopy (AFM)

All AFM images were collected on an Ntegra system using a SFC050LNTF AFM Head on an inverted microscope (Olympus IX71). The probes were Tap300AI probes (budgetsensors.com) and all images were collected using dynamic mode. The silicon probe had a length of 125μm, a mean width of 30μm, and thickness of 4μm. The tip's height was 17μm, and its radius was less than 10nm. All samples were collected in air. AFM images were collected with help from Nur Uddin Ahamad and Graham Galway from Dr. Anatoli Ianoul's laboratory at Carleton University, Ottawa.

2.2.6.1 Control sample

A control sample was prepared by immersing a gold-coated optical fiber in DNA buffer solution for four hours. It was then rinsed with deionized water and dried in air before imaging.

2.2.6.2 Thiolated DNA deposition

The DNA used for this experiment was also the aptamer for thrombin, with a 5'-thiol-C6 modifier. A gold-plated fiber was immersed in a 25μM solution of the aptamer in DNA buffer for four hours. The fiber was then rinsed with deionized water and dried in air before imaging.

2.2.6.3 Thrombin binding on an aptamer-deposited fiber

A gold-plated fiber was immersed in a 25μM solution of the thiolated aptamer for a period of four hours. The fiber was then rinsed with DNA buffer and immersed in a 30μM solution of α-thrombin in protein buffer for approximately 12 hours. After immersion, the fiber was rinsed with deionized water and dried in air before imaging.

2.2.6.4 Thrombin on a gold-coated fiber control sample

A gold-plated fiber without aptamer deposition was immersed in a 30μM solution of α-thrombin for approximately 15 hours. After immersion, the fiber was rinsed with deionized water and dried in air before imaging.

2.3 Results and Discussion

2.3.1 Experiment objectives

The primary objective of this project was to make an optical fiber-based surface plasmon resonance biosensor, in which the biomolecular interaction of a surface-immobilized aptamer with its target would result in a measurable response. As surface plasmon resonance sensors are sensitive to changes in refractive index, it was important to show that the changes observed in the surface plasmon were due to the attachment of the aptamer and its target to the surface and not due to other factors, such as the evaporation of the buffer solution. Evaporation of the buffer during the experiment would make the salt content of the environment surrounding the fiber more concentrated, which would affect the propagation of the surface plasmon and create false-positive changes in the observed spectra.

Therefore, another objective of the project was to prove that the desired biological interactions were taking place on the gold-plated surface of the fiber. This was done using microscopic image-based methods, which allowed the observation of the chemisorption of the aptamer strand onto the surface, and the aptamer-target interactions that occurred when the thrombin target was introduced. The adsorption of the aptamer onto the surface of the fiber, and the subsequent binding of the aptamer to its target, may create a change in the effective refractive index surrounding the optical fiber sensor. Correlating a change in plasmon frequency or amplitude to the physical observation of the aptamer deposition and target binding would provide evidence of the value of this sensor design.

2.3.2 Ellman's test

Ellman's test is a simple experiment that indicates the presence of thiol (-SH) in a given sample. The great advantage of this test is that it is very easy to perform, can be confirmed visually and requires only the preparation of two solutions of equal molarity. Ellman's test was an important diagnostic test in this experiment, since the thiol group on the aptamer for thrombin was necessary to ensure that the aptamer could bind to the gold surface of the fiber.

Previous work[55] showed that the optimal concentration to use for the solutions of 5,5'-dithiobis-(2-nitrobenzoic acid) (DTNB) and DNA was 30μM. This concentration gave the most

accurate visualization of the DTNB and nitrothiobenzoate (TNB) peaks using UV-Vis spectrometry, and the colour change also made the presence of thiols observable by simply looking at the reaction.

A control sample of DTNB was prepared by mixing equal parts of 30μM DTNB solution in DNA buffer with pure DNA buffer. The Ellman's test samples were prepared by mixing equal parts of a 30μM DTNB solution with a 30μM solution of the aptamer for thrombin. A successful Ellman's test, in which it was seen that the DNA in the sample was thiolated, is depicted in Figure 2.12. The DTNB sample showed an absorbance maximum at 323nm. Over time during the test, the formation of TNB was observed by the increasing absorbance peak at 410nm, and the decrease of the DTNB peak at 323nm. After two hours of reaction, it was observed that the formation of TNB was slowing, indicating that the DTNB had been almost completely converted in two hours. The absorbance of the peak at 410nm after two hours corresponds to a TNB concentration of 28μM, indicating an almost complete formation. The large spike in absorbance at approximately 300nm was due to the large amount of DNA present in the sample (DNA absorbs strongly at 260nm, and the onset of the absorbance is seen at 300nm).

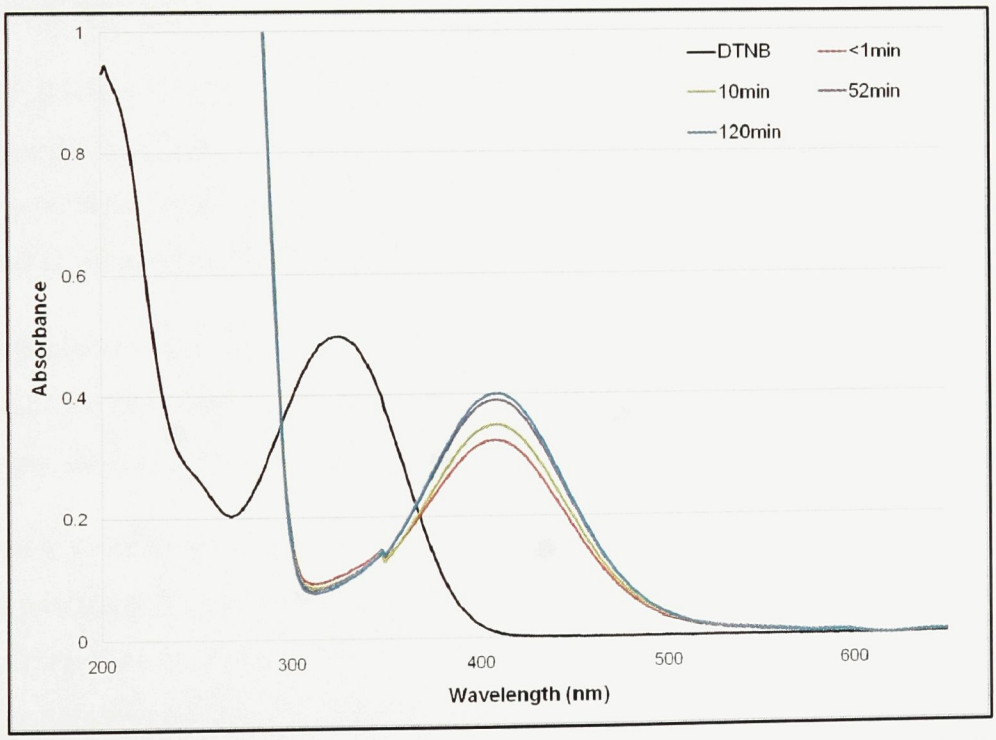

Figure 2.12. UV-Vis spectrum of 30μM DTNB solution (black) and Ellman's test solution at t = <1 min (red), t = 10 min (green), t = 52 min (purple) and t = 120 min (blue). Solutions were prepared in the DNA buffer solution. The DNA strand used in the Ellman's test was thiolated aptamer for thrombin.

Oxidation of the thiol groups on the aptamers in solution, which may have occurred if the aptamers were exposed to air, could have resulted in the formation of disulphide bonds, as shown by the equation[56]

$$2(R–S) \rightarrow R\text{-}S\text{-}S\text{-}R + 2H^{+} + 2e^{-}$$

This would also result in the inability to cleave DTNB in the Ellman's test, therefore a negative Ellman's test is characterized by the lack of formation of a TNB absorbance peak at 412nm. The formation of a disulphide bond from two thiol groups would decrease the ability of the sulphur to bind to the gold surface on the fiber.

The disulphide bond, if it is formed, can be reduced back to two thiol groups using tris(2-carboxyethyl) phosphine hydrochloride (TCEP). This is also a simple process, where an excess of TCEP in solution can be added to a solution of disulphides to reform the thiol groups. TCEP can be used to reduce a disulphide to two thiols as shown below:[57]

$$(HOOC(CH_2)_2)_3P + RSSR + H_2O \rightarrow (HOOC(CH_2)_2)_3P{=}O + 2RSH$$

2.3.3 Confocal microscopy

Since thrombin does not naturally fluoresce, using confocal microscopy to monitor thrombin-aptamer binding was not possible. However, by modifying DNA strands with a cyanine-derived fluorescent dye (Cyanine 3, also known as Cy3), the binding of the aptamer to the surface of the fiber could be easily observed.

Cy3 dye was a convenient dye to use for these experiments. The commercial availability of the dye allowed the ordering of DNA sequences with the Cy3 dye incorporated at the 3'-end of the sequence during synthesis, reducing the number of steps needed to prepare the DNA.

A study conducted by Sanborn *et al.*[47] reported that the fluorescence intensity of Cy3 increased approximately 4-fold when Cy3 was attached to the 5'-end of an 18-mer DNA strand compared to free Cy3 in solution. In the same study, it was found that the maximum excitation and emission wavelengths were red-shifted by approximately 4 nm when the dye was bound to the DNA. These findings both demonstrated that Cy3 dye molecules possess characteristics desirable for these confocal experiments. A fluorescence intensity increase upon binding to DNA

creates more distinction between the desirable DNA-bound dye and undesirable non-specifically bound free dye. As a result, background fluorescence caused by the non-specific binding of Cy3 to the gold-plated fibers would have been less apparent in the confocal images than Cy3 attached to DNA on the surface of the fiber. Also, since DNA-bound Cy3 has excitation and emission maxima at higher wavelengths than free Cy3, tuning of the laser and detector on the confocal microscope would allow for better visualization of the DNA-bound Cy3 compared to free Cy3. Although the performed experiments differ from Sanborn's study since the dye molecules were attached to the 3'-end of the DNA strand as opposed to the 5'-end, it is possible that these effects could be observed for the dye attached at the 3' end.

2.3.3.1 Preparing microscope slides

The fibers were mounted on the microscope slides using a solution that was 50% glycerol in deionized water and covered with a cover slip. This was done while the fiber was still intact and threaded through the ferrule, after which the fiber was cut using a razor blade. This method was used because cutting the fiber before mounting it on the slide resulted in scratches to the gold-coating since the fiber would slide along the surface it was on (slide, lab bench, etc.), causing damage to the gold coating. Holding or moving the fiber by holding it with fingers or tongs after it was cut may have resulted in damage to the DNA on the gold surface, or the gold coating itself. As a result, a different way of ensuring that the fiber did not move after being cut was needed. Mounting the fiber before cutting it proved to be an effective solution to the problem.

Research by Sanborn *et al.*[47] showed that free Cy3 in pure glycerol had a quantum yield approximately nine times higher than free Cy3 in a Tris buffer solution. The reason given for this is that the viscosity of the glycerol prevents the formation of a photoisomer (the *cis* form of the Cy3 molecule), which is formed when light is absorbed by the dye molecule. This photoisomer competes with the fluorescence of the dye, and as a result the observed overall fluorescence is diminished. Although this was not tested with DNA-bound Cy3, the results

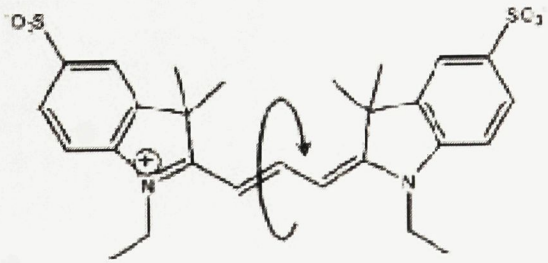

Figure 2.13. The molecular rotation for cyanine isomerization.[47] Rotation from the *trans*-isomer to the *cis*-isomer causes a reduction in the observed fluorescence.

discussed in Sanborn's paper indicate that mounting the fiber in a glycerol solution may have helped the imaging by reducing photoisomerization and increasing the fluorescent yield of the dye.

2.3.3.2 Positive and negative Cy3 samples

Cy3-positive and Cy3-negative solution samples were prepared by depositing several drops of a 30uM solution of Cy3 in DNA buffer and several drops of DNA buffer on a slide, respectively. The slides were then dried overnight, and prepared for microscopy as described in Section 2.2.5.1.

The Cy3-positive sample was used to ensure that Cy3 fluorescence could be seen using the microscope at the given excitation and emission wavelengths. As shown in Figure 2.14, the dye was clearly visible using a 63x-magnified objective lens. No images of the dye were taken with an objective lens with a lower magnification.

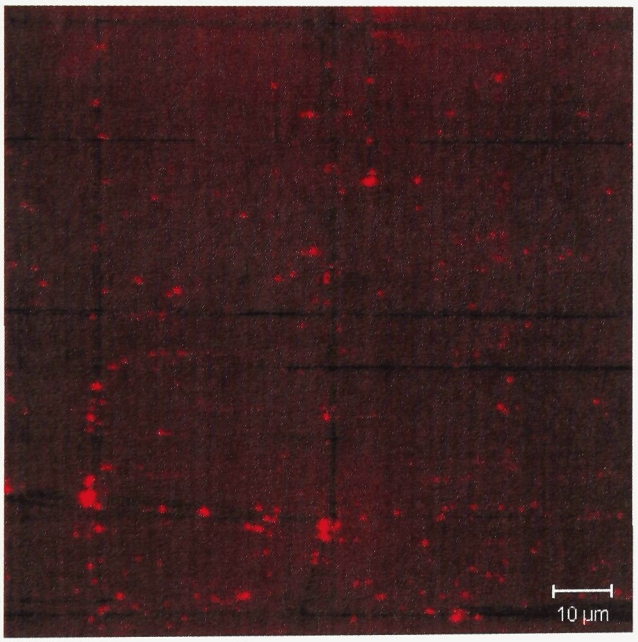

Figure 2.14. Confocal microscope image of Cy3 solution deposited on a slide. Excitation 550nm, emission 570nm, 10% laser strength, detector pinhole width 23µm, 63x magnification.

The Cy3-negative sample was prepared to show that no fluorescence in the images would be due to a component present in the DNA buffer solution. The images were taken with the same laser and detector settings as the single-strand DNA trials (see Section 2.3.3.4). As seen in Figure

A-2.1 in the Appendix, no fluorescence can be observed at these detector settings. Therefore, no fluorescence in any images was the result of the buffer that was used to make the solutions.

2.3.3.3 Background fluorescence from the Cy3 dye

To see whether any fluorescence seen in the images may have come from free Cy3 dye in solution binding non-specifically to the gold plating, a fiber was submerged in a solution of Cy3 dye dissolved in DNA buffer for 20 hours. This was the same length of time that the fiber was submerged in the Cy3-tagged DNA solutions for the deposition experiments. Confocal microscope images were then obtained with the same laser and detector settings used in the single-stranded DNA trials. From Figure A-2.2 in the Appendix, it was observed that no fluorescence could be seen at the settings used for the DNA experiments. When the power of the laser was increased to a setting approximately eight times higher than the original level, a faint fluorescence could be seen, as shown in Figure A-2.2b.

From Figure A-2.2b, it can be seen that there was an interaction between the gold on the fiber and the dye. To make the dye more water-soluble, two sulphite (SO_3^{2-}) groups were functionalized onto the dye structure. These groups are classified as borderline bases,[58] and as a result can interact with gold, a soft acid. The resulting interaction resulted in a faint background glow, as well as the appearance of some clusters. However, this fluorescence was not seen with the same laser intensity and detector pinhole size as were used to see fluorescence with the single-stranded DNA experiments (see below). This shows that the background fluorescence caused by the interaction between the gold-coating and unreacted Cy3 dye does not influence the observed fluorescence in the aptamer adsorption experiments. Also, since the non-specific adsorption of the dye to the gold surface may have been based on a borderline base/soft acid interaction, the interaction may have been replaced by the favoured gold-thiol bond during the deposition of the aptamer. This suggests that the fluorescence seen in the single-stranded attachment images came from the dye-tagged DNA attaching to the gold-plated surface.

2.3.3.4 Dye-tagged DNA attachment

In this experiment, the DNA aptamer was attached to a gold-plated optical fiber using the gold-thiol reaction, as described in Chapter 1, Section 1.1.7.2. The formation of thiolated self-assembled monolayers (SAMs) on gold surfaces has been useful in the development of

electrochemical and SPR-based biosensors.[59] The reaction progresses as a two-step process, with the thiolated DNA adsorbing quickly to the gold surface, and rearranging on the surface over time.[60] This mechanism would result in the observation of some aptamers being bound quickly to the surface, with more aptamers attaching to the surface the longer that the fiber was left in the DNA solution.

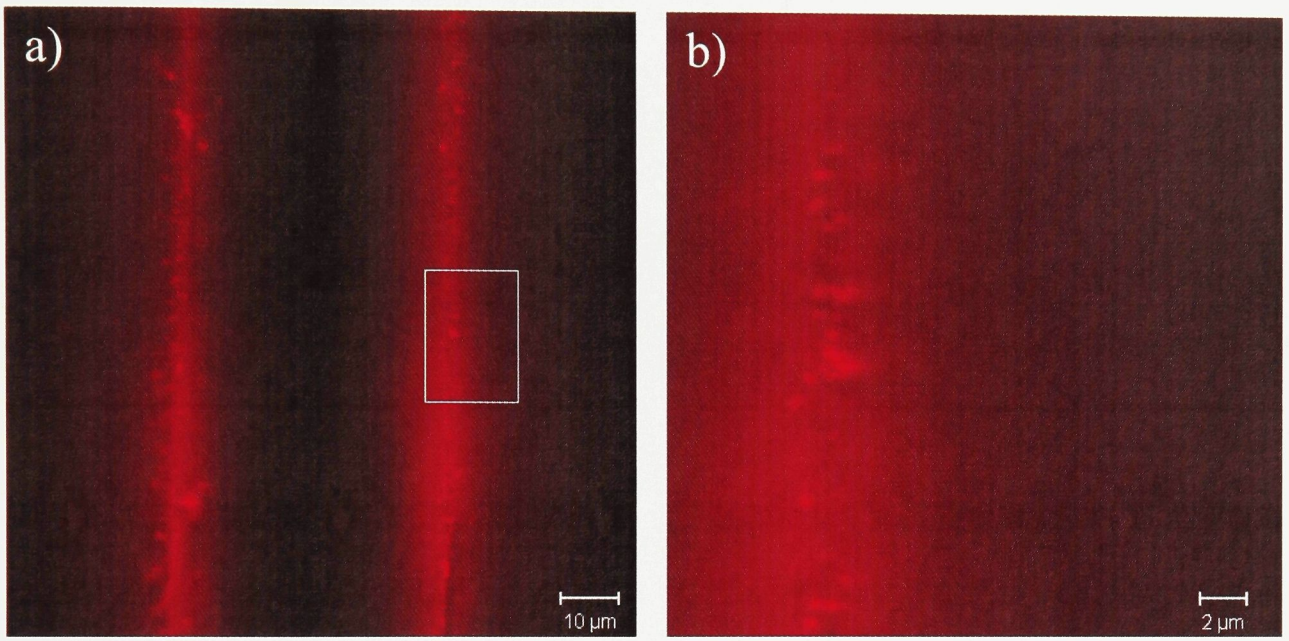

Figure 2.15. Confocal microscope images of an optical fiber immersed in a 45µM Cy3- and thiol-modified DNA solution for 20 hours. a) Excitation 550nm, emission 570nm, 11% laser strength, detector pinhole width 55µm, 63X magnification; b) A zoom-in of 2.15a, the area of which is marked by a white box in a).

From Figure 2.15, it can be seen that fluorescence from the Cy3 dye was observed. It should be noted that the confocal microscope only takes images at a certain focal depth, meaning that the fluorescence seen is only from the dye present at the depth of the picture. It should also be noted that the images in Figure 2.15 do not show the entire fiber, although the contours of the fluorescence give the appearance of the sides of the fiber. Figure 2.16 is a schematic diagram of the plane of the confocal microscope image with respect to the optical fiber. The figure shows that at a particular image depth, the surface of the fiber could only be seen as two columns. This was the result of imaging a curved surface with a horizontal image plane. As the depth of the image increased, the distance between the fluorescent columns in the image became wider.

The results of this experiment, with consideration to the control experiments discussed in Sections 2.3.2.2 and 2.3.2.3, indicated that the fluorescence seen in Figure 2.15 was the result of the dye-tagged thiolated aptamer sequence binding to the gold surface of the fiber. The strength

of the chemisorptive bond between the thiol and the gold surface is somewhat strong (40-45 kcal mol^{-1}),[61] and the gold-thiol bond was strong enough to withstand post-deposition rinsing with water. The free dye, however, was rinsed off with washings, if it had been bound to the surface at all. From the zoomed-in Figure 2.15b, it was observed that the individual fluorescence features were approximately 0.5 to 1μm in diameter. This may have been the radius of the fluorescence emission of one dye molecule on an immobilized aptamer strand. Another possibility is that the large fluorescence features were caused by the aggregation of the aptamers on the surface of the fiber, since from the images it appeared as though some of the fluorescence features were from many sources grouped together, and not single sources spread evenly over the surface of the fiber. From magnification of the fluorescence features of Figure 2.14, it appeared as though single features were about the same size. Nevertheless, these images provide evidence for the binding of the thiolated aptamer strands to the gold-plated fiber surface.

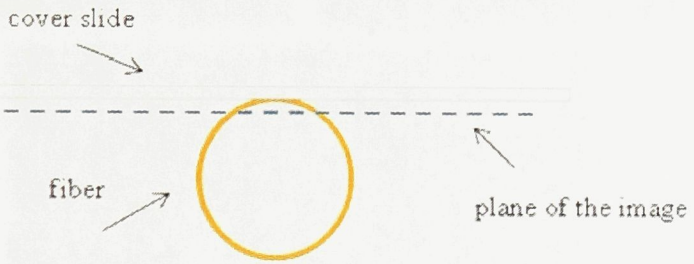

Figure 2.16. Diagram of the confocal image plane with respect to the optical fiber and cover slide.

This result was essential to the overall concept of the aptamer-based biosensor. The biosensor is based on the specific binding of surface-immobilized aptamer sequences with their targets. An aptamer sequence not bound or non-specifically bound to the fiber would not affect the surface plasmon resonance upon binding with the target, since this would not change the density of biological matter on the surface of the fiber. The fact that the signal remained after washing suggested that the bond between the dye-labelled DNA and the gold surface was stronger than a non-specific binding interaction, and was due to the covalent binding of the aptamer to the fiber.

To observe the extent of DNA attachment in a time frame more analogous to the plasmon measurement experiments that were being conducted (see Section 2.3.5), confocal microscopy images were collected after a gold-plated optical fiber was immersed in the same DNA solution

for 3.25 hours instead of 20, and rinsed with DNA buffer as was done in the previous experiments.

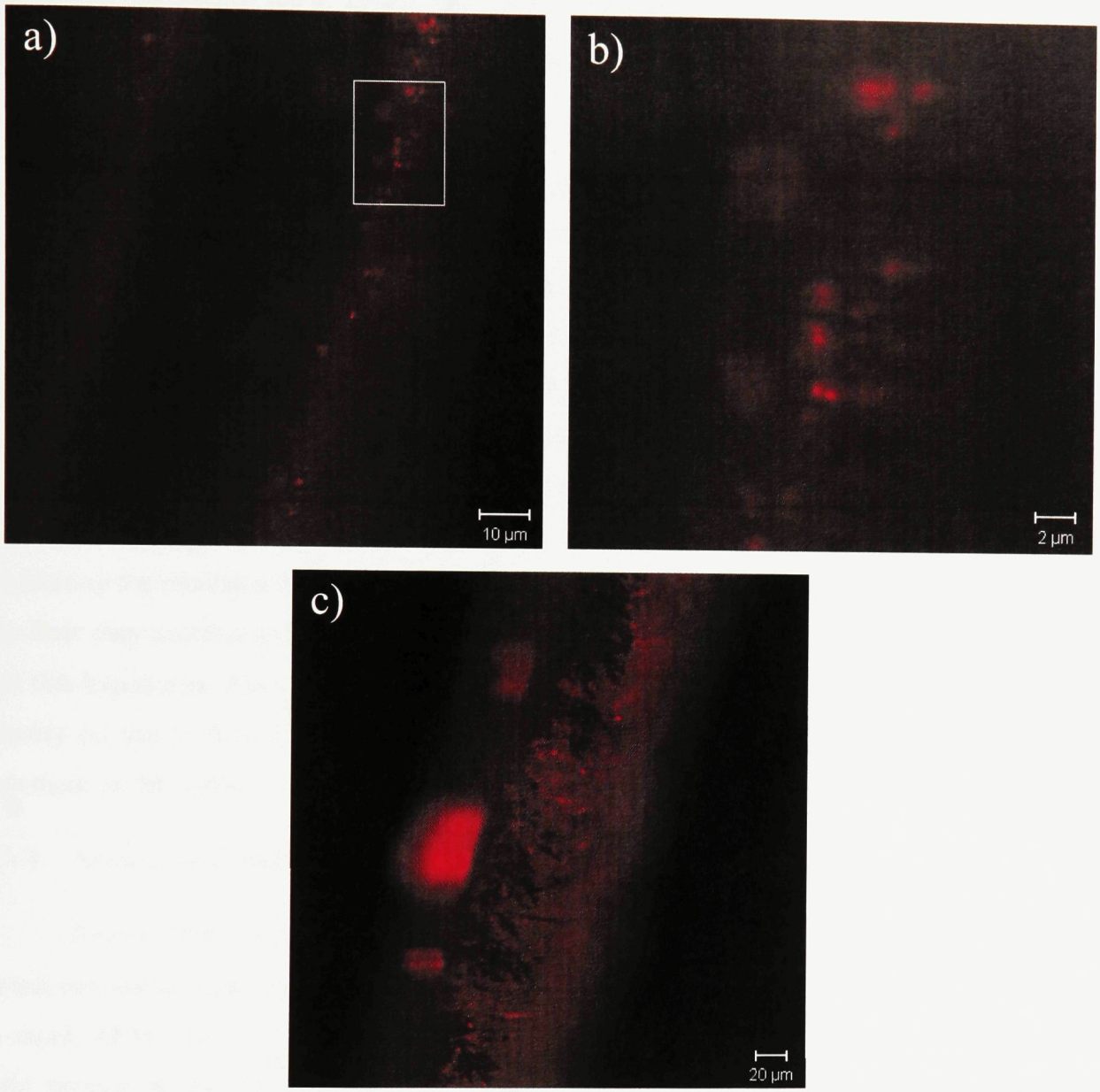

Figure 2.17. Confocal microscope images of an optical fiber immersed in a 45µM Cy3- and thiol-modified DNA solution for 3.25 hours. a) Excitation 550nm, emission 570nm, 11% laser strength, detector pinhole width 55µm, 63X magnification; b) A zoom-in of 2.17a, the area of which is marked by a white box; c) Excitation 550nm, emission 570nm, 11% laser strength, detector pinhole width 55µm, 20X magnification.

The images in Figure 2.17 were captured with the same laser and detector settings as the other deposition experiments. As shown by the images, the dye-tagged DNA was bound to the gold surface, even with the shorter deposition time. This was expected, as the first step of the binding of the thiol groups to the gold surface progresses quickly.[60] The size of the fluorescence

features was similar to those seen in Figure 2.16, with single features (see Figure 2.16b) being approximately 0.5 to 1μm in size. It was noticed, however, that the intensity of the fluorescence seen in the images was not as strong compared to the images of the fiber that had been immersed in the DNA solution for 20 hours. This suggests that less DNA was bound to the surface of the fiber during the shorter deposition time.

The lower concentration of DNA on the surface of the fiber may possibly be due to initial non-specific binding of the DNA to the surface of the fiber hindering the formation of the covalent gold-thiol bond. Non-specific binding between the DNA and the surface of the fiber would result in the "laying down" of the DNA on the surface. These interactions can be replaced by the stronger covalent binding of the thiol group of the DNA over time, and times of around 12 to 36 hours are typical in order to form an ordered layer on the gold surface.[60] The Mg^{2+} ions in the DNA buffer solution were included to allow the aptamers to form a more ordered, denser layer on the gold surface by neutralizing the negative charges of the DNA backbone, and decreasing the repulsion between DNA strands. A higher aptamer concentration on the surface of the fiber may increase the sensitivity of the biosensor, although more study would be required to test this hypothesis. Also, work to discover the relationship between deposition time and aptamer density on the surface may prove to be useful, and determine the optimal surface density of aptamers on the surface for use in the biosensor.

2.3.4 Atomic force microscopy

Atomic force microscopy (AFM) is a powerful physical technique, and can be used to detect nanometre-sized features of many types of samples on many types of surfaces.[62] With this in mind, AFM was chosen in order to show that the aptamer for thrombin was attaching to the gold surface of the fiber, and that aptamer-protein binding was taking place on the surface. Thrombin-aptamer binding on mica has also been studied using AFM, and in both cases individual thrombin proteins were observed.[29]

2.3.4.1 Gold-plated fiber

For comparison purposes, a gold-plated fiber was placed in DNA buffer for four hours and analyzed using AFM. The results obtained are shown in Figure 2.18.

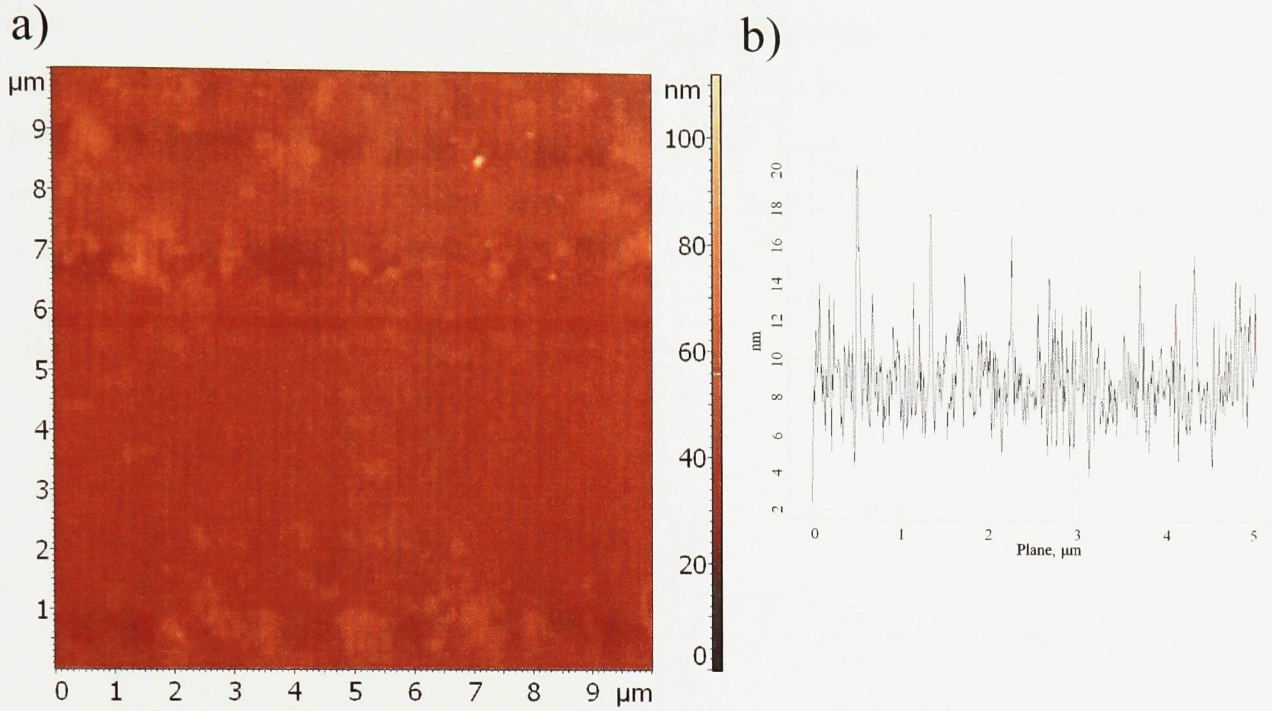

Figure 2.18. a) Atomic force microscope image of a gold-plated optical fiber. b) A cross-section of the same gold-plated optical fiber.

Results of this experiment showed a flat surface with an average roughness of the surface of 2.5nm. This roughness may have been due to inconsistencies in the surface caused by the sputtering technique used to layer the gold on the optical fiber. It has been shown that using the sputtering technique to form a gold coating in air at a pressure of 0.0003 bar resulted in the formation of islands, which coarsened with layer thickness.[63] The cross-section of the image, shown in Figure 2.18b, showed that there was an oscillation of the height of the cantilever of about 4nm to 6nm. It is possible that the larger features seen in the image were from salt or dust that was collected on the surface of the gold before the images were taken. It is also possible that the oscillation was due to the upward and downward motion of the fiber when it was contacted by the tip. This may have happened if the fiber was not fastened down properly on the glass slide before analysis.

2.3.4.2 Aptamers deposited on the gold surface

Since the aptamer for thrombin consists of 15 nucleotides, its length was estimated to be approximately 5nm. This, hypothetically, made it possible for the presence of the aptamer on the gold surface of the fiber to be detected using AFM. The gold-plated fiber was left in a 25µM solution of the aptamer for thrombin for four hours before imaging. The fiber was rinsed with

deionized water after deposition to help remove any aptamer that was bound non-specifically to the fiber. From Figure 2.19, the topography of the DNA-deposited fiber was similar to that of the bare gold-coated fiber. The surface was found to be mostly flat, with features ranging from 10nm to 40nm in height. From the cross-section, it was observed that the background fluctuations were slightly less than the bare fiber sample, with fluctuations in the surface of about 2nm to 3nm.

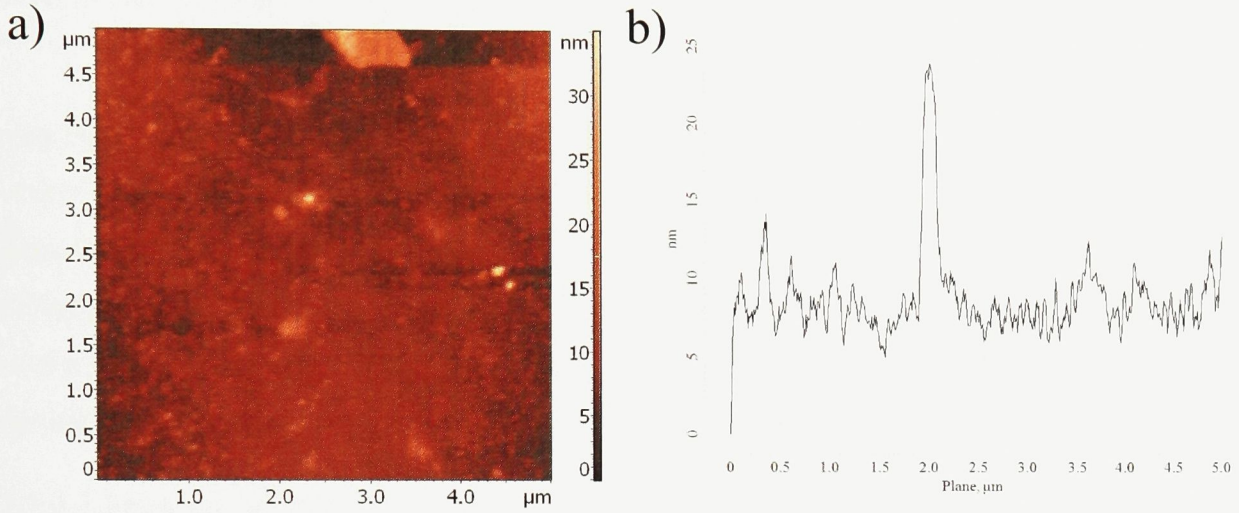

Figure 2.19. a) Atomic force microscope image of thiolated aptamer for thrombin deposited on a gold-plated optical fiber. b) A cross-section of the image.

From the images, there did not appear to be any sections that would indicate the presence of DNA on the surface. This may have been the result of the aptamer strands laying flat on the gold surface during imaging, either through interaction of the DNA with the gold surface or from the influence of the AFM tip. The DNA may be more likely to stand out from the surface if hydrated, or influenced by surrounding DNA strands, if there was a high concentration of covalently-bound aptamers in a certain area. Depending on the resolution of the AFM, this arrangement of aptamers may have appeared as a wide feature raised 5nm above the surface, or as a series of 5nm-tall peaks. As seen in the cross-section, small features with heights of approximately 5nm can be seen. These features may have been the result of a group of attached DNA segments. However, since features this size were also observed in the bare gold surface it was difficult to state with certainty that these features were due to DNA deposition. The similarity of the two surfaces may also be the result of the aptamers not being bound to the gold surface of the fiber, although this is not likely since the confocal microscopy results showed that the thiolated aptamer for thrombin was able to bind to the gold after three hours (see Section 2.3.3.4).

One difference that was observed between the bare gold and aptamer-deposited samples was the average roughness, which was 2.5nm and 2.0nm respectively. This 20% difference may have been due to the binding of the aptamer to the gold, as a surface with an ordered layer of bound DNA may be less rough compared to a gold surface. However, the difference in roughness of about 0.5nm may be too small to be conclusive. More study would be required in order to find a clear relation between DNA deposition and the unevenness of a surface.

The absence of distinctive 5nm peaks in the AFM image of the aptamer-deposited sample may have also been the result of the G-tetrad formed by the aptamer for thrombin. The G-tetrad, which would have shortened the height of the aptamer, can be formed in the presence of sodium ions, which were present in the DNA buffer.[64] The formation of G-tetrads would make a group of deposited aptamer strands appear to be a slightly raised surface. Considering the inconsistency of the surface seen in the AFM image of the bare gold surface, it would have been difficult to distinguish a raised area of the gold surface from a group of bound aptamers.

2.3.4.3 Aptamer-thrombin interaction

To see if the aptamer-thrombin interaction could be imaged on the gold-coated fiber, a fiber was immersed in a 30μM solution of thrombin in protein buffer for approximately 12 hours. The fiber was then rinsed in deionized water prior to imaging to remove the non-specifically bound proteins.

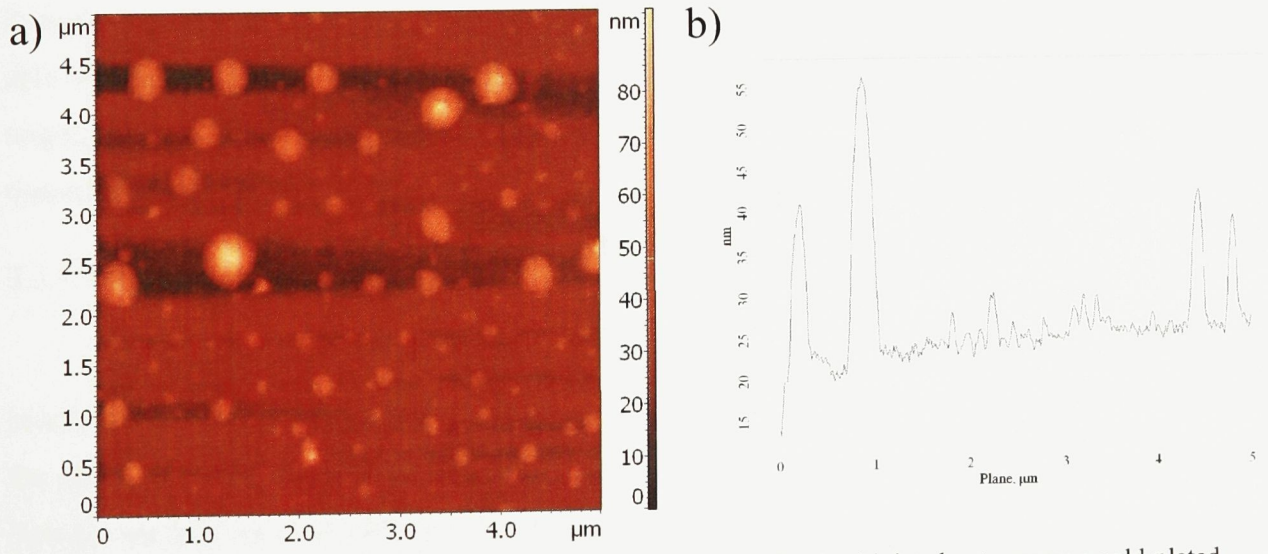

Figure 2.20. a) An atomic force microscope image of thrombin bound to its thiolated aptamer on a gold-plated optical fiber. b) A cross section of a section of the image.

From Figure 2.20, features can be seen on the gold surface, which are clearly distinguished from the baseline oscillation. The heights of these features ranged from 4nm to approximately 100nm. The size of the thrombin protein is 4.1nm by 4.1nm,[29] therefore the features created by a single thrombin protein bound to a single aptamer would be slightly taller than four nanometres, and approximately four nanometres wide. Some features that were observed (refer to the left side of Figure 2.20b) were a size that indicated the presence of an aptamer-bound protein, but many features were larger than expected. One reason for this may be the accumulation of dust or salt on the surface of the fiber.

Another explanation for this result may be the binding of the thrombin proteins to an aggregate of aptamers on the surface. From the confocal microscope images taken in Section 2.3.3, it appeared as though some of the fluorescence seen in the images was due to an accumulation of dye-tagged aptamers in one spot. This was observed particularly for the images in which the aptamers were left in the aptamer solution for a shorter period of time, and was possibly due to the fact that not enough time was given for the aptamers to form an ordered layer on the surface. It may have also been due to inconsistencies of the gold layer from the sputtering process, resulting in increased binding of the aptamers in certain regions, and no aptamer binding in other regions. If this was also the case for the deposition of the aptamers and subsequent binding to thrombin during the AFM experiments, the result may have been many individual thrombin proteins agglomerating in a small area, causing the large features seen in the AFM images. It is not understood, however, if an agglomerate of aptamers on the surface would be able to bind to their targets, or if they would detach from the agglomerate after binding to the target. A study in which the aptamers are deposited for a longer period of time before the thrombin is added may provide insight into why the large features were present in this sample.

2.3.4.4 Non-specific interactions of thrombin with a gold-plated fiber

In order to ensure that the features seen on the aptamer-modified fiber exposed to a solution of thrombin (see Figure 2.20) were not from the non-specific deposition of thrombin on the gold surface, a gold-plated fiber was placed in a thrombin solution for a period of time, and then the surface was analyzed by AFM. The image is shown in Figure 2.21.

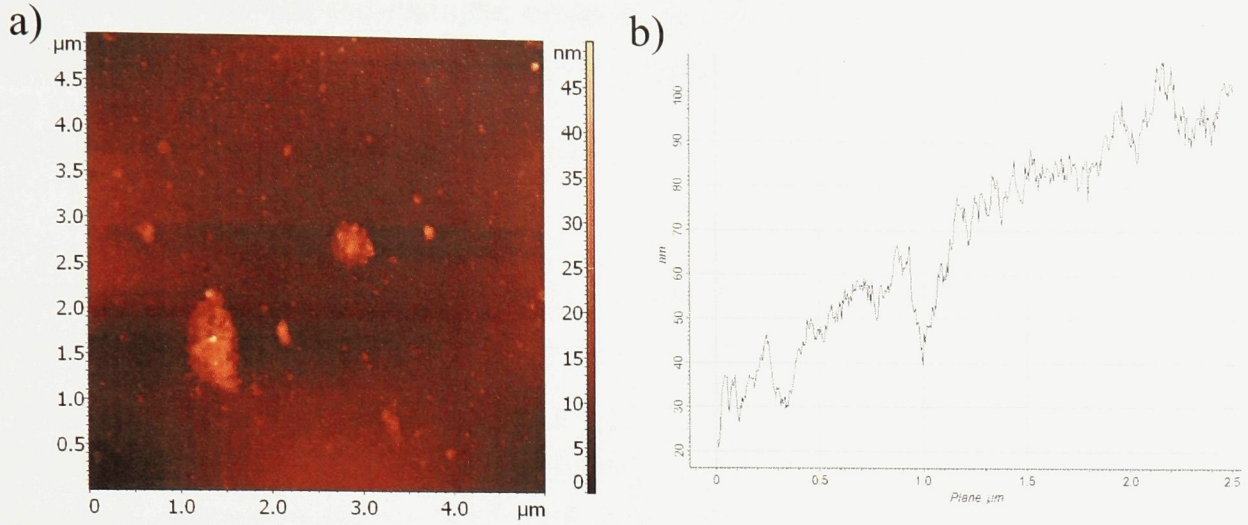

Figure 2.21. a) An atomic force microscope image of thrombin exposed to a gold-plated optical fiber. b) A cross section of a segment of the same fiber.

From the image, it was observed that the features present in the aptamer-thrombin sample were not present in the control sample. From the cross section of the AFM image (Figure 2.21b), the few features that were observed were not much larger than the noise, and may have been from the sample being dirty. The features may have also been due to the roughness of the gold surface.

2.3.5 Surface plasmon resonance

Many different methods were used to position the fiber during the SPR measurements. The first method was inserting the fiber into a long glass tube, which was filled with the buffer or DNA or thrombin solution (similar to the setup in Figure 2.11). This method was advantageous, since the sample size could be limited to approximately 200µL and there was no problem with the evaporation of the solution. However, allowing the fiber to be free in the solution affected the curvature of the fiber, especially when the fiber had to be removed to switch the solutions, which made the referencing of the signals more difficult. Therefore, both of the ends of the fibers had to be fixed onto a platform, and initially this was done by laying the fiber on a slide and covering the gold-plated portion of the fiber with the solution. However, the evaporation of the solution occurred fairly quickly with this setup. The refractive index change caused by the evaporation of the solution made it difficult to tell if the shift in the surface plasmon resonance was due to the binding of the aptamer to the surface, or simply due to the increase in salt concentration. The final design of the sensing platform, shown in Figure 2.10, allowed both ends of the fiber to be

fixed in place, and also prevented the evaporation of the solution. However, a downside of the design was that it required larger samples to be used during the analyses.

2.3.5.1 Aptamers deposited on the gold surface

As a reference sample, the fiber was immersed in the DNA buffer solution, and measurements were taken over time. In order to match the refractive index of the buffer solution with a buffer solution with DNA dissolved in it (the DNA dissolved in the solution increased its refractive index), sodium chloride was added until the desired refractive index was reached. During the experiment, the change in amplitude of the cladding resonance at 1536.6nm was measured, as it was one of the wavelengths contained in the envelope of the surface plasmon. With the fiber in the buffer solution, no change in the amplitude of the resonance was observed, which indicated that no change in refractive index around the fiber was occurring (TG89 in Figure 2.22). This also indicated that no evaporation of the sample was occurring.

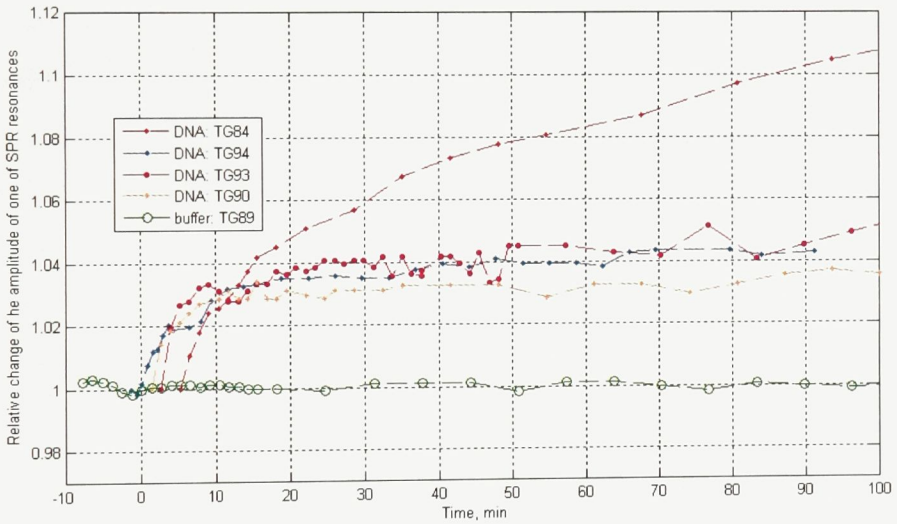

Figure 2.22. Relative amplitude intensities of the cladding resonance measured at a single wavelength for gold-plated optical fibers in the DNA buffer solution (green line) or a 15μM solution of thiol-modified aptamer for thrombin (other lines).

With the addition of the thiolated DNA, however, an increase in the resonance at the observed wavelength of approximately 4% was observed (all other curves in Figure 2.22). The amplitude readings taken during the experiment were compared to the amplitude of the resonance at the same wavelength in the buffer solution, giving the relative amplitude value that was plotted. The increase in resonance was the result of a change in the refractive index on the

fiber surface due to the attachment of the DNA to the surface, and the responsive shift in the resonance characteristics of the surface plasmon. The increase in amplitude occurred for the first seven minutes, which suggested that most of the attachment of the thiolated aptamer to the surface occurred within the first ten minutes. This was consistent with the reported observations of the attachment of thiolated molecules to a gold surface.[60] The amplitude of the resonance did not change considerably over the next 90 minutes, indicating that the amount of DNA on the surface of the fiber did not change during this time. There was a slight increase in the amplitude, though, which may have been due to completion of the slower process of the formation of a denser and more ordered thiolated DNA layer on the fiber. The response of TG84 during the deposition of the aptamer continued to increase, even after the time taken for the responses of the other fibers to plateau had passed. This may have been due to the evaporation of some of the DNA solution, which would have increased the concentration of salts and DNA, and increased the refractive index of the solution.

For the graphing of the relative responses, the wavelengths which gave the largest changes in amplitude were chosen and plotted. This may have been due to the difference in the gratings for each fiber, or the environments in which the readings took place. For sensing purposes, this would make the sensor more complicated, since instead of needing to monitor only one wavelength the whole light spectrum would need to be monitored. This may also be advantageous, since samples prepared in different solution environments could be analyzed and give amplitude responses that are reproducible and concentration-dependent. This would make the preparation of working samples more straightforward, since they would not have to be adjusted to the correct refractive index before analysis. More study will be required to examine the concentration dependence of the response and verify the validity of this hypothesis.

Although the step in which the aptamer was immobilized on the fiber surface would not be performed during practical use of the sensor, it was encouraging that a measurable response was observed for the deposition of the aptamer.

2.3.5.2 Aptamer-thrombin interaction

Of the four fibers tested in the experiments listed above, two fibers were used to test whether the binding of thrombin to its aptamer on the surface of the fiber could also be observed

by monitoring the transmission spectrum. The relative increase in amplitude at a particular wavelength over time is shown in Figure 2.23. It was observed that one fiber (TG90) had a signal increase of approximately 7% after two hours, while the other fiber (TG94) showed an increase of 5% after 90 minutes of exposure to the thrombin target. The amplitude values were still increasing at the time the experiment was stopped, the reason for which was not discovered. A possibility for the increase may be the evaporation of the buffer solution during the deposition. Readings over a longer period of time would have provided a better idea of the increase that could be shown by the binding of the aptamer to its target. The greater response from the thrombin binding may have been due to the greater size of thrombin (MW = 36700 g mol^{-1}) compared to its aptamer (4726 g mol^{-1}).

The different responses in amplitude observed between the two fibers may have been due to differences in the density of the aptamer layers on the gold surfaces of the fibers that were used. A higher concentration of aptamers immobilized on the fiber surface would allow more binding of the thrombin target, which would contribute to a greater change in the effective refractive index around the fiber, and provide a better response. To confirm this, a study of the effect of aptamer deposition time on the observed amplitude change when thrombin is introduced may be helpful.

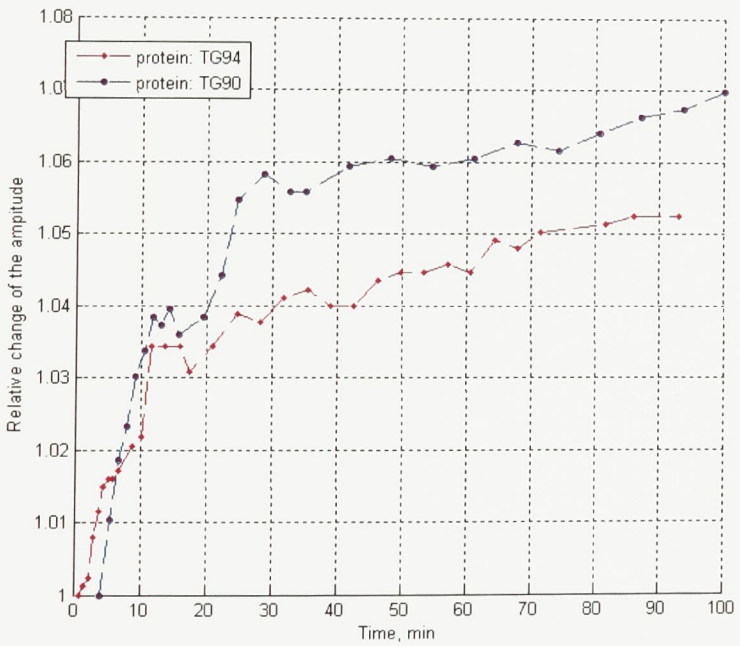

Figure 2.23. Relative amplitude intensities of the cladding resonance measured at a single wavelength for two different aptamer-modified optical fibers in a 30μM solution of thrombin.

The thrombin concentration used for detection in these experiments was fairly high, in order to ensure that the binding of the aptamer to thrombin was observed. The concentrations used were approximately 1000 times larger than other studies in which thrombin-aptamer interactions were monitored using surface plasmon resonance.[65, 66] Future experiments will be required to test thrombin concentrations in the nanomolar range, in order to examine the detection abilities of the sensor against other reported sensors.

2.4 Conclusions

The experiments described above showed that the designed TFBG surface plasmon resonance sensor was able to detect the presence of thrombin in solution via the binding of the thrombin to a surface-immobilized aptamer. The detection was possible due to the change in the effective refractive index around the fiber that was caused by the accumulation of the thrombin at the surface of the fiber during the binding process. The immobilization of the DNA aptamers also provided a measurable signal, showing that the sensor may be adequately sensitive to detect small molecules as well as larger molecules.

In order to show that the SPR responses were due to the attachment of the aptamer to the surface and the subsequent binding of thrombin to the surface-immobilised fiber, microscopy techniques were used to show that the binding of the aptamer and thrombin-aptamer interactions occurred under the same conditions of the experiments. Confocal microscopy was used to observe the binding of a dye-tagged, thiol-modified aptamer for thrombin to gold-plated optical fibers after three hours of immersion in a solution of the DNA. Atomic force microscopy showed features that may have corresponded to thrombin bound at the surface of an aptamer-modified optical fiber, although more study would be required to confirm this.

This study described the beginning of a project to develop a sensitive, label-free, compact sensor that may be modified to be used in the detection of a number of targets. More study will be necessary to show the sensor's sensitivity and full analytical abilities (limits of detection, detection ranges), but preliminary testing showed considerable promise for this design as a viable sensing platform.

2.5 References

(1) D'Orazio, P. *Clin. Chim. Acta* **2003**, *334*, 41-69.

(2) Leung, A.; Shankar, P. M.; Mutharasan, R. *Sens. Actuators, B* **2007**, *125*, 688-703.

(3) Manera, M. G.; Spadavecchia, J.; Leone, A.; Quaranta, F.; Rella, R.; Dell'atti, D.; Minunni, M.; Mascini, M.; Siciliano, P. *Sens. Actuators, B* **2008**, *130*, 82-87.

(4) Mernagh, D. R.; Janscak, P.; Firman, K.; Kneale, G. G. *Biol. Chem.* **1998**, *379*, 497-503.

(5) Sota, H.; Hasegawa, Y.; Iwakura, M. *Anal. Chem.* **1998**, *70*, 2019-2024.

(6) Wang, J.; Zhou, H. S. *Anal. Chem.* **2008**, *80*, 7174-7178.

(7) Goff, D. R. *Fiber Optic Reference Guide: a practical guide to the technology;* Focal Press: Boston, MA, 1996; p 11.

(8) Hecht, J. *Understanding Fiber Optics*, 4th ed.; Prentice Hall: Upper Saddle River, NJ, 2002; Chapter 1.

(9) Murata, H. *Handbook of Optical Fibers and Cables*, 2nd ed.; Marcel Dekker, Inc.: New York, NY, 1996; p 17.

(10) Yu, F. T. S.; Yang, X. *Introduction to Optical Engineering;* Cambridge University Press: New York, NY, 1997; Chapter 12.

(11) Homola, J.; Yee, S. S.; Myszka, D. Surface Plasmon Resonance Biosensors. In *Optical Biosensors: Present and Future*; Ligler, F. S., Rowe Taitt, C. S., Eds.; Elsevier: Boston, MA, 2002; Chapter 7.

(12) Hill, K. O.; Fujii, Y.; Johnson, D. C.; Kawasaki, B. S. *Appl. Phys. Lett.* **1978**, *32*, 647-649.

(13) Fan, X.; White, I. M.; Shopova, S. I.; Zhu, H.; Suter, J. D.; Sun, Y. *Anal. Chim. Acta* **2008**, *620*, 8-26.

(14) Kersey, A. D.; Davis, M. A.; Patrick, H. J.; LeBlanc, M.; Koo, K. P.; Askins, C. G.; Putnam, M. A.; Friebele, E. J. *J. Lightwave Technol.* **1997**, *15*, 1442-1463.

(15) Rao, Y.-J. *Meas. Sci. Technol.* **1997**, *8*, 355-375.

(16) Gangopadhyay, T. K. *Sens. Actuators, A* **2004**, *113*, 20-38.

(17) Lee, B. *Opt. Fiber Technol.* **2003**, *9*, 57-79.

(18) Guo, T.; Ivanov, A.; Chen, C.; Albert, J. *Opt. Lett.* **2008**, *33*, 1004-1006.

(19) Chen, C.; Albert, J. *Electron. Lett.* **2006**, *42*, 1027-1028.

(20) Guo, T.; Chen, C.; Laronche, A.; Albert, J. *IEEE Photon. Technol. Lett.* **2008**, *20*, 635-637.

(21) Shevchenko, Y. Y.; Albert, J. *Opt. Lett.* **2007**, *32*, 211-213.

(22) Binnig, G.; Quate, C. F.; Gerber, C. *Phys. Rev. Lett.* **1986**, *56*, 930-933.

(23) Morris, V. J.; Kirby, A. R.; Gunning, A. P. *Atomic Force Microscopy for Biologists;* Imperial College Press: London, England, 1999; Chapters 1-2.

(24) Jalili, N.; Laxminarayana, K. *Mechatronics* **2004**, *14*, 907-945.

(25) Hinterdorfer, P.; Dufrêne, Y. F. *Nat. Methods* **2006**, *3*, 347-355.

(26) Hansma, H. G. *Annu. Rev. Phys. Chem.* **2001**, *52*, 71-92.

(27) Dufrêne, Y. F. *Nat. Rev. Microbiol.* **2008**, *6*, 674-680.

(28) Müller, D. J.; Dufrêne, Y. F. *Nat. Nanotechnol.* **2008**, *3*, 261-269.

(29) Rinker, S.; Ke, Y.; Liu, Y.; Chaabra, R.; Yan, H. *Nat. Nanotechnol.* **2008**, *3*, 418-422.

(30) Liu, Y.; Lin, C.; Li, H.; Yan, H. *Angew. Chem. Int. Ed.* **2005**, *44*, 4333-4338.

(31) Basnar, B.; Elnathan, R.; Willner, I. *Anal. Chem.* **2006**, *78*, 3638-3642.

(32) Hepler, P. K.; Gunning, B. E. S. *Protoplasma* **1998**, *201*, 121-157.

(33) Sheppard, C. J. R.; Shotton, D. M. *Confocal Laser Scanning Microscopy;* Springer-Verlag New York Inc.: New York, NY, USA, 1997; Chapter 1.

(34) Ferrando, M.; Spiess, W. E. L. *Food Sci. Tech. Int.* **2000**, *6*, 267-284.

(35) Shotton, D. M. *Histochem. Cell Biol.* **1995**, *104*, 97-137.

(36) Paddock, S. W. *BioTechniques* **1999**, *27*, 992-1004.

(37) Tadrous, P. J. *J. Pathol.* **2000**, *191*, 345-354.

(38) Peng, X.; Du, J.; Fan, J.; Wang, J.; Wu, Y.; Zhao, J.; Sun, S.; Xu, T. *J. Am. Chem. Soc.* **2007**, *129*, 1500-1501.

(39) Krämer, S. D.; Wunderli-Allenspach, H. *Biochim. Biophys. Acta* **2003**, *1609*, 161-169.

(40) Slaughter, G. E.; Bieberich, E.; Wnek, G. E.; Wynne, K. J.; Guiseppi-Elie, A. *Langmuir* **2004**, *20*, 7189-7200.

(41) Xu, L.; Davies, S.; Schofield, A. B.; Weitz, D. A. *Phys. Rev. Lett.* **2008**, *101*, 094502.

(42) Shepherd, J. L.; Kell, A.; Chung, E.; Sinclar, C. W.; Workentin, M. S.; Bizzotto, D. *J. Am. Chem. Soc.* **2004**, *126*, 8329-8335.

(43) Shepherd, J. L.; Bizzotto, D. *Langmuir* **2006**, *22*, 4869-4876.

(44) Mujumdar, R. B.; Ernst, L. A.; Mujumdar, S. R.; Lewis, C. J.; Waggoner, A. S. *Bioconjugate Chem.* **1993**, *4*, 105-111.

(45) Randolph, J. B.; Waggoner, A. S. *Nucleic Acids Res.* **1997**, *25*, 2923-2929.

(46) Ha, T. *Methods* **2001**, *25*, 78-86.

(47) Sanborn, M. E.; Connolly, B. K.; Gurunathan, K.; Levitus, M. *J. Phys. Chem. B* **2007**, *111*, 11064-11074.

(48) Jares-Erijman, E. A.; Jovin, T. M. *J. Mol. Biol.* **1996**, *257*, 597-617.

(49) Kozlov, A. G.; Lohman, T. M. *Biochemistry* **2002**, *41*, 6032-6044.

(50) Kenworthy, A. K. *Methods* **2001**, *24*, 289-296.

(51) Ellman, G. L. *Arch. Biochem. Biophys.* **1958**, *74*, 443-450.

(52) Riddles, P. W.; Blakeley, R. L.; Zerner, B. *Methods Enzymol.* **1983**, *91*, 49-60.

(53) Shevchenko, Y. Y. *Surface plasmon resonance sensor based on the tilted fiber Bragg grating*, Carleton University, Ottawa, ON, 2007.

(54) Corning Incorporated. *Corning® SMF-28™ Optical Fiber: Product information*. **2002**. *http://www.ee.byu.edu/photonics/FiberOpticConnectors.parts/images/smf28.pdf* (accessed November 18, 2008, 2008).

(55) Chan, J. Y. S. *Towards an Aptamer for L-Homocysteine*, Carleton University, Ottawa, ON, 2007.

(56) Clayden, J. P.; Greeves, N.; Warren, S.; Wothers, P. D. *Organic Chemistry;* Oxford University Press: New York, NY, 2001; p 1355.

(57) Burns, J. A.; Butler, J. C.; Moran, J.; Whitesides, G. M. *J. Org. Chem.* **1991**, *56*, 2648-2650.

(58) Miessler, G. L.; Tarr, D. A. *Inorganic Chemistry*, 3rd ed.; Prentice Hall: Upper Saddle River, NJ, 2004; p 183.

(59) Chaki, N. K.; Vijayamohanan, K. *Biosens. Bioelectron.* **2002**, *17*, 1-12.

(60) Xu, J.; Li, H.-L. *J. Colloid Interface Sci.* **1995**, *176*, 138-149.

(61) DeBono, R. F.; Loucks, G. D.; Della Manna, D.; Krull, U. J. *Can. J. Chem.* **1996**, *74*, 677-688.

(62) Frommer, J. *Angew. Chem. Int. Ed.* **1992**, *31*, 1298-1328.

(63) Schug, C.; Schempp, S.; Lamparter, P.; Steeb, S. *Surf. Interface Anal.* **1999**, *27*, 670-677.

(64) Smargiasso, N.; Rosu, F.; Hsia, W.; Colson, P.; Baker, E. S.; Bowers, M. T.; De Pauw, E.; Gabelica, V. *J. Am. Chem. Soc.* **2008**, *130*, 10208-10216.

(65) Ostatná, V.; Vaisocherová, H.; Homola, J.; Hianik, T. *Anal. Bioanal. Chem.* **2008**, *391*, 1861-1869.

(66) Tang, Q.; Su, X.; Loh, K. P. *J. Colloid Interface Sci.* **2007**, *315*, 99-106.

APPENDIX

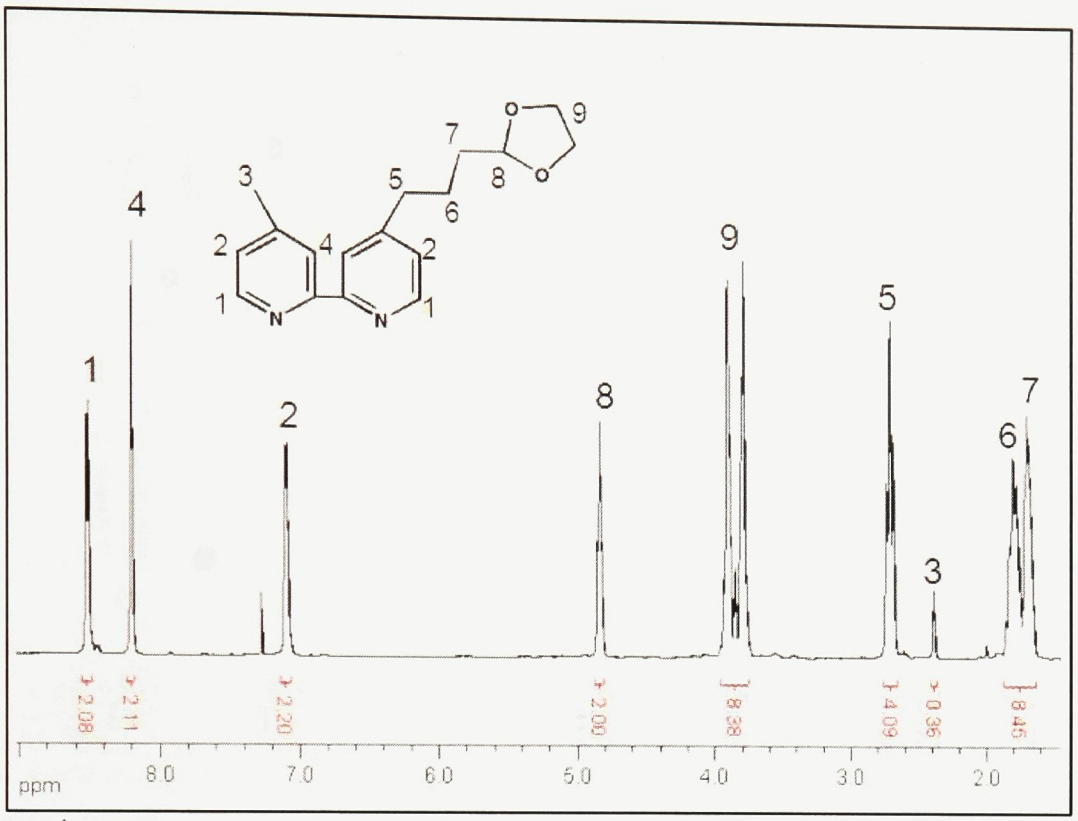

Figure A-1.1. ^{1}H NMR spectrum (300 MHz, $CDCl_3$) and peak assignments of a mixture of 4-[3-(1,3-dioxolan-2-yl)propyl]-4'-methyl-2,2'-bipyridine and 4,4'-[3-(1,3-dioxolan-2-yl)propyl]-2,2'-bipyridine, as discussed in Section 1.3.2.1.

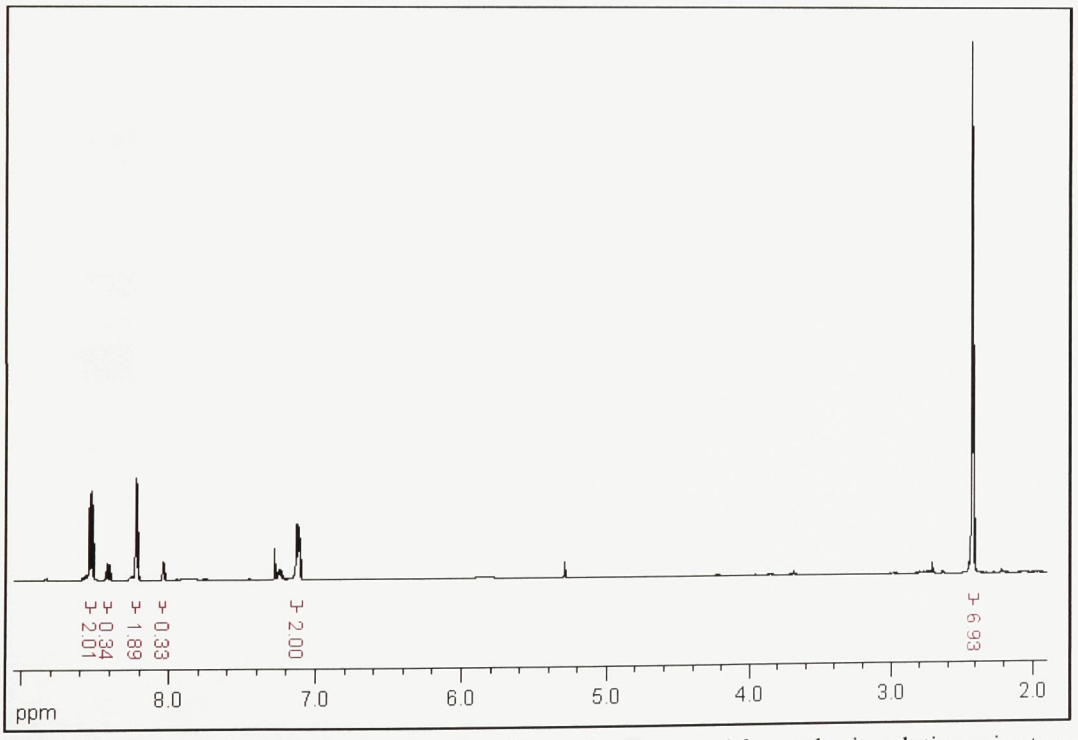

Figure A-1.2. ^{1}H NMR spectrum (300 MHz, $CDCl_3$) of impurites extracted from a basic solution prior to acification eand extraction of bipy', as discussed in Section 1.3.2.3.

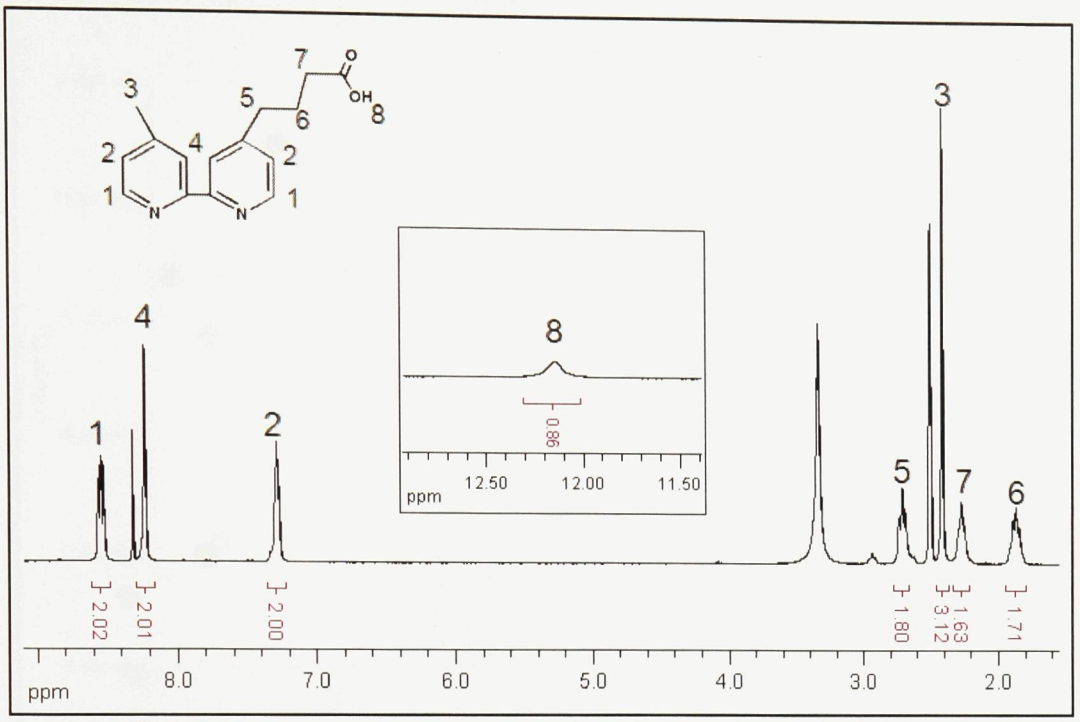

Figure A-1.3. ^{1}H NMR spectrum (300 MHz, $CDCl_3$) and peak assignments of 4-(3-carboxypropyl)-4'-methyl-2,2'-bipyridine, extracted after being in acidic solution for five months, as discussed in Section 1.3.2.4.

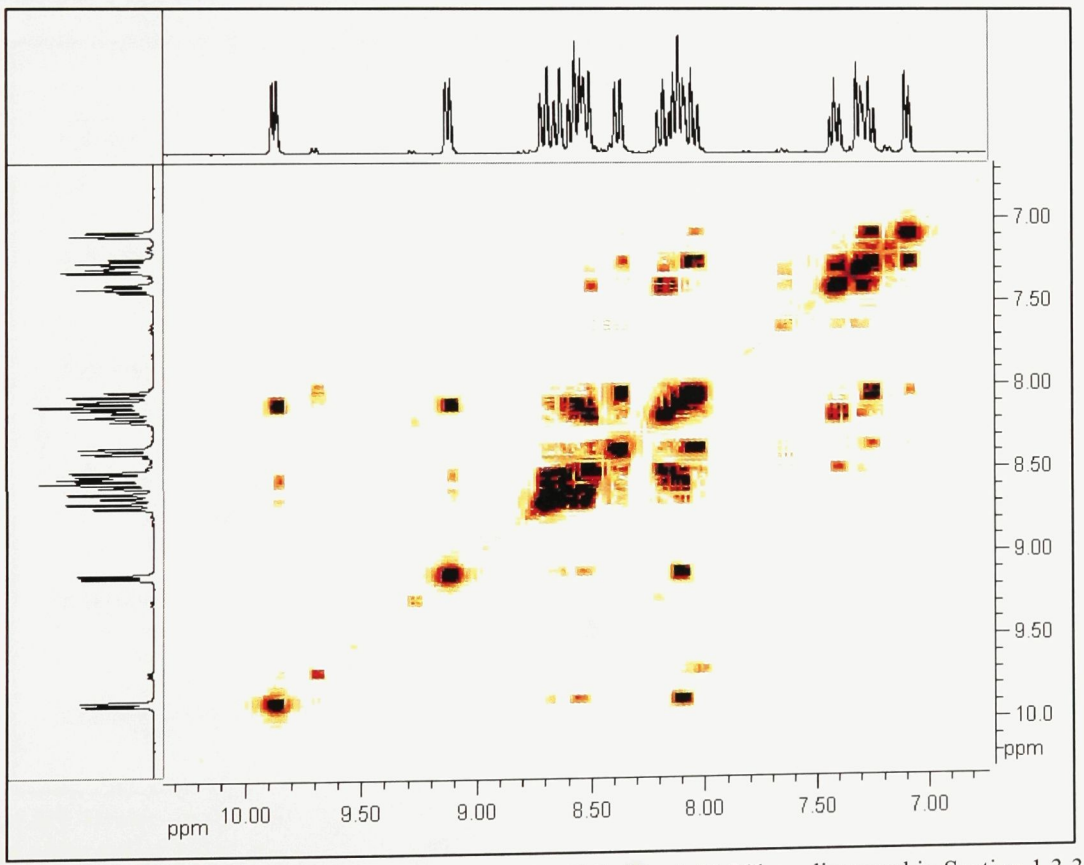

Figure A-1.4. ^{1}H NMR COSY spectrum (300 MHz, D_2O) of $[Co(bipy)_2Cl_2]Cl$, as discussed in Section 1.3.3.

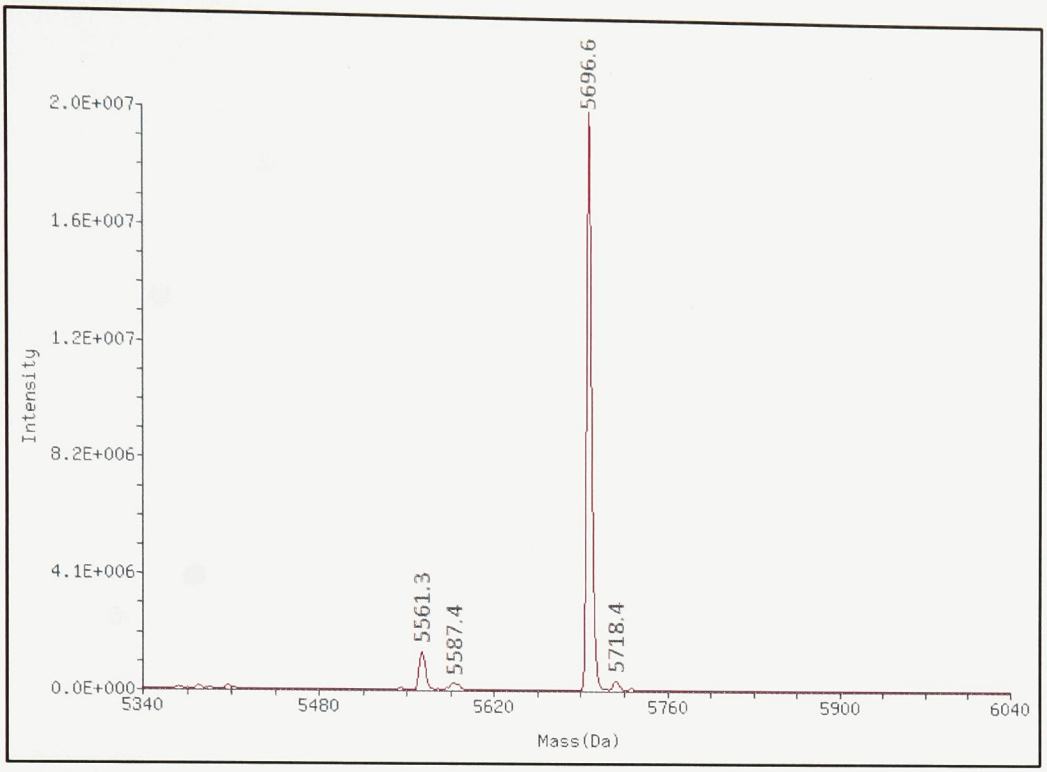

Figure A-1.5.1. Deconvoluted mass spectrum of an HPLC fraction (retention time = 9min) from a bipy'-DNA coupling reaction with PyBOP, as discussed in Section 1.3.7.2.

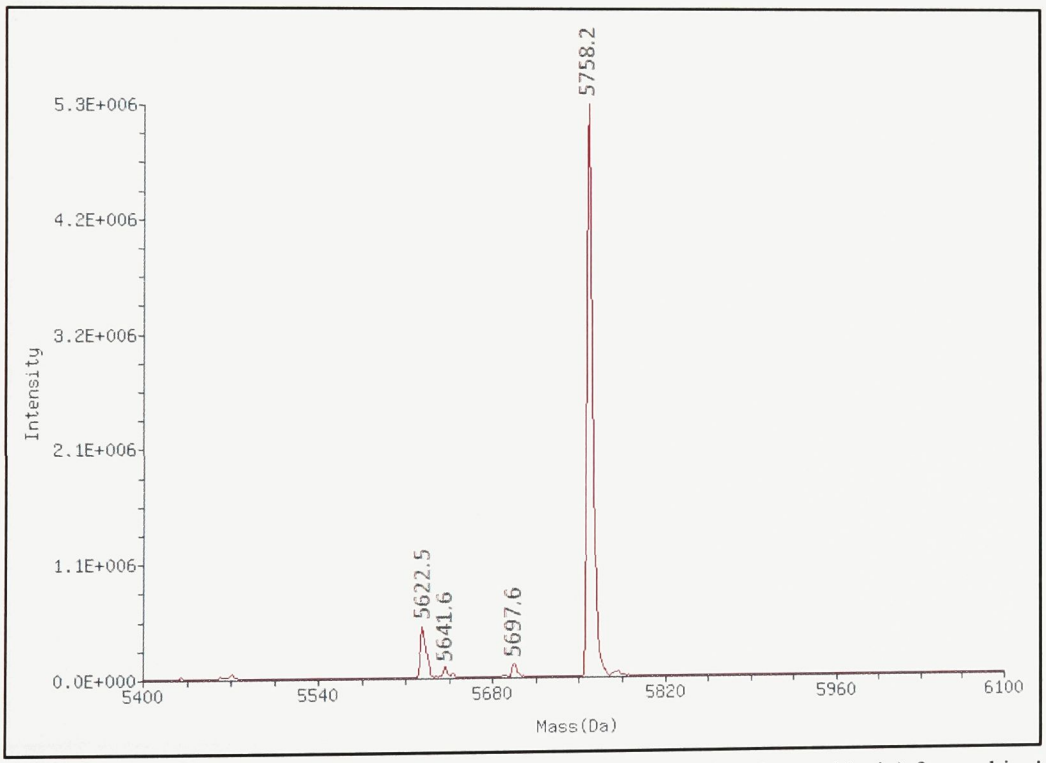

Figure A-1.5.2. Deconvoluted mass spectrum of an HPLC fraction (retention time = 11min) from a bipy'-DNA coupling reaction with PyBOP, as discussed in Section 1.3.7.2.

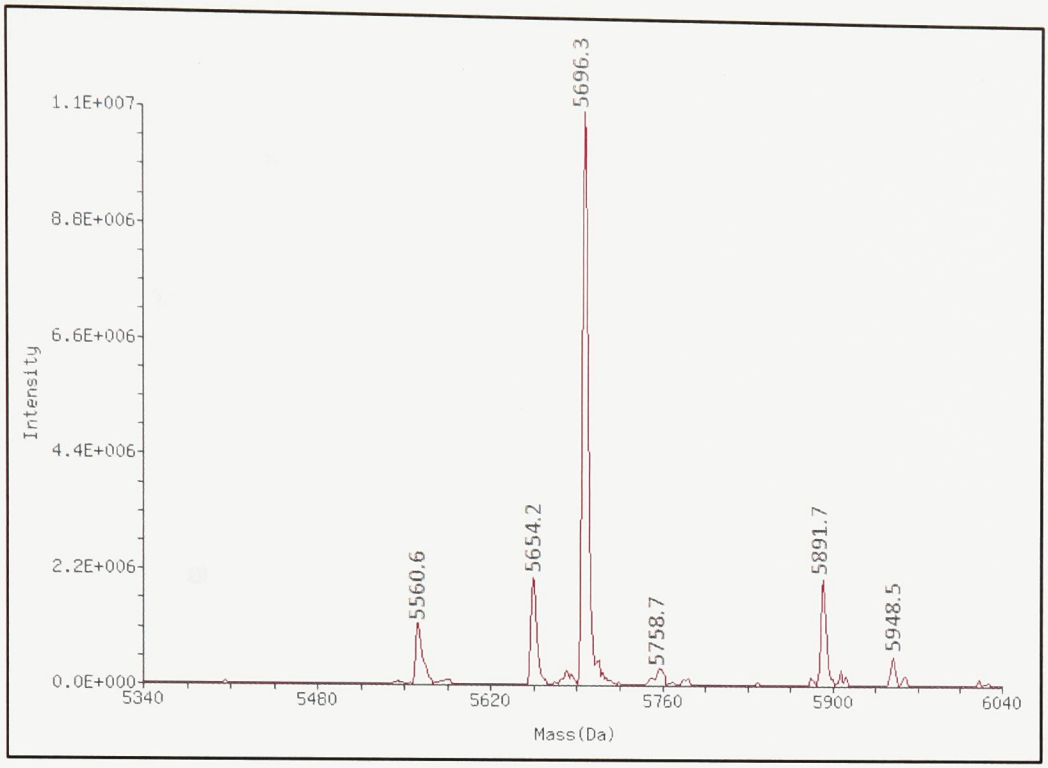

Figure A-1.6.1. Deconvoluted mass spectrum of an HPLC fraction (retention time = 5.5min) from a $[Co(bipy)_2(bipy')](PF_6)_3$-DNA coupling reaction with PyBOP, as discussed in Section 1.3.7.2.

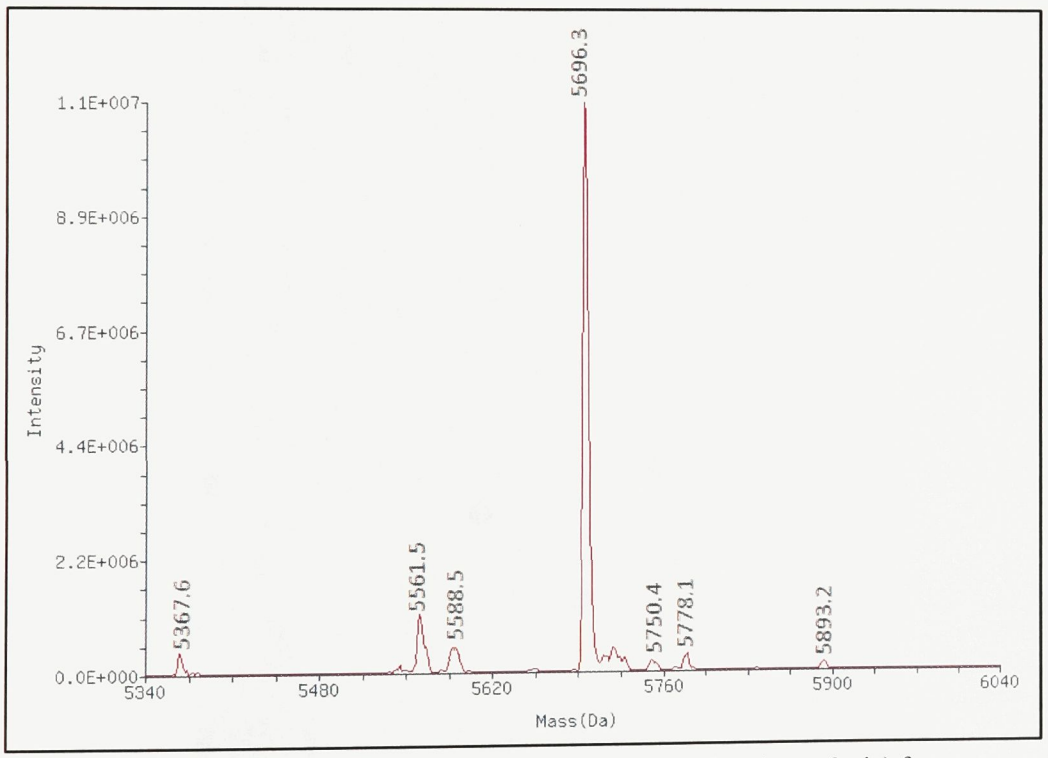

Figure A-1.6.2. Deconvoluted mass spectrum of an HPLC fraction (retention time = 9min) from a $[Co(bipy)_2(bipy')](PF_6)_3$-DNA coupling reaction with PyBOP, as discussed in Section 1.3.7.2.

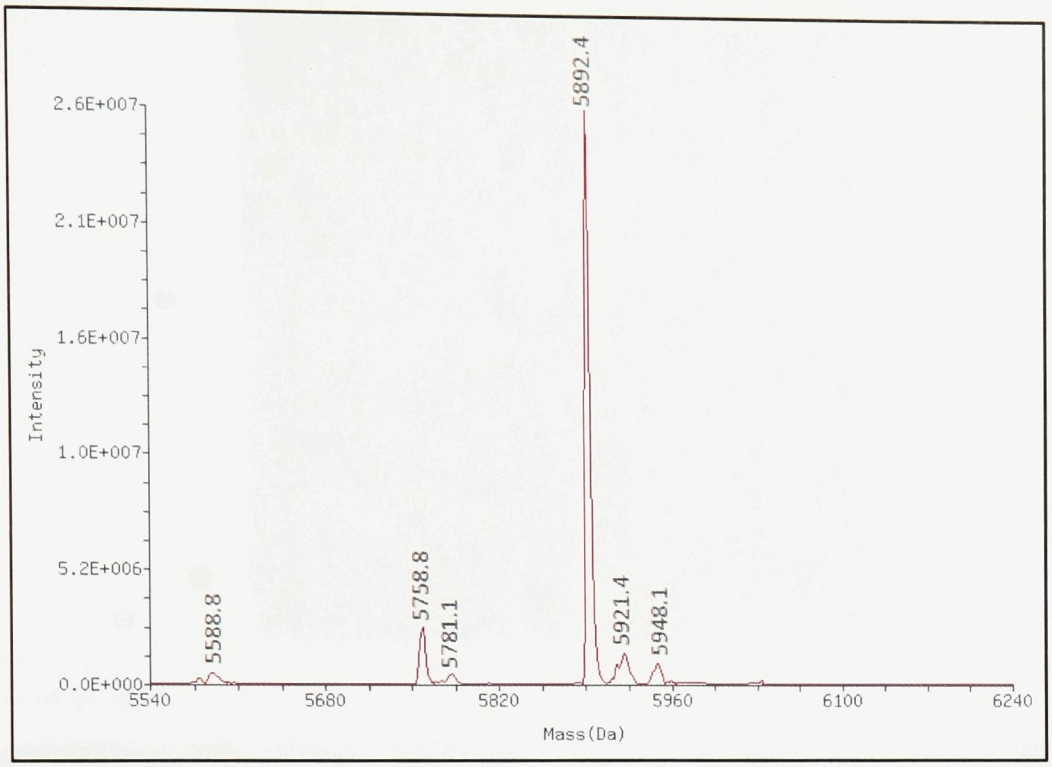

Figure A-1.6.3. Deconvoluted mass spectrum of an HPLC fraction (retention time = 17min) from a $[Co(bipy)_2(bipy')](PF_6)_3$-DNA coupling reaction with PyBOP, as discussed in Section 1.3.7.2.

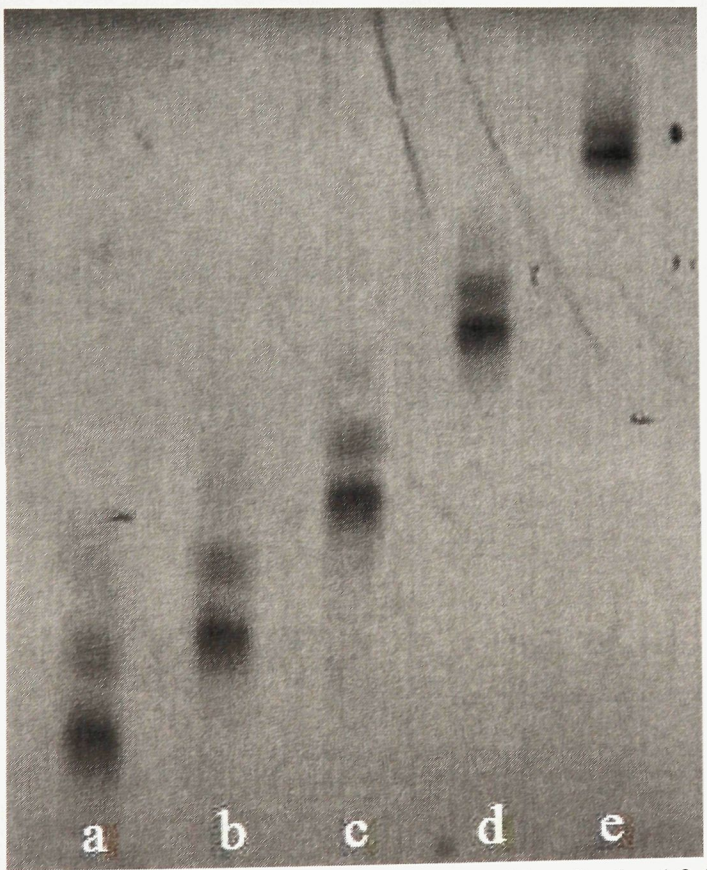

Figure A-1.7. PAGE results for the amine-modified 10-mer DNA strand (see Section 1.2.6.5). Bands were created by the migration of the DNA for a) 2.5 hours, b) 2 hours, c) 1.5 hours, d) 1 hour, and e) 30 minutes.

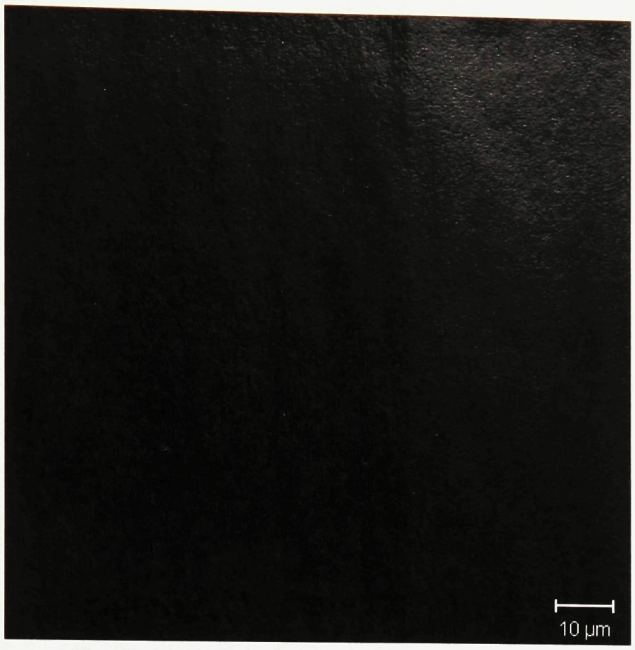

Figure A-2.1. Confocal microscope image of DNA buffer deposited on a slide. Excitation 550nm, emission 570nm, 11% laser strength, detector pinhole width 55µm, 63X magnification.

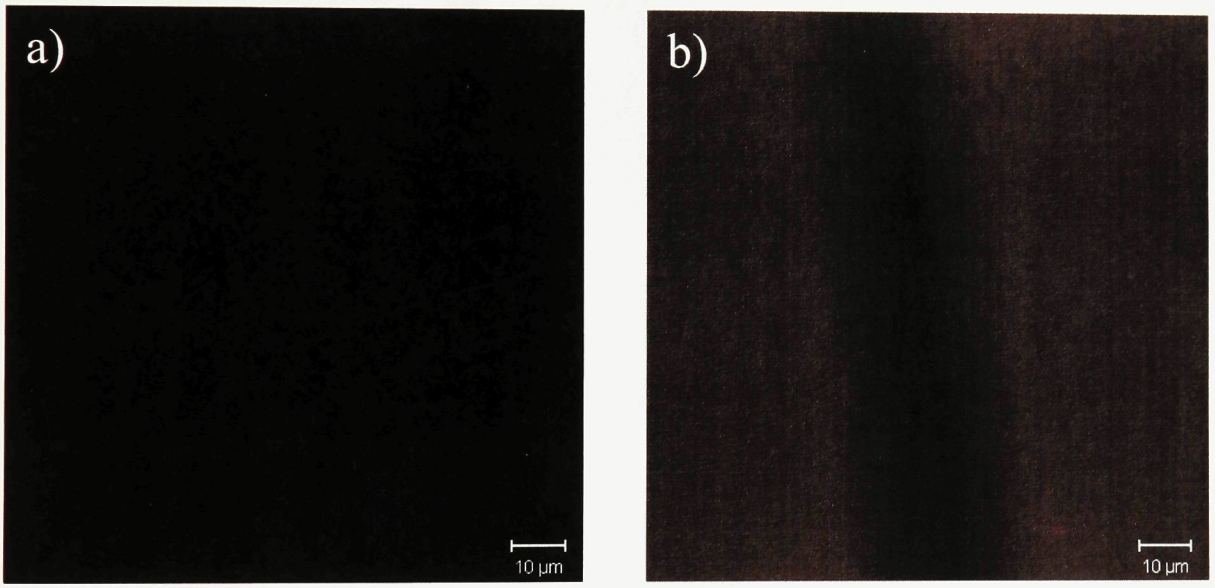

Figure A-2.2. Confocal microscope images of optical fibers immersed in a 30µM Cy3 solution for 20 hours.
a) Excitation 550nm, emission 570nm, 11% laser strength, detector pinhole width 55µm, 63X magnification;
b) Excitation 550nm, emission 570nm, 80% laser strength, detector pinhole width 55µm, 63X magnification.